Università degli Studi di Padova

Sede Amministrativa: Università degli Studi di Padova
Dipartimento di medicina animale produzioni e salute

CORSO DI DOTTORATO DI RICERCA IN SCIENZE VETERINARIE
CICLO: XXIX

THREE-DIMENSIONAL COMPUTATION OF FEMORAL CANINE MORPHOLOGICAL PARAMETERS: FROM THE THEORY TO THE SURGERY APPLICATION

Coordinatore: Ch.mo Prof. Alessandro Zotti
Supervisore: Ch.mo Prof. Maurizio Isola
Co-Supervisore: Ch.mo Prof. Roberto Busetto

Dottorando: Federico Longo

“ A little history of nothing..”

Every page of this brief manuscript was written in Cordovado, my secret lost paradise.
Every breathe, thought and smile is entirely dedicated to my Grand Parents, Maria Pia and Piero.

I love you.

INDEX

ABBREVIATION LIST

aLDFA	Anatomic lateral distal femoral angle
aLPFA	Anatomic lateral proximal femoral angle
Cd	Caudal
Cr	Cranial
CORA	Center of rotation of angulation
DFLA	Distal femoral long axis
DJD	Degenerative joint disease
FL	Femur length
FNA	Femoral neck angle
FNHA	Femoral head and neck axis
FTA	Femoral torsion angle
FVA	Femoral varus angle
H Dist	Distance of the center of the head from DFLA
HU	Hounsfield units
H Rad	Head radius
HJOL	Hip joint orientation line
MA	Mechanical axis
mLDFA	Mechanical lateral distal femoral angle
mLPFA	Mechanical lateral proximal femoral angle
PFLA	Proximal femoral long axis
STL	Stereolotigraphy
TCA	Transcondylar axis

CHAPTER 1

INTRODUCTION

Angular deformities of the canine pelvic limb are relatively frequent and well documented.[1,2]

Skeletal malformations may be a consequence of changes occurred in the metaphysis of young animals. Possible causes include genetic predisposition, as well as growth disturbances such as premature and asymmetric physeal closure induced by metabolic or traumatic alterations.[3,4] Furthermore, angular deformities of the long bone could be the result of malunions resulting from inveterate fractures or inappropriate surgical treatment. [1,5-7]

Additionally, bone deformities are often related to some leading and increasingly recurrent causes of canine pelvic limb lameness including hip dysplasia, cranial cruciate ligament rupture and medial patellar luxation.[1-5] For instance, femoral angular deformities such as varus, valgus, and torsional anomalies, have been increasingly associated with these common orthopaedic pathologies.[6-9]

Whereas the relationship of these structural bone malformations to the pathogenesis of the cited pathologies is still unclear,[2] the biomechanical factors involved have been recently studied to accurately evaluate preoperative surgical planning. It has been stated, for instance, that an inadequate correction of femoral or tibial deformities may be a recurrent and persistent cause of MPL.[2, 10-12]

Traditionally, state of art for the morphological computation of angles and axes in the canine femur has been limited for several years to a multiple orthogonal radiographic study.[10-13]

Advantages of a radiographic study are related to its world-wide diffusion in veterinary practices, relatively affordable cost of the examination and reported repeatability, reproducibility and accuracy of some measurements. [6-10]

Following this tendency, bunch of papers in the last two decades proposed several values calculated trough x-ray films that are still considered as reference parameters when a femur deformity has to be detected. Additionally, some of these articles introduced angles pertinent to different breeds, offering to the orthopaedic surgeon solid terms of comparison in the process of decision-making .[6-12]

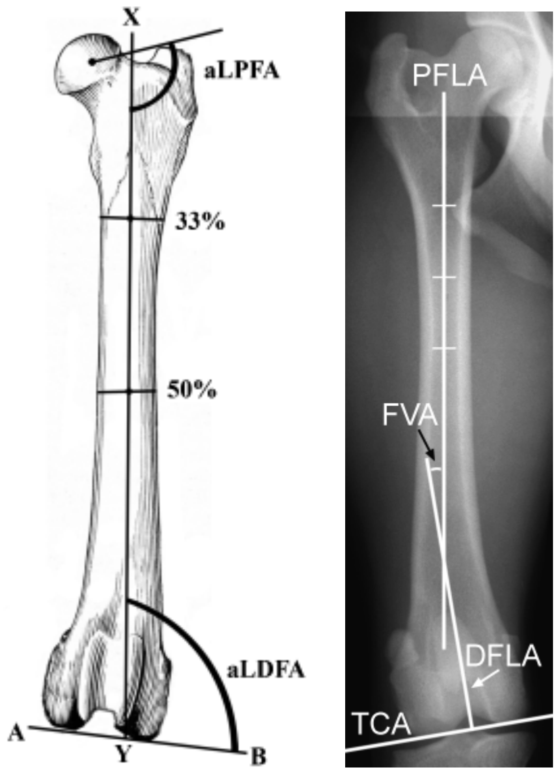

Fig. 1: PFLA and TCA outlined in cranio-caudal drawn and radiographic images. aLPFA and aLDFA are measured in the image on the left, while FVA is found in the image on the right. (Images taken from Tomlison et al., 2007; and Dudley et al., 2006).

However, literature highlighted some limitations for computing precise measurements through radiographs that could prevent an accurate assessment and quantification of bone deformities .[8,13,14] Among the well-known limits of the biplanar radiographic imaging techniques we firstly mention the fact that standard radiography is often technically challenging, time-consuming and operator dependent. [8]

In fact, one of the most relevant constraints of a radiographic evaluation is due to its sensitivity to the rotational positioning of long bones, such as the femur, induced by their natural procurvatum.[15] Some authors describe that excessive femoral external rotation during the positioning of the patient increases the apparent varus deformity. Alternatively, excessive femoral internal rotation increases the apparent valgus deformity.[6,15]

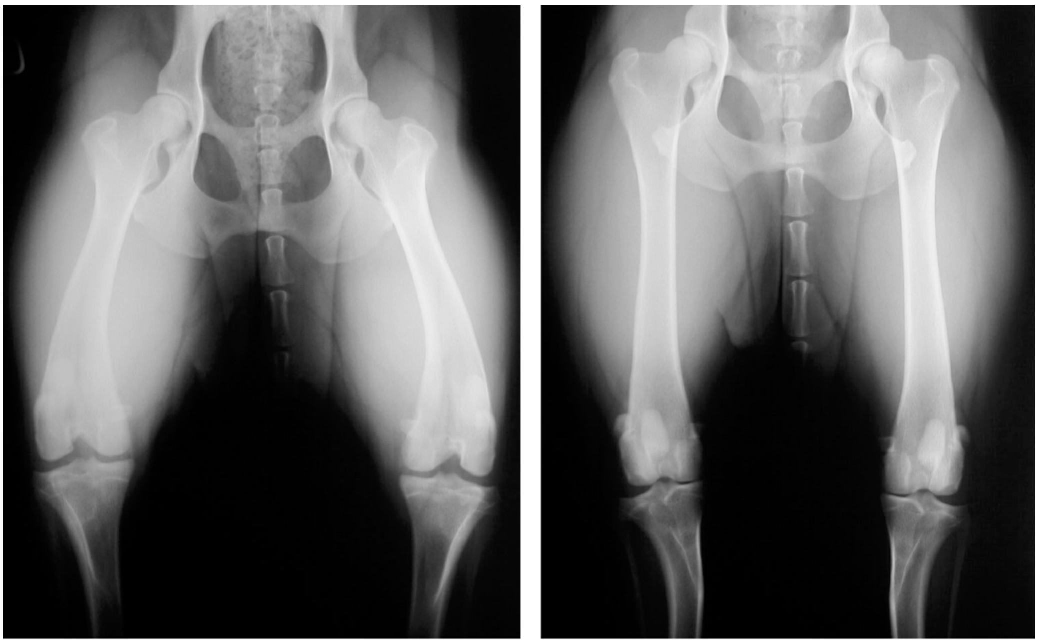

Fig. 2: image of the same dog (Golden retriever of 3 years old) obtained with different radiographic positioning. On the left, femurs were not hyperextended and intra-rotated, thus a varus deformity is present. On the right, a standard ventro-dorsal projection shows no frontal deformity.

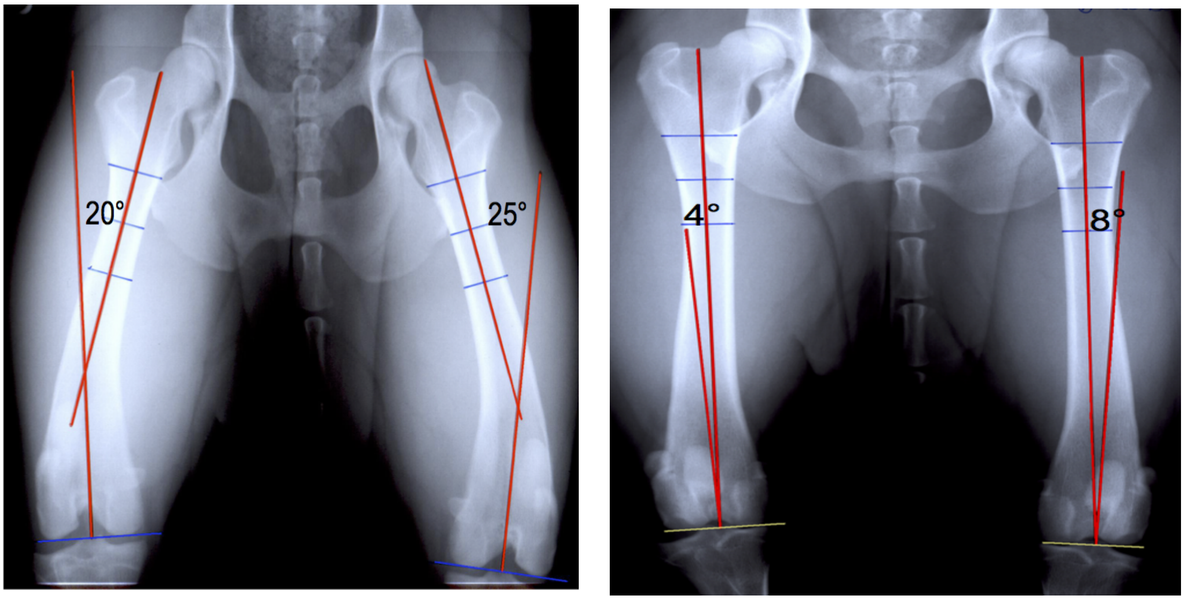

Fig. 3: FVA measurement in the same patient (Rottweiler 2 years old) performed in x-ray films obtained through an incorrect positioning (left) and a correct projection (right).

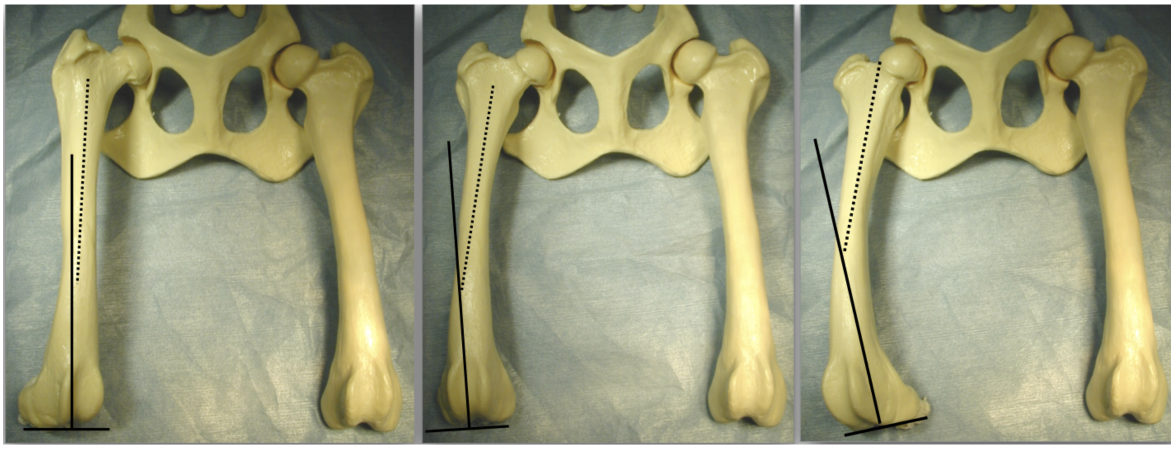

Fig. 4: a bone model was used to show the changes in PFLA, DFLA and TCA axes when internal or external torsion of the femur are applied. The images in both sides evidence that excessive internal torsion cause the decreasing of the FVA, while an excessive external torsion determines a false increase of the FVA. In the central image is represented a correct positioning of the femoral trochlea.

Therefore, it's mandatory to correctly position the patient in the radiographic table to achieve a radiographic film in which the orthopaedic surgeon could get reliable measurements related to the bone morphology. General indications for the patient positing recommend that the patient must be in dorsal decumbency, with a standard or sitting position (more advisable), with the femur parallel to the radiographic cassette and the x-beam perpendicular to the femur, hip extended as well as pelvic limbs internally rotated.[6-8]

Taking into account the complexity of the execution of a correct radiographic study of the hip, especially with patients affected by hip dysplasia or arthritis, some authors suggested the use of the fluoroscopy to improve the view of the femur as well as decrease the variability of the perceived varus angle related to the patient positioning. [8]

Fig. 5: radiographic positioning of dogs performed using a standard ventro-dorsal approach (left image) and a sitting position (right picture). The second positioning is preferred as the femur is more parallel to the radiographic cassette.

Furthermore, specific criteria for the determination through radiograph of an appropriate femoral orientation have been proposed to overcome possible bias in diagnostic evaluation.[6-8]

Currently, accepted guidelines for patient positioning require a single radiographic study for each femur, with neutral hip rotation, as well as the patella firmly centred on the trocheal groove.[2-4,15] Moreover, to obtain a true sagittal femoral projection, nearly 50 % of the lesser trochanter has to be visible; the proximal femoral nutrient foramen is occasionally observed within the diaphysis and fabellae have to be cortically bisected.[8]

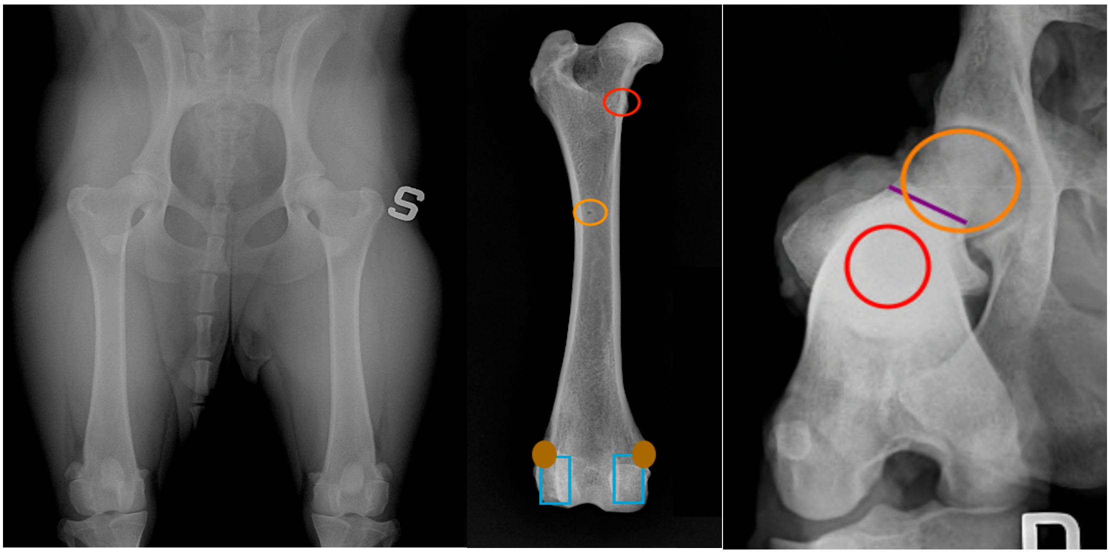

Fig. 6: Radiographic films of correctly positioned canine pelvis, cranio-caudal and axial femur positioning. Anatomical landmarks to check in the cranio-caudal projection from proximal to distal direction are: the lesser trochanter (partially visible), end-on view of the nutrient foramen, fabellae bisected and vertical walls of intercondylar notch must be parallel. In the axial view the intramedullary canal has to be visible and femoral head and neck observable.

As reported by several authors, these radiographic guidelines are necessary to improve the quality of diagnostic evaluation for deformities and to assess clinical cases with a standardized protocol as well.[6-10] However, some of these recommendations have been recently questioned.[16]; for instance the reliability of the bisection of the fabellae for the evaluation of a correct positioning of a femoral cranio-caudal projection was discussed by Aiken et al. and defined as an unreliable parameter.[16]

The second limitation of a radiographic study is ascribable to its biplanar properties that may not be precise enough to detect multiapical deformities, defined as multiple bone deformations in different planes. [17]

Specifically, the femur has a complex three-dimensional (3D) configuration characterized by the presence of physiological procurvatum (sagittal deformity) and varus (frontal deformity).

Therefore, even when orthogonal radiographic projections are satisfactory, they merely provide two-dimensional indications of limb anatomy. Indeed, two-dimensional assessment conceals rotations along the longitudinal axis of the bone and, as a result, could induce a misinterpretation of the corrective parameters. [15,18]

The third relevant shortcoming is the absence of a universal definition for the same computational feature.[19,20] In the atlas of "clinical goniometry and radiographic measurement proposed by Petazzoni, we can find the substance of this criticism. In fact, in this book several methods to find the same axis or angle are shown.[20] As a result, the variability and the inaccuracy of femoral measurements may rise.

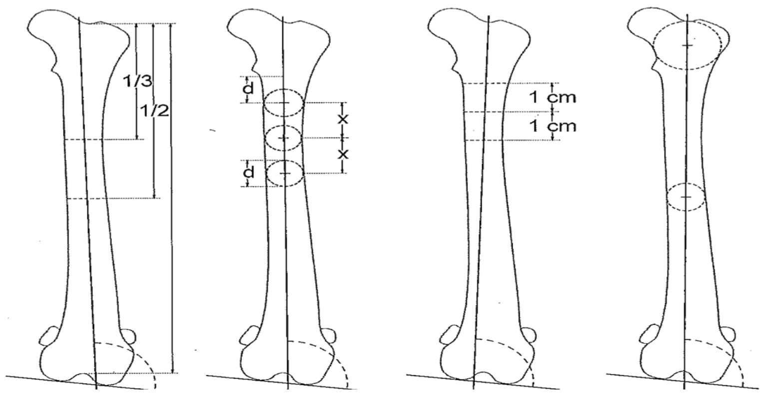

Fig. 7: image showing four different methods for drawing the PFLA. (Image taken from Miles JE et al., 2015).

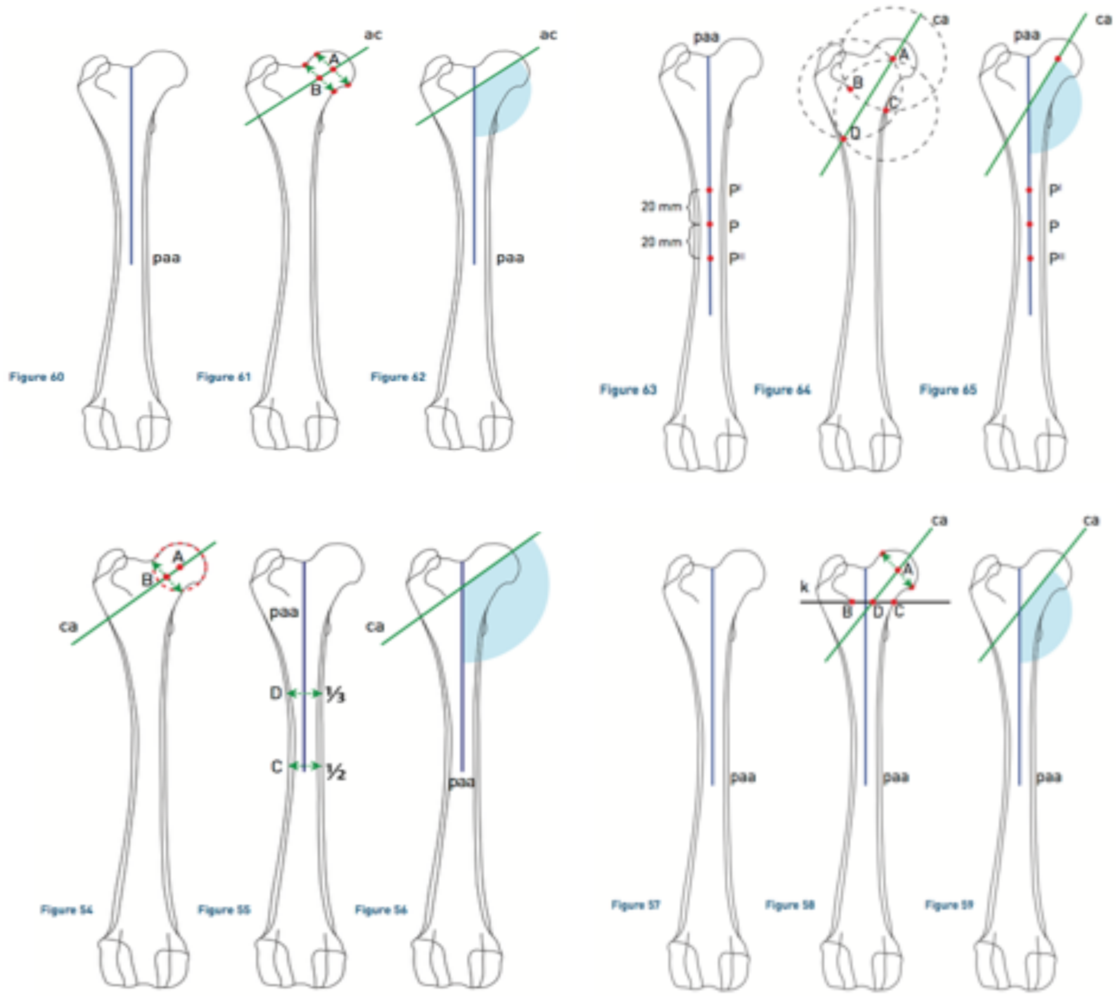

Fig. 8: pictures describing four methodologies reported in the literature to calculate the FNA. (Petazzoni M and Jaerger G, 2008).

Another discussion topic relative to the radiographic measurements, proposed by veterinary literature, is that many of the angles suggested were calculated in specific breeds, most of all medium to large size dogs. On one hand, these measurements exemplify reliable reference parameters for surgeons but their pertinence to only few breeds could represent, in the author point of view, a significant constraint. In fact, medial patellar luxation (MPL) is a pathology that reportedly affects several small and toy breed dogs.[21-23] Since that, quite often this frequent orthopaedic disease is present bilaterally, and so surgeons cannot rely on reference parameters taken from the not affected limb, the general tendency to refer to those parameters is at least questionable, and opens the spot to the following question: could we consider reference angles obtained, for instance, in Labrador retrievers adaptable to breeds such as Pinschers, Dachshunds or Bulldogs, in case of femoral deformity? If we look at the different morphological characteristics of the bone (dolicomorphus versus chondrodystrofic breed) this is may not practicable and encourage future studies approaching this topic.

AUTHOR	SUBJECTS	METHOD	aLDFA (°)	aLPFA (°)	mLDFA (°)	mLPFA (°)
Dudley et al. 2006	18 femurs 20-30 Kg	Cranio-caudal Radiographs	99.4 ± 2.3	-	-	-
		Radiographs	99.2 ± 3.3	-	-	-
		Computerized Tomography	98.8 ± 3.3	-	-	-
		Anatomic Preparation	97.4 ± 3.9	-	-	-
Swiderski et al. 2008	10 femurs	Radiographs	95.8 ± 1.0	-	-	-
		Anatomic Specimen	95.2 ± 2.1	-	-	-
Tomlinson et al. 2007	100 Golden Retriever femurs	Radiographs	97 ± 2.8	98 ± 5.7	100 ± 2.3	95 ± 5.2
	100 Labrador Retriever femurs		97 ± 3.2	103 ± 6.4	100 ± 2.6	100 ± 6.0
	100 German Shepherd femurs		94 ± 3.3	101 ± 5.0	97 ± 3.1	97 ± 4.5
	100 Rottweiler femurs		98 ± 3.5	96 ± 5.3	100 ± 2.7	93 ± 4.7
Dismukes et al. 2008	101 Femurs	Cadaveric radiographs	-	-	98.6 ± 2.5	103.7 ± 5.4

Tab. 1: Reference table for aLDFA measurement. Author of the study, subject and breed as well as method used are outlined. (Petazzoni M and Jaerger G, 2008).

Breeds	Number of Subjects	Number of femurs evaluated	Mean femoral neck angle (°) +/- standard deviation
Anatolian Shepherd	10	20	**138.60 ± 1.29**
Dobermann	20	40	**127.04 ± 1.07**
Golden Retriever	10	20	**129.25 ± 2.75**
Labrador Retriever	42	84	**131.61 ± 0.76**
German Shepherd Dog	88	166	**129.9 ± 0.46**
Pointer	26	52	**129.84 ± 0.98**
Irish Setter	12	24	**128.91 ± 1.51**

Tab. 2: breed reference table for FNA measurements (Petazzoni M and Jaerger G, 2008).

The last criticism about the radiographic study is related to the prolonged anaesthesia time for the patient and the protracted exposition to the x-rays for the operators.

Recent advancements within the veterinary imaging field, such as computed tomography (CT),[24-29] and magnetic resonance (MRI),[30,31] with the aim of overcome the limitations related to the radiographic study led to a change in diagnostic evaluation of bone deformities establishing their superiority over plain radiographies. The inaccuracy due to femoral malposition has been investigated and statistically quantified using CT and MRI. [15] For instance, a paper from Oaxley et al. (2013) suggests that a CT standardized, repeatable and reproducible protocol is advocated to accurately detect femoral malalignment and, hypothetically, decrease surgical planning errors that a radiographic study is not entirely able to detect.

In general, CT and MRI have been used to assess femoral conformational deformities,[8, 26-29] detect geometry and joint changes mediated by surgical treatment

[24,25] as well as quantify and monitor joint disease for early diagnosis of hip dysplasia.[28]

The coming of these technologies has several benefits. First of all, most of the time the acquisition process of data is faster that a radiographic exam. Secondly, the malpositioning issue can be efficiently bypassed as the three-dimensional handling of the bone template allows the operator to entirely visualize the bone model without any problems concerning the orientation and visualization of it. Lastly, an underrated but crucial point is the avoidance of any x-ray exposition for the operator. [8,9]

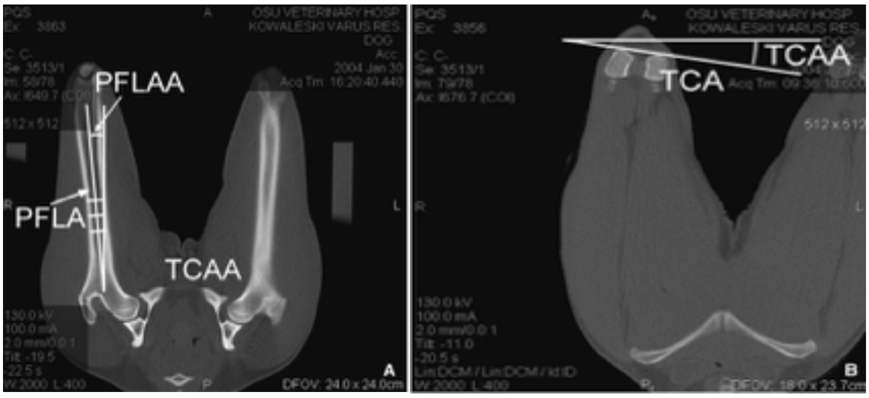

Fig. 9: tomographic measurement of aLDFA. TCA and PFLA drawing are shown. (Images taken from Dudley et al., 2006).

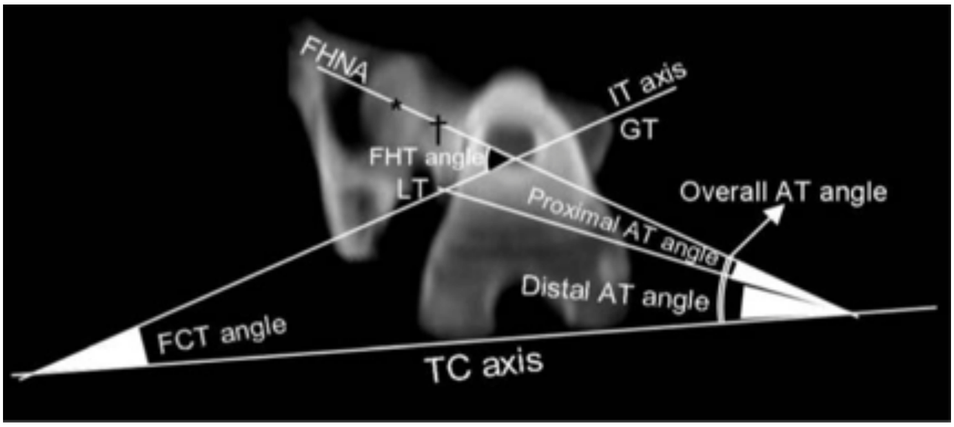

Fig. 10: tomographic computation of FTA. TCA and FHNA are firstly detected. The torsion angle (AT angle) is the result of the sum of the proximal and distal AT angle. (Image taken from Mostafa et al., 2012).

Although difficulty related to the positioning of the patient can be effectively reduced using CT and MRI, these techniques allow only to improve femoral orientation and visualization of specific anatomic landmarks, since the measurement of femoral angles and axes is still achieved with two-dimensional imaging (2D). Thus, the preferred assessment of femoral morphometric parameters is still debated and unclear.[7,8,27]

To temper this trend, efforts to develop consistent and standardized imaging protocols contributed to an ever-increasing accuracy for the assessment and quantification of femoral deformities.[15,27]

Human medical research has focused on developing imaging modalities with the purpose of generating precise morphometric analyses of bone surfaces through the reconstruction of 3D geometric models. Reportedly, 3D femoral surface models are constructed with data acquired from bi-planar radiographs,[32,33] CT,[34,35] MRI,[36] and surface meshing software.[37-40]

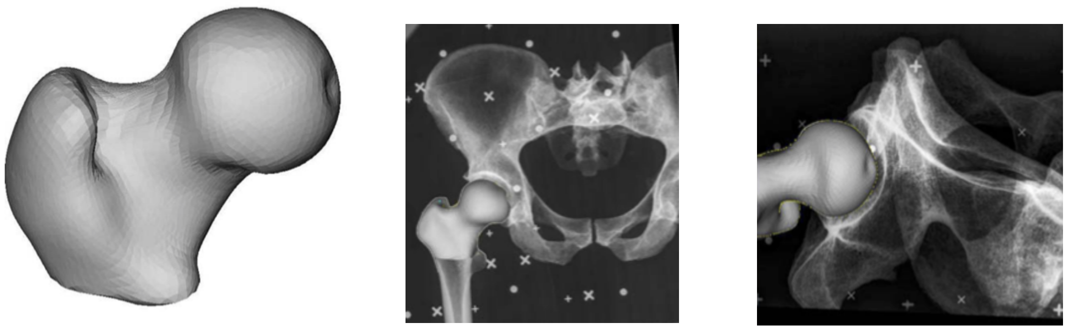

Fig. 11: femur 3D model obtained through calibrated x-rays images. In the central and the right pictures, a perfect superimposition between the reconstructed bone model and the projections of the femur in the x-rays is observed.

(Images taken from Zheng G et al., 2009).

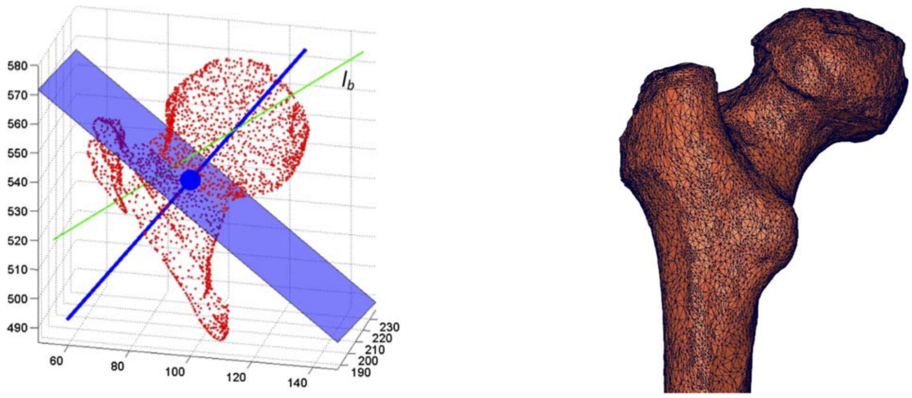

Fig. 12: in the left picture, the FHNA is drawn with an orientation that is perpendicular to the normal (blue plain). On the right, a 3D reconstructed model of pathological femur is shown. (Pictures presented in Cerveri P et al., 2010)

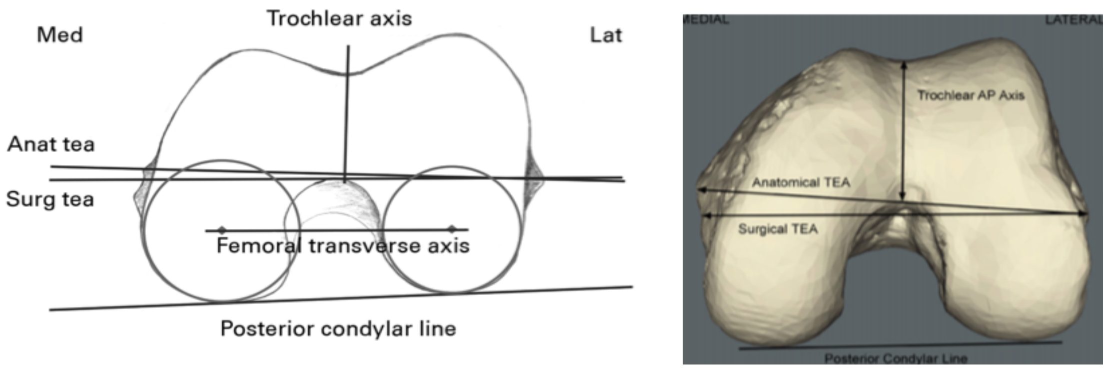

Fig. 13: diagram showing the axis drawn to study the rotational alignment of the distal femur (left). Anatomic and surgical tea represent the trans-epicondylar axes. The right picture is a translated image on a reconstructed CT-scan. (From Victor J et al., 2009).

Although, 3D models are a well-established diagnostic tool for human medicine, in veterinary medicine they represent a novel topic that is progressively growing. In fact, computation on 3D geometric models has been recently introduced.[41-50] as source of 3D prototypes modelling that offer reliable data for investigating several areas of interest within the veterinary orthopaedic field such as canine hip joint osteoarthritic degeneration,[41,42] designing of bone templates,[43-45] analysis of the femoral surface,[46] as well as for in-vivo kinematics research.[47,48] Reportedly, 3D geometrical models have been, also, used for volume measurements and evaluation of joint congruency,[49] as well as experimental trials in which deformed bones were rotated at a desired orientation, creating cross-sectional views from any position.[50]

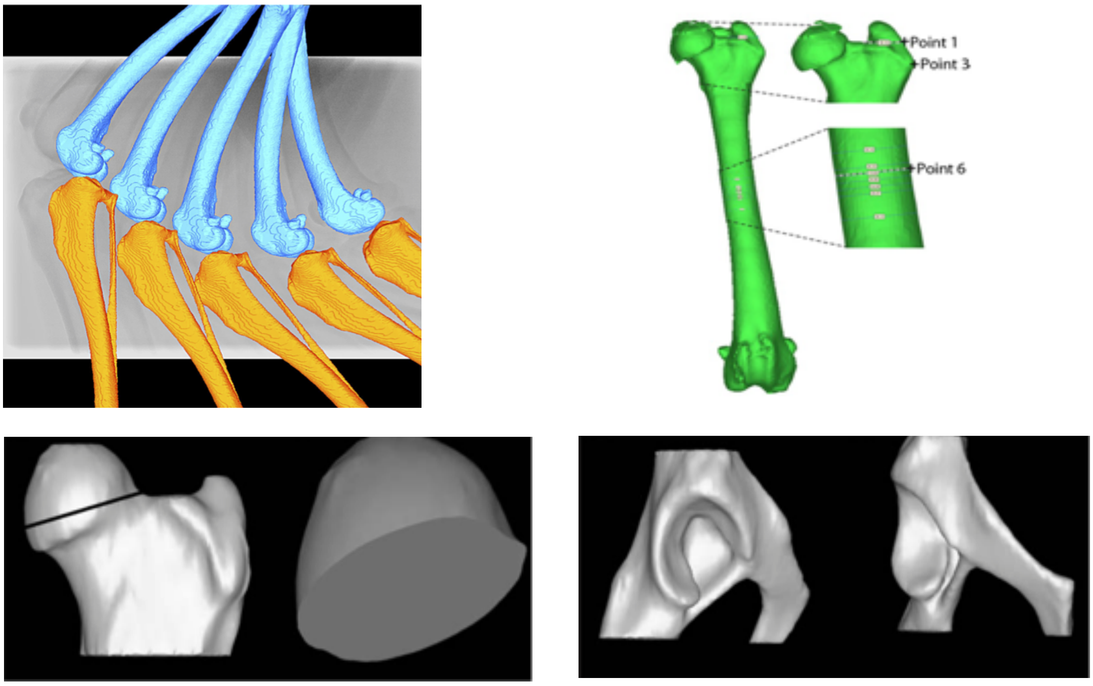

Fig. 14: examples of 3D model femur analysis described in veterinary literature. An in-vivo 3D kinematic stifle study (A: Kim S et al., 2014); a surface femoral evaluation (B: Zamprogno H et al.; 2014) and a coxo-femoral joint isolation for the investigation of joint laxity and degenerative diseases in the canine hip (C: D'Amico L et al.; 2011)

So, even if in the recent past an increased emphasis on 3D evaluation is gradually rising, little if any attention was devoted to 3D measurements, thus the assessment of canine femoral axes and angles is still not reported in veterinary medicine. As a matter of fact, currently available canine femoral measurements related to frontal, sagittal and transverse deformities have only been computed in bi-planar projections, whether acquired from 2D or 3D imaging models.[7,8,12,13,21]

A recent example of the cited studies is the recent paper of Yasukawa et al. (2016), whose objective was that the evaluation of femoral deformities through CT scan-reconstructed 3D images. Nevertheless, Yasukawa et al provide femoral measurements calculated in CT frontal or lateral view, thus in bi-planar projections without reporting 3D measurements.

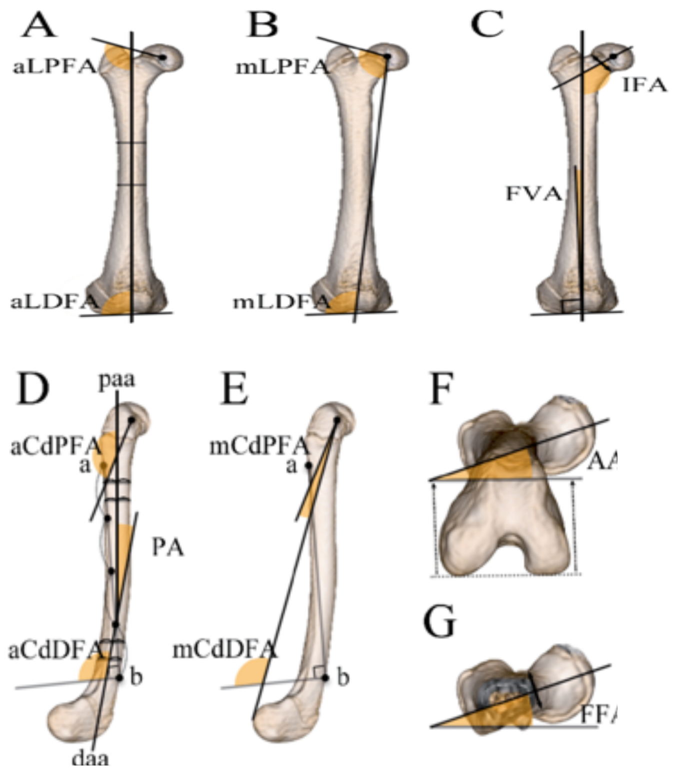

Fig. 15: CT pictures of Toy Poodles femurs in which femoral angles were computed in biplanar images. Measurement of anatomical/mechanical, proximal/distal LFA (A, B); FVA (C); anatomical/mechanical, proximal/distal CdFA as well as FTA (F) are shown. (Yasukawa et al.; 2016).

As concerns human medicine, three-dimensional organic models have been proven to be very advantageous for both preoperative planning and computer-aided surgeries .[6,14,]

In fact, human limb deformities are generally assessed through geometrical prototypes acquired from CT, 3D scanners and MRI computed tomography.[51-53]

The acceptance of computed-based technology in human orthopaedics has strongly encouraged the use of 3D surface models of patient organs, to provide image guidance and enhanced visualization in surgical planning. Currently available CT scans and MRI, aided by up-to-date image-enhancing tools including segmentation and surface meshing software, support an accurate and realistic reconstruction of 3D organic models. The integrated computed approach to diagnosis and planning permits an acceptable estimation of the clinical parameters essential for the most appropriate surgical strategy development, and correct follow up evaluation.[51-53]

In veterinary, the use of the cited diagnostic teqniques as a source of three-dimensional reconstruction models is gradually increasing.[54-56] A more detailed preoperative planning does not only represent the only benefit of working with mesh and geometrical models, but also their pertinence to the surgical field.

Corrective osteotomies are performed to treat limb deformity with the aim of re-establishing physiological alignment, limiting articular damages and chronic pain, and decreasing osteoarthritis evolution in the medium and long term.[17,53,56] Thus, a detailed preoperative evaluation is mandatory to achieve a satisfactory surgical outcome.

Starting from the definition, it is conceivable to consider that a bone reconstruction that contemplates all three axes in the space could be very useful to surgeons dealing with diagnostic evaluation of long bones affected, for instance, by physiological bone deformity such as natural procurvatum (femur and radius), or complex deformity corrections (uniapical oblique and biapical non-compensated deformities).[17,54]

In this sense, the concept of computer-aided surgeries is progressively growing in veterinary orthopaedics. In fact, some papers, recently, reported the design of customized intraoperative surgical devices obtained by 3D organic models. These saw guides are extremely useful to select accurately the osteotomy corrective point on bone surfaces and therefore precisely performing an accurate wedge osteotomy in the planned location-Cora and through the appropriate planes of an angular deformity.[55,56]

REFERENCES

1. Piermattei DL, Flo GL: The stifle joint, in Piermattei DL, Flo GL (eds): *Brinker, Piermattei & Flo's Handbook of Small Animal Orthopaedics and Fracture Repair*. Philadelphia, PA, Saunders, 2015, pp 516–580

2. Kowaleski MP, Boudrieau RJ, Pozzi A: Stifle joint in Tobias K and Johnston S (eds): *Veterinary surgery small animal*. St. Louis, MO, Elsevier, 2012 pp 906-998

3. Hauptman J, Cardinet GH, Morgan JP, et al: Angle of inclination and anteroversion in hip dysplasia in the dog. *Am J Vet Res* 1985; 46:2033-2036

4. Gibbons SE, Macias C, Tonzing MA, et al: Patellar luxation in 70 large breed dogs. *J Small Anim Pract* 2006;47:3-9

5. Johnson AL, Broaddus KD, Hauptman JG, et al: Vertical patellar position in large-breed dogs with clinically normal stifles and large-breed dogs with medial patellar luxation. *Vet Surg* 2006;35:78-81

6. Palmer RH, Ikuta CL, Cadmus JM: Comparison of femoral angulation measurement between radiographs and anatomic specimens across a broad range of varus conformations. *Vet Surg* 2011;40:1023-1028

7. Swiderski JK, Radecki SV, Park RD, et al: Comparison of radiographic and anatomic femoral varus angle measurements in normal dogs. *Vet Surg* 2008;37:43-48

8. Dudley RM, Kowaleski MP, Drost WT, et al: Radiographic and computed tomographic determination of femoral varus and torsion in the dog. *Vet Radiol Ultrasound* 2006;47:546-552

9. Mostafa AA, Griffon DJ, Thomas MW, et al: Proximodistal alignment of the canine patella: radiographic evaluation and association with medial and lateral patellar luxation. *Vet Surg* 2008;31:201-211

10. Bardet JF, Rudy RL, Hohn RB: Measurement of femoral torsion in dogs using a biplanar method. *Vet Surg* 1983;12:1-6

11. Montavon PM, Hohn RB, Olmestead ML, et al: inclination and anteroversion angles of the femoral head and neck in the dog evaluation of a standard method of measurement. *Vet Surg* 1985;14:272-282

12. Tomlison J, Fox D, Cook JL, et al: Measurement of femoral angles in four dogs breeds. *Vet Surg* 2007;36:593-598

13. Jackson GM, Wendelburg KL: Evaluation of the effect of distal femoral elevation on radiographic measurement of the anatomic lateral distal femoral angle. *Vet Surg* 2012;41:994–1001

14. Dueland RT, Adams WM, Fialkowski JP, et al: Effect of pubic symphysiodesis in dysplastic puppies. *Vet Surg 2001*;30:201-217

15. Oxley B, Gemmill TJ, Pink J, et al: Precision of a novel computed tomographic method for quantification of femoral varus in dogs and an assessment of the effect of femoral malpositioning. *Vet Surg* 2013;42:751-758

16. Aiken M, Barnes D: Are the fabellae bisected by the femoral cortices in a true craniocaudal pelvic limb radiograph? *J Small Anim Pract* 2014;55:465–470

17. Paley D: Principles of Deformity correction. Berlin. Germany, Springer-Verlag, 2003

18. Towle HA, Griffon DJ, Thomas MW, et al: Pre-and postoperative radiographic and computed tomographic evaluation of dogs with medial patellar luxation. *Vet Surg* 2005;34:265-272

19. Miles J, Mortensen M, Svalastoga E, et al: A comparison of anatomical lateral distal femoral angles obtained with four femoral axis methods in canine femora. *Vet Comp Orthop Traumatol* 2015;3:193-198

20. Petazzoni M: Radiographic measurements of the femur in Petazzoni M and Jaerger GH (eds): *Atlas of clinical goniometry and radiographic measurements of the canine pelvic limb*. Duluth, GA, Merial, 2008, pp 34-54

21. Yasukawa S, Edamura K, Tanegashima K, et al: Evaluation of bone deformities of the femur, tibia, and patella in Toy Poodles with medial patellar luxation using computed tomography. *Vet Comp Orthop Traumatol* 2016; 29: 29–38

22. O'Neil DG, Meeson RL, Sheridan A, et al.: The epidemiology of patellar luxation in dogs attending primary-care veterinary practices in England. *Canine Genetics and Epidemiology* 2016; 3:4

23. Alam MR, Lee JI, Kang HS, et al.: Frequency and distribution of patellar luxation in dogs - 134 cases (2000 to 2005). *Vet Comp Orthopaed*. 2007;20(1):59–64

24. Sarilier M, Yildrim IG, Ocal MK: Effect of triple pelvic osteotomy on the proximal femoral geometry in dysplastic dogs. *Res Vet Sci* 2012;92:142-146

25. Fujiki M, Misumi K, Sakamoto H: Laxity of canine hip joint in two positions with computed tomography. *J Ver Med Sci* 2004;66:1003-1006

26. Ginja MM, Gonzalo-Orden JM, Jesus SS, et al: Measurement of the femoral neck anteversion angle in the dog using computed tomography. *Vet J* 2007;174:378-383

27. Barnes DM, Anderson AA, Frost C, et al: Repeatability and reproducibility of measurements of femoral and tibial alignment using a computed tomography multiplanar reconstructions. *Vet Surg* 2015;44:85-93

28. Palierne S, Asimus E, Mathon D, et al: Geometric analysis of the proximal femur in a diverse sample of dogs. *Res Vet Sci* 2006;80:243–252

29. Lopez MJ, Davis KM, Jeffrey-Borger SL, et al: Interobserver repeatibility of measurements on computed tomography images of lax canine hip joints from youth to maturity. *Vet Surg* 2009;38:920-926

30. Kaiser S, Cornely D, Golder W, et al: The correlation of canine patellar luxation and the anteversion angle as measured using magnetic resonance images. *Vet Radiol Ultrasound* 2001;42:113-118

31. Ginja MM, Ferreira AJ, Jesus SS, et al: Comparison of clinical, radiographic, computed tomographic, and magnetic resonance imaging methods for early prediction of canine hip laxity and dysplasia. *Vet Radiol Ultrasound* 2009;50:135-143

32. Gamage P, Xie SQ, Delmas P, et al: diagnostic radiograph based 3D bone reconstruction framework: application to the femur. *Comput Med Imag Grap* 2011; 35:427-437

33. Koh K, Kim YH, Kim K, et al: Reconstruction of patient-specific femurs using X-ray and sparse CT images. *Comput Biol Med* 2011;41:421-426

34. Otomaru I, Nakamoto M, Kagiyama Y, et al: Automated preoperative planning of femoral stem in total hip arthoplasty from 3D CT data: atlas-based approach and comparative study. *Med Image Anal* 2012;16:415-426

35. Metzler P, Geiger EJ, Alcon A, et al: Three-dimensional virtual surgery accuracy for free fibula mandibular reconstruction: planned versus actual results. *J Oral Maxillofac Surg* 2014;72:2601-2612

36. Zhu Z, Li G: Construction of 3D human distal femoral surface models using a 3D statistical deformable models. *J Biomech* 2011;44:2362–2368

37. Cerveri P, Marchente M, Bartels W, et al: Automated method for computing the morphological and clinical parameters of the proximal femur using heuristic modeling techniques. *Ann Biomed Eng* 2010;38:1752-1766

38. Kang Y, Engelke K, Fuchs C, et al: An anatomic coordinate system of the femoral neck for highly reproducible BMD measurements using 3D QCT. *Comput Med Imag Grap* 2005;29:533-541

39. Victor J: Rotational alignment of the distal femur: a literature review. *Orthop Traumatol Surg Res* 2009;95:365-372

40. Victor J, Van Doninck D, Labey L, et al: A common reference frame for describing rotation of the distal femur. A CT-BASED kinematic study using cadavers. *Bone Joint J* 2009;91-B:683-690

41. Lopez MJ, Lewis BP, Swaab ME, et al: Measurements obtained by use of computed tomography and radiography and scores of cartilage microdamage in hip joints with moderate to severe joint laxity of adult dogs. *Am J Vet Res* 2008;69:362-370

42. Andronescu A, Kelly L, Kearney MT, et al: Associations between early radiographic and computed tomographic measures and canine hip joint osteoarthritis at maturity. *Am J Vet Res* 2015;76:19-27

43. Savio G, Baroni T, Concheri G, et al: Mesh processing for morphological and clinical parameters computation in dog femur. *Research in Interactive Design* (Vol. 4) Springer 2016; 302-307

44. Wang C, Wang J, Zhang Y, et al: A canine model of femoral head osteonecrosis induced by an ethanol injection n navigated by a novel template. *Int J Med Sci* 2013;10:1451-1458

45. Fitzwater KL, Marcellin-Little DJ, Harrysson OL, et al: Evaluation of the effect of computed tomography scan protocols and freeform fabrications methods on bone biomodel accuracy. *Am J Vet Res* 2011;72:1178-1185

46. Zamprogno H, Nelson N, Schaeffer DJ, et al: Three Dimensional Morphologic Analysis of the Lateral Surface of the Canine Femur. *Vet surg* 2014;9999:1-7

47. Kim SE, Jones SC, Lewis DD, et al: In-vivo three-dimensional knee kinematics during daily activities in dogs. *J Orthop Res* 2015;33:1603–1610

48. Jones SC, Kim SE, Banks SA, et al: Accuracy of noninvasive, single-plane fluoroscopic analysis for measurement of three-dimensional femorotibial joint poses in dogs. *Am J Vet Res* 2014;75:477–485

49. D'Amico LL, Xie L, Abell LK, et al: Relationship of hip joint volume ratios with degrees of joint laxity and degenerative disease from youth to maturity in a canine population predisposed to hip joint osteoarthritis. *Am J Vet Res* 2011;72:376-383

50. Verim O, Tasgetiren S, Er MS, et al: Anatomical evaluation and stress distribution of intact canine femur. *Int J Med Robotics Comput Assist Surg* 2013;9:103–108.

51. Di Angelo L, Di Stefano P: Bilateral symmetry estimation of human face. International Journal on Interactive Design and Manufacturing 2013; 7(4):217-225

52. Lattanzi R, Baruffaldi S, Zannoni C, et al: Specialised CT scan protocols for 3-D pre-operative planning of total hip replacement*. Med Eng Phys* 2004;26:237–245

53. Dobbe J, du Prè KJ, Kloen P, et al: Computer-assisted and patient-specific 3-D planning and evaluation of a single-cut rotational osteotomy for complex long-bone deformity. *Med Biol Eng Comput* 2011;49:1363-1370

54. Dismukes DI, Fox DB, Tomlinson JL, et al: Use of radiographic measures and three-dimensional computed tomographic imaging in surgical correction of an antebrachial deformity in a dog. *J Am Vet Med Assoc* 2008; 232:68–73

55. Crosse KR, Worth AJ: Computer-assisted surgical correction of an antebrachial deformity in a dog. *Vet Comp Orthop Traumatol* 2010;23:354–361

56. Domenech L, Soler C, Soriano J: Development of a customized device for correction of angular deformities of long bones in small animals. A case report. *17th Conference of the European Society of Veterinary Orthopaedics and Traumatology*. October 2-4, 20

CHAPTER 2

AIMS OF THE RESEARCH

The present research was envisioned as a project defined by multiple studies that are strictly correlated each other. The report of the birth, development and practical application to the diagnostic and surgery fields of a novel 3D approach for the computation of femoral measurements was the first aim. Moreover, in the authors' purpose the description of the translational value of the proposed procedure enhanced with its plausible utility to the daily practice of orthopaedic surgeons, represented another focal point.

In this sense, the research started from the validation of the 3D assessment of femoral morphometric parameters. Veterinary literature reports tons of papers describing several methodologies for obtaining femoral measurements through different diagnostic techniques. Furthermore, bibliography presents lot of angles values that are currently adopted and considered as reference parameters for most of the corrective osteotomies. Additionally, in the recent past an increased emphasis on 3D approach grown but little if any attention was devoted to 3D measurements. This trend represented in the authors' mind the gap with the current knowledge and, thus, an area to be deeply investigated. Indeed, to the best of author knowledge, there were no papers documenting the assessment of 3D femoral axes and angles in veterinary medicine, with no 3D protocol described. In addition, currently available canine femoral measurements related to frontal, sagittal and transverse deformities have only been computed in bi-planar projections, whether acquired from 2D or 3D imaging models.

Therefore, starting from the accepted human methods and from the features definition in veterinary literature, we proposed a new approach.

The first study was designed to define a 3D methodology, introducing a consistent and quantitative method for the assessment of femoral morphometric parameters in 3D geometrical models. To validate the proposed approach, accurate geometric data were necessary and, therefore, we opted for meshes obtained by a 3D scanner, instead of CT images. Once the validation of the was stated, our focus was directed towards the evaluation of the precision of the proposed 3D protocol.

The validation of a novel diagnostic test requires verification of the repeatability, defined as the strength of agreement between repeated measurements of the same samples performed from one examiner, and the reproducibility as well, that express the same variance but between a group of observers.

Furthermore, the accuracy of the measurements indicates how close the measurements took with the investigated technique to a true value (gold standard). Therefore, a second project was designed to test the precision of three diagnostic techniques, two largely diffuse (Rx and TC) one recently introduced in veterinary (3D), for the measurement of femoral angles.

The second purpose of this study was the investigation of the potential application of the algorithm implemented in a computer-aided-design (CAD) software, using CT data. Considering that for the first study we worked with 3D scanner data, the main aim at this point of the research was represented by the enhancement of the presented 3D protocol for diagnostic purposes. In the author opinion, changing the source of data was necessary because of the availability of CT and MRI equipment in veterinary practice.

Finally, the last goal of this project was the translation of the application of 3D computation to the surgical field. The current research contemplates the fact that the augmented interest on 3D computation is not only relevant for diagnostic reasons, but also for surgery. Thus, the correlation between the diagnostic utility of the 3D approach and its plausible practice for surgery purposes was the object of the final study. The starting point was suggested by veterinary literature that reports in few papers the development and application of surgical devices used to perform assisted-correction of bone deformities.

These surgical tools are designed through 3D geometrical models and act both as precise intraoperative localizers of osteotomy corrective landmarks and surgical saw guides.

Three-dimensional assessment of a bone conformation may improve the understanding and evaluation of bone deformities and occurring joints malalignment. In this sense, the localization of the CORA as well as the accuracy of the orientation of the osteotomy-cutting plane may be significantly upgraded through a 3D approach.

CHAPTER 3

MESH PROCESSING WITH RHINOCEROS:

A PRESENTATION OF AN ALGORTHIM FOR

THE COMPUTATION OF MORHOMETRIC

PARAMETERS IN THE CANINE FEMUR

This chapter was adapted from: Savio G, Baroni T, Conchieri G, Isola M, Baroni E, Meneghello R, Turchetto M and Filippi S: Mesh processing for morphological and clinical parameters computation in dog femur. *Research in interactive design*; 2016: published.

SUMMARY

Mesh processing is a fast-increasing area of engineering research that adapts concepts from applied mathematics, computer science and engineering to design algorithms for the acquisition, reconstruction, analysis, manipulation as well as transmission of complex 3D models. In the last decades, the popularity of triangle meshes has been grown as irregular triangle meshes have developed into a suitable alternative to more traditional spline surfaces.

A lot of programs were designed and created with the aim of being able to manipulate 3D geometrical models and thus create, for instance, printed prototypes valuable for several fields of interest.

In this chapter, we present a commercially available CAD software (*Rhinoceros*) that we used in the current research as well as a newly developed algorithm that was added to *Rhinoceros* tool to execute the computation of morphological femoral parameters.

MESH PROCESSING

Mesh processing or geometry processing is an imaging technique that employs concepts from applied mathematics, computer science and engineering to design efficient algorithms for the acquisition, reconstruction, analysis, manipulation and transmission of complex 3D models.[1-3]

Geometry processing involves working with a shape, usually in 2D or 3D. The modelling of a shape usually implicates three stages, which are known as its life cycle. At the beginning of the process, a shape can be instantiated through one of three methods: a model, a mathematical representation, or a scan. After that, the shape can be analysed and edited repeatedly in a cycle. This usually involves acquiring different measurements, such as the distances between the points of the shape, the smoothness of the shape. The user can, also, produces substantial transformations of the model through, for instance, deforming or de-noising function. Finally, at the final stage of the process, the shape is finalized and could be ready for 3D printing and used as a physical model.

Mesh processing, usually, involves the use of polygonal meshes. A polygon mesh is a collection of vertices, edges and faces that defines the shape of a polyhedral object in 3D computer graphics and modelling.[4,5] The faces usually consist of triangles (triangle mesh), quadrilaterals, or other simple convex polygons, since this simplifies rendering, but may also be composed of more general concave polygons, or polygons with holes.

Several programs are freely available on the web to manipulate, modify and accurately cut a 3D geometrical model. Among them, we mention: *Meshlab, Rhinoceros, Polyga, VRMesh, Gmsh, Mesh slicer*.

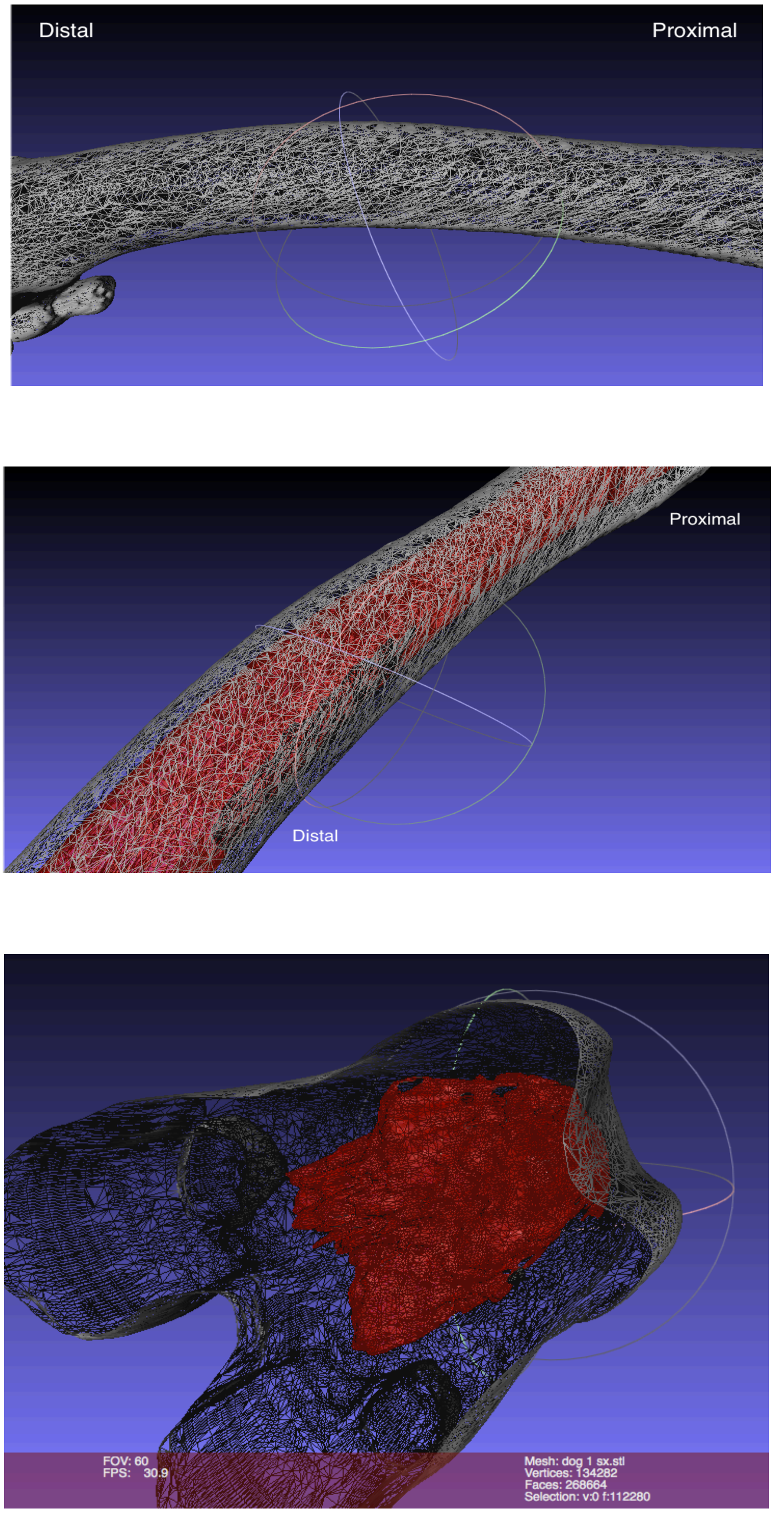

Fig.16: example of a mesh processing with *Meshlab***.** In the image at the top, the triangular shape of the vertices is observable. In the central picture the difference between the internal (highlighted in red) and external meshes is shown. The image at the bottom of the page is a view of the distalfemoral epiphysis with the internal mesh outlined.

OVERVIEW OF RHINOCEROS

For the development of our research we used tools available in *"www.food4rhino.com/project/rp"* developed in Rhinoceros version 5.0 environment.

Rhinoceros is a temporarily free surface modeller and is defined as a library for advanced scientific computation that has a computer-aided design (CAD) software. This application employs the NURBS mathematical model which focuses on producing mathematically precise representation of curves and freeform surfaces in computer graphics (as opposed to polygon mesh-based applications).

This commercial 3D computer graphics is versatile, indeed its application is broadly reported in several and different fields that include architecture, product and industrial design, as well as graphic and multimedia prototyping. It has been, also, used in medical science for surface rendering or analysis.

For our studies, we selected this CAD software for several reasons. First of all, Rhino supports the management of mesh surfaces, for instance mesh visualization, mesh data structure management, geometric center calculation, sphere fitting. Moreover, it allows for the implementation of dedicated procedures for femur analysis. Secondly, Rhinoceros' application architecture is very handy and enables the user to customize the interface and create custom commands and menus. This represents a suitable advantage when a surface analysis of features characterized by a complex structure such as the bones, is needed.

Third benefit to keep in mind is the multiple sources of data available. The user can work with meshes derived from the most popular 3D imaging techniques like TC, MRI and 3D scanner.

This represented a high valuable advantage for our research since we used both 3D scanner and TC data.

Another point to mention is the fact that there are dozens of plug-ins existing that complement and expand *Rhinoceros'* capabilities in specific fields like rendering and animation, architecture, engineering, prototyping, and others.

In our case, we developed in *Rhinoceros* some plugins such as using *IronPython* and *Meta.Numerics* accessible at *"www.meta-numerics.net".*

As regard the compatibility of this CAD software, it supports over 30 CAD file formats for importing and exporting dataset. Among the image files and CAD formats that are natively supported (without use of external plugins), we mention: STL, FBX, IGES, STEP, .3ds and OBJ.

In our study we used STL files that are defined as file formats native to the stereolithography CAD software created by 3D systems. This type of file format is supported by many other software packages; it is widely used for rapid prototyping, 3D printing and computer-aided manufacturing. STL files describe only the surface geometry of a three-dimensional object without any representation of colour, texture or other common CAD model attributes. Specifically, an STL file describes a raw unstructured triangulated surface by the unit normal and vertices (ordered by the right-hand rule) of the triangles using a three-dimensional Cartesian coordinate system.

Finally, another advantage that we pondered using *Rhino,* is its ability to support the 3D printing function. In fact, Rhinoceros 3D relies on some plug-ins that facilitate 3D printing and allows the export of the STL and .OBJ file formats, both of which are supported by numerous 3D printers and 3D printing services.

ALGORITHM

With the aim of computing all the 3D femoral measurements, an algorithm implemented in *Rhinoceros* environment was developed. The algorithm was, also, created with the intention of simplifying as much as possible the computation process, decreasing the user inputs and shortening the computational time as well.

The algorithm is freely available in *IronPython.net* and ready to be used in *Rhinoceros.* After the completion of the download, the file must be saved in the computer memory storage. Afterward, *Rhino* is opened and the file is dragged into it. The new function will appear in the program toolbar like a femur icon entitled "*dog*".

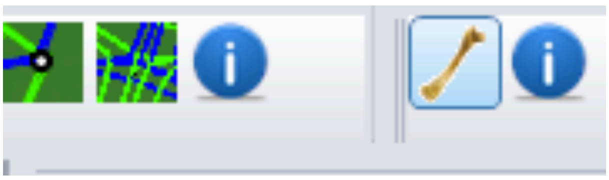

Fig. 17: the femur icon appears in the *Rhinoceros* toolbar (in the upper right corner).

When a femur, saved as a STL file, is imported in *Rhino*, the user must select the femur icon and, secondly, a point onto the femur head. Thirdly, before the starting of the computation, the user must set the segmentation parameters (Fig. 18).

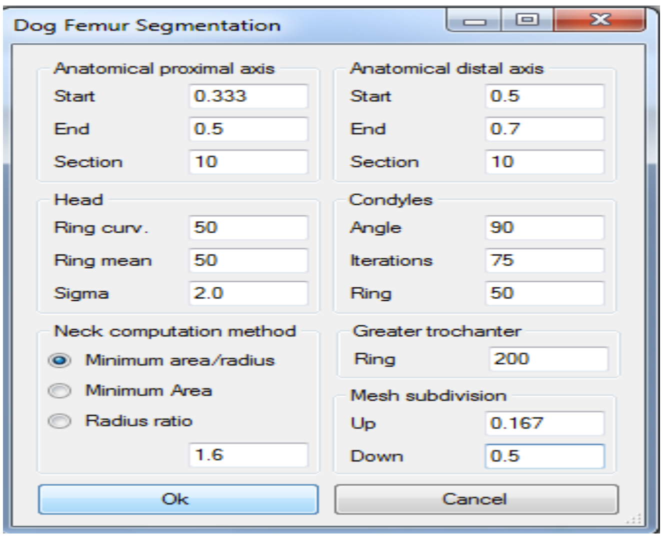

Fig. 18: dog femur segmentation window. For this study, the above values were used for the femoral analysis.

Next, the algorithm starts the analysis of the bone with the following procedure.[6-8]

In the proposed approach, the *proximal femoral long axis* identifies the z-axis of the reference frame. Firstly, the femur is approximately placed lengthwise along the z-axis (Fig. 19 A). This positioning is obtained aligning the principal axis of inertia, having the maximum moment of inertia, along the z-axis. The femur length is measured from the most proximal aspect of the greater trochanter to the most distal point of the lateral femoral condyle along the z-axis (Fig. 19 B). Then the proximal femoral long axis is preliminarily assessed in the portion comprised between one-third and one-half of the femur length, where 10 equally spaced sections, perpendicular to the z-axis are found (Fig. 19 B). The geometric center of each section is calculated and the line (that is the proximal femoral long axis) fitting through the geometric centers is computed (Fig. 19 C). Then the femur is re-oriented aligning the fitting line on the z-axis (Fig. 19 D) and the actual proximal femoral long axis is re-computed repeating the above procedure.

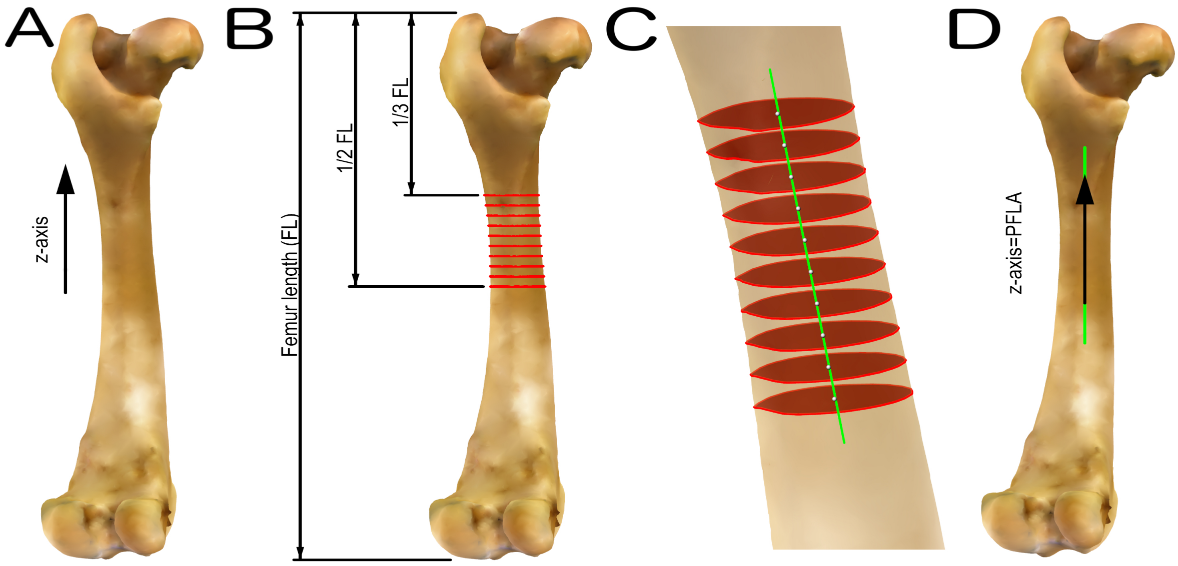

Fig. 19: PFLA computation. Femur is approximately oriented along the z-axis (A). The femoral length is measured along the z-axis and 10 equally spaced sections, perpendicular to the z-axis, in a range of space between one-third and one –half of femoral length, are identified (B). The geometric centers (grey dots) for each section are found and fitted by a line (green line) (C). The femur is re-oriented aligning the fitting line on the z-axis.

The *femoral head* is obtained by fitting a sphere on a specific set of points (red vertices in Fig. 20). The selection of mesh vertices is based on a curvature analysis computed by a local quadratic fitting with 4 coefficients, according to the method proposed by Savio et al.[7] In detail, starting from the selected point on the femoral head, the algorithm implemented finds the upper vertex of the femoral head (vertex having the maximum value of the z-coordinate in the head), searching, in the connected vertices, those with greater z-coordinate and repeating this task on the last vertex found, until no vertex with higher z-coordinate is found. The curvatures of the vertices located inside a neighbourhood of the upper vertex of the head are then computed (in this study a spherical neighbourhood of radius equal to one-fiftieth of the femur length was assumed). A mean value (KM) and a standard deviation (SD) of the curvature of the selected vertices are calculated. Finally, all the vertices mutually connected having a curvature in the range KM±2*SD, are automatically selected and used to calculate the fitting sphere. Consequently, the number of vertices adopted in the spherical fitting is closely related to the number of vertices in the femoral head and depends to the mesh resolution (meshes adopted in this study have approximately 100,000 vertices, but the method was also tested on mesh ranging between 10,000 and 1,000,000 of vertices, without significant differences in the results).

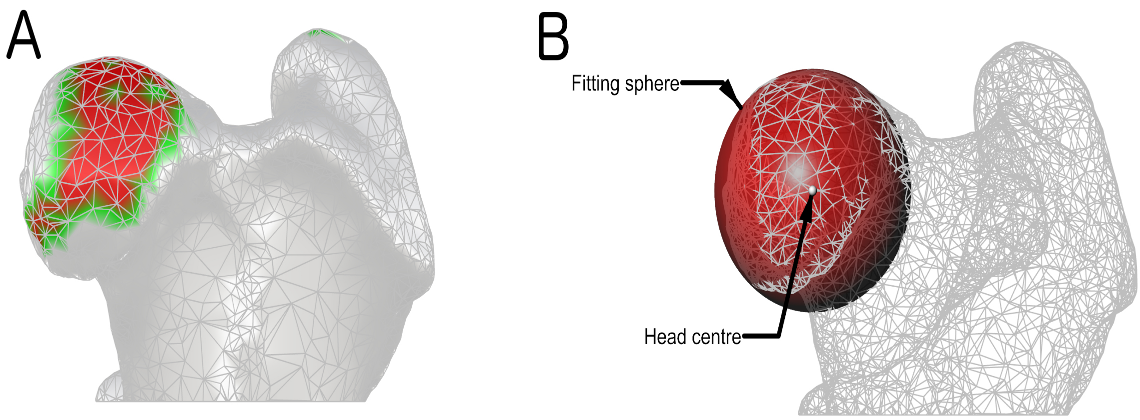

Fig. 20: femoral head analysis. Based on curvature analysis on green and red vertices, a set of vertices are selected in the femoral head (red vertices) (A). Selected vertices are fitted by a sphere that is superimposed to the femoral head (the center of the sphere is the head center) (B).

Femoral head and neck axis is the line connecting the center of the femoral head with the center of the femoral neck, which is computed sectioning the neck by a sphere concentric with the head center (Fig. 21 C, D). More in detail, the center of the neck is assumed as the geometric center of the spherical portion inside the femur. The radius of the spherical portion is selected to minimize the ratio between the area of the spherical portion and the radius itself.[5] Minimizing this ratio was achieved by the bisection method, limiting the iterations to a radius variation less than 5‰ of the head radius (e.g. 0.05 mm of radius variation on 10 mm of head radius). Specific procedures were implemented to avoid local minimum convergence.

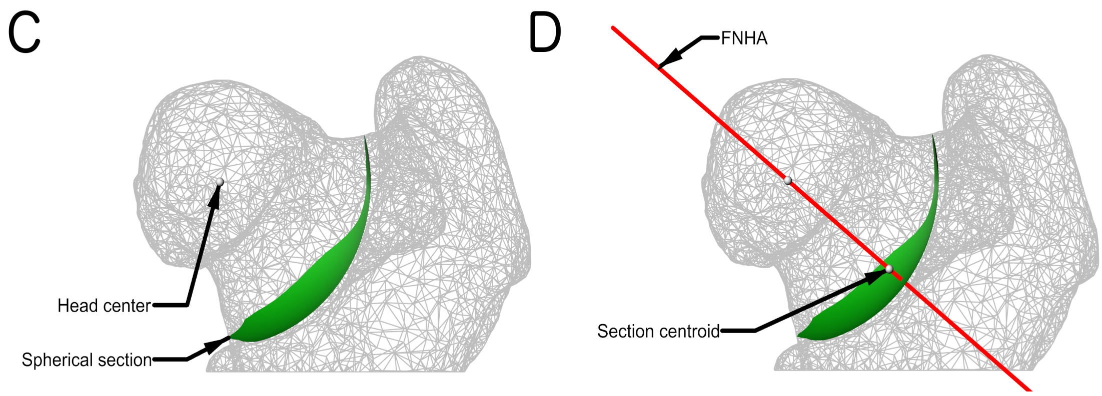

Fig. 21: femoral neck analysis. A sphere having a center into the head center is built and the portion inside the femur neck (a spherical section) is exhibited (C). The FNHA is then obtained, connecting the head center and the geometric center of the spherical section (section centroid) (D).

The *hip joint orientation line* is assumed as the axis connecting the center of the femoral head with the tip of the greater trochanter.[9] This point is computed as the highest of a 6 coefficients quadratic surface that fits the greater trochanter tip. The greater trochanter lies in the opposite side of the femoral head, with respect to the proximal femur long axis. Considering the upper point of the femoral head, the opposite point with respect to the proximal femoral long axis is identified. In a similar way of the upper vertex of the femoral head, starting from the mesh closest point to the opposite point, the greater trochanter tip is identified. Then, all the vertices in a spherical neighborhood of radius 1/200 of the femur length are adopted for the surface fitting.

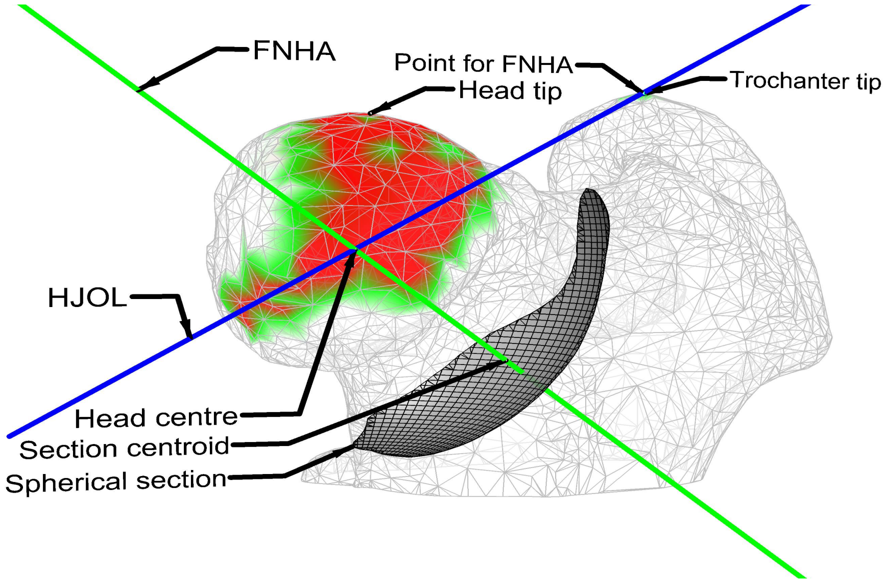

Fig. 22: Analysis of the proximal femoral epiphysis. FNHA is the green line , whereas the blue line represents the HJOL. At the top of the great trochanter an area with green vertices is visible. This landmark is one of two points along which the HJOL passes. The other one is the center of the femoral head. Notice, also, the grey section with its own centroid in the femoral neck.

The analysis of the condyles is necessary to place the *transcondylar* and *mechanical axes*. Locally, the condyles (articular surface) could be approximated by spheres fitting the points of the mesh near to the tibial plateau.[10] Consequently, the transcondylar axis can be defined as a line connecting the contact points between two spheres, simulating the condyles, and a plane, simulating the tibial plateau (Fig. 23).

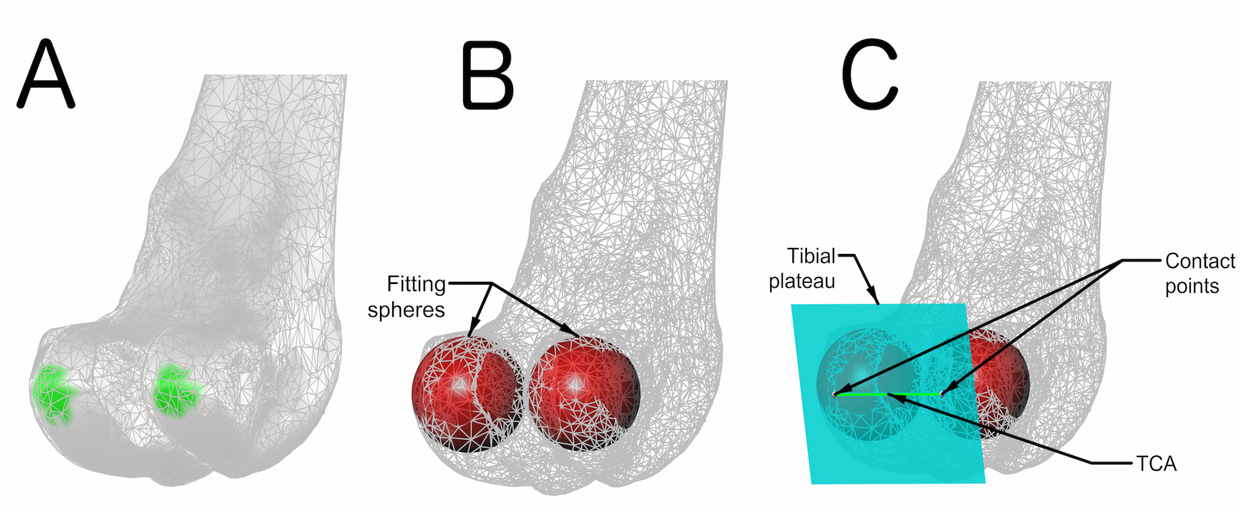

Fig. 23: TCA computation. A set of vertices (green vertices) are selected in each condyle (A). The vertices selected are fitted by two spheres that are superimposed to the condyles (B). A plane representing the tibial plateau is put in contact with the spheres, and the TCA is found as the line connecting the contact point between the tibial plateau and the spheres.

A symmetry plane of the distal portion was computed following the methodologies proposed in literature.[6-8] In depth, the plane is computed through the following summarized methodology:

- A starting mirror plane is defined
- The distal portion is then mirrored referring to the initial mirror plane
- The mirrored plane is copied
- The registration of the mirror portion with the distal portion is carried out moving in the together the copy of the mirror plane
- The final symmetry plane is the mid plane that results from the starting plane and its copy after the recording.

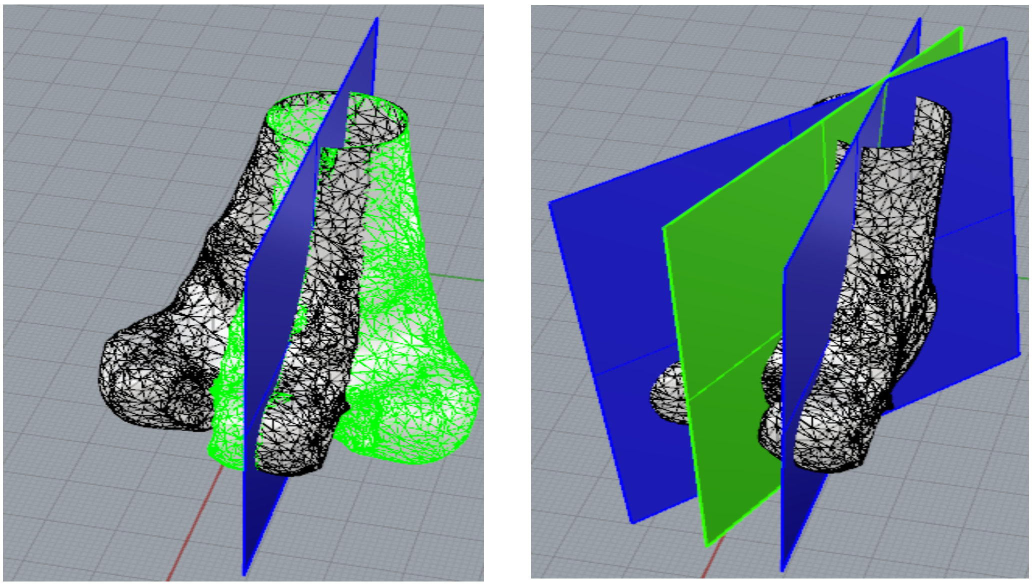

Fig. 24: Computation of the Symmetry plane of the distal femora portion (SPD). A first mirror plane is found (blue plane on the left image); then a mirroring of the blue plane in the distal femoral portion, is performed (green area in the left picture). The starting mirror plane is copied to be, then, translated in the contralateral part. Finally, the symmetry plane (green plane on the right image) is found between the two mirror planes.

On this plane a line is built at an established angle with respect to the proximal femoral long axis (this angle represents the inclination between the normal to the tibial plateau and the proximal femoral long axis). In front of the condyles, a plane perpendicular to the previous line, representing the tibial plateau, is outlined (the direction is established using the position of the geometric center of a portion of the distal femur, that is between the proximal femoral long axis and the condyles).

Then the closest points to this plane are found: one vertex for the medial and one for the lateral condyle. For each vertex, all the vertices in a spherical neighbourhood of radius 1/50 of the femur length are selected for the fitting spheres computation. Transcondylar axis can assume different positions depending on the rotation between femur and tibia.

In our research, an angle of 90° is assumed between the normal to the tibial plateau and the proximal femoral long axis.

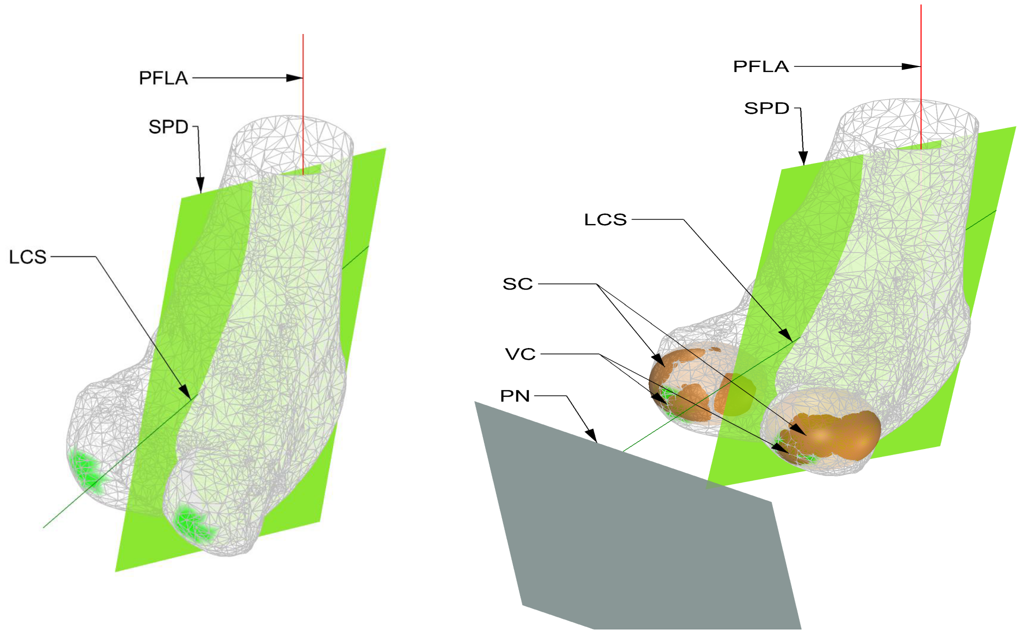

Fig. 25: a line (LCS) into the SPD is drawn and is rotated with respect to the PFLA with an establish angle that is found between the PFLA and the tibial plateau (left picture). A plane with an orientation of 90° in relation to the LCS, is drawn (PN, right image). The vertices (VC) of the femoral condyles are fitted with two spheres (Brown spheres on the right image).

Transcondylar axis (TCA) is traditionally defined as a line tangential to the femoral condyles. However, this axis assumes different positions depending on the rotation between femur and tibia. In the proposed 3D approach, FTA is the connecting line resulting from the contact points between condyles and a plane, the tibial plateau, and not a line.

Specifically, the line that connects the centers of the spheres is defined as the *femoral transverse axis (FT).* A point of minimum distance (PMD) from the Ft with respect to the PFLA is found. Then, a reference plane (RP) passing through the FT and PMD is built. Spheres are consequently sectioned with a plane (PFTA) obtaining two circles

(CC). PFTA is found rotating the RP and is necessary to compute the contact point between the tibial plateau and femoral condyles.

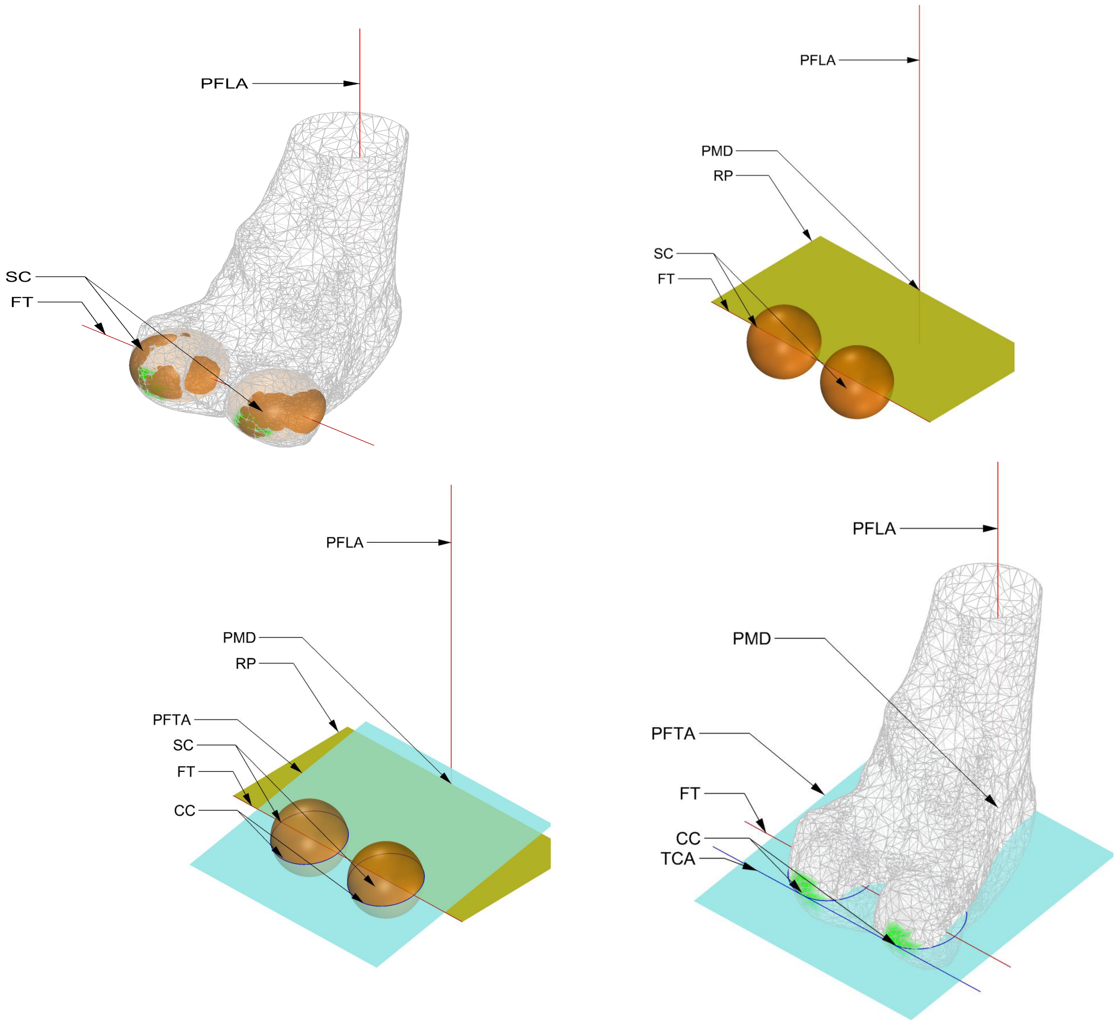

Fig. 26: Femoral transverse axis (FT) and transcondylar axis (TCA) computation. Notice the red line (FT) that passes through the centers of the condylar spheres. A point of minimum distance between FT and PFLA is located (PMD) and a reference plane is then constructed (brown plane, RP). An additional plane (blue plane, PFTA) is obtained through the rotation of RP. PFTA sections the two spheres, obtaining two circles called CC. Moreover, PFTA finds the contact points between the tibial plateau and condyles, hence defining the points to draw the TCA.

The *mechanical axis* is, finally, obtained connecting the center of the head to the midpoint of the transcondylar axis.

Fig. 27: Mechanical axis (MA) computation. To obtain this axis is necessary to find the center of the femoral head as well as the TCA.

Femoral angles (Fig. 28) that could be computed adopting the algorithm developed, are here defined and listed:

- the *anatomic lateral proximal femoral angle* (aLPFA), between the hip joint orientation line and the proximal femoral long axis;
- the *mechanical lateral proximal femoral angle* (mLPFA), between the hip joint orientation line and the mechanical axis;
- the *anatomic lateral distal femoral angle* (aLDFA) between the transcondylar axis and the proximal femoral long axis;

- the *mechanical lateral distal femoral angle* (mLDFA), between the transcondylar axis and the proximal femoral long axis;
- the *femoral neck angle* (FNA), between the femoral head and neck axis and the proximal femoral long axis;
- the *femoral torsion angle* (FTA), between the transcondylar axis and the femoral head and neck axis;
- *the femoral varus angle* (FVA), between a plane perpendicular to the transcondylar axis and the proximal femoral long axis

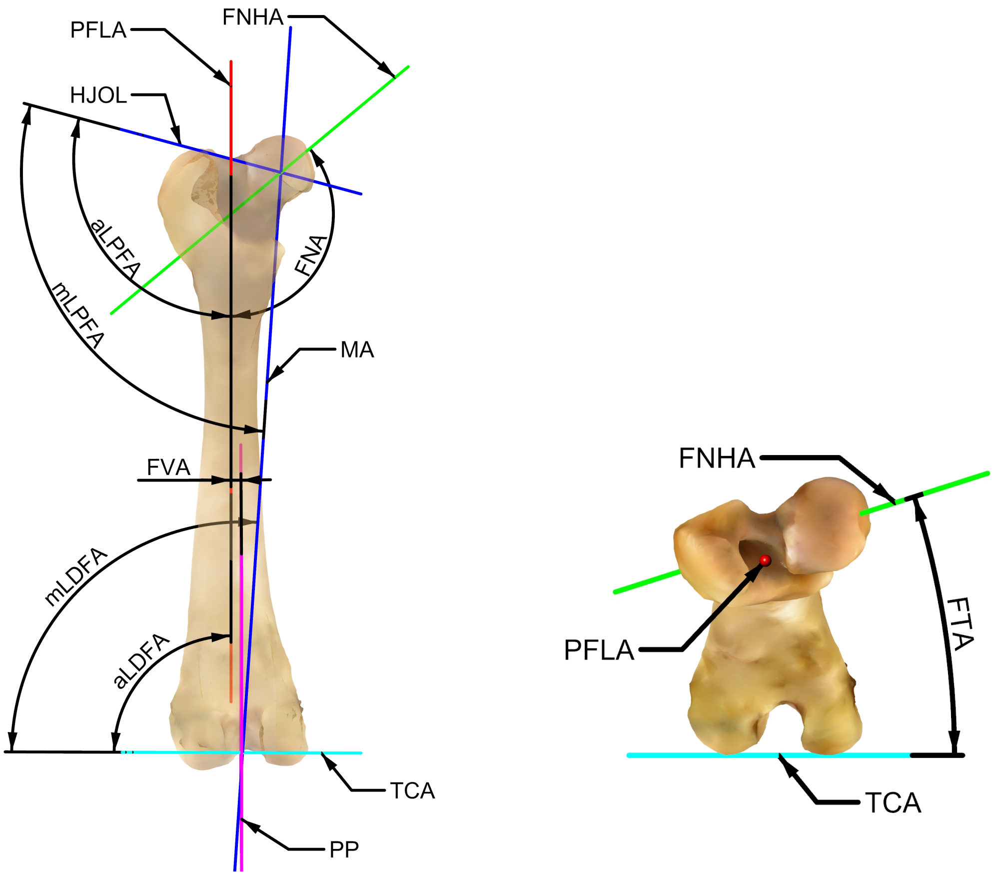

Fig. 28: computation of femoral angles and axes. On the left image, FNA, aLPFA and mLPFA are found in the proximal femoral epiphysis. The FVA is measured in the most distal part of the diaphysis, while the aLDFA and mLDFA are shown in the distal epiphysis. In the right image, FTA computation in a proximal to distal axial view of the femur.

REFERENCES

1. Botsch M: Surface representations, mesh data structures in Botsch M, Kobbelt L, Pauly M (eds*)* *Polygon Mesh Processing*. AK Peters ltd, MA, USA 2010, pp 1-28
2. Levy B, Petitjean S, Ray N at al.: Least squares conformal maps for automatic texture atlas generation in *ACM SIGGRAPH conference proceedings*, ACM, 2002
3. M. Agrawala, A. Beers, and M. Levoy: 3D painting on scanned surfaces. In *Proc. 1995 Symposium on Interactive 3D Graphics*, 1995.
4. M. Floater. Parametrization and smooth approximation of surface triangulations. *Computer Aided Geometric Design*1997; 3:231–250
5. A. Hubeli and M. Gross: Multiresolution features extraction from unstructured meshes. In *Proc. of IEEE Visualization Conf.,* 2001.
6. Di Angelo L. and Di Stefano P. Bilateral symmetry estimation of human face. *Inter J Inter Des Manufact* 2013; 7: 217-225
7. Savio G, Meneghello R, Concheri G: Optical Properties of Spectacle Lenses Computed by Surfaces Differential Quantities. *Advi Sci Lett* 2013; 19:595-600
8. Savio G, Baroni T, Concheri G, et al: Mesh processing for morphological and clinical parameters computation in dog femur. *Research in Interactive Design* 2016; 4:302-307
9. Petazzoni M: Radiographic measurements of the femur in Petazzoni M and Jaerger GH (eds): *Atlas of clinical goniometry and radiographic measurements of the canine pelvic limb*. Duluth, GA, Merial, 2008, pp 34-54
10. Victor J, Van Doninck D, Labey L, et al: A common reference frame for describing rotation of the distal femur. A CT-BASED kinematic study using cadavers. *Bone Joint J* 2009;91-B:683-690

CHAPTER 4

A THREE-DIMENSIONAL DIAGNOSTIC TECHNIQUE FOR THE COMPUTATION OF FEMORAL CANINE MORPHOMETRIC PARAMETERS

This chapter was adapted from: Savio G, Baroni T, Conchieri G, Baroni G, Meneghello R, Longo F and Isola M.: Computation of femoral canine morphometric parameters in three-dimensional geometrical models. *Veterinary Surgery* 2016: published.

SUMMARY

A prospective study was designed to define and validate a method for the measurement of three-dimensional (3D) morphometric parameters in polygonal mesh models of canine femora. Sixteen femora from 8 medium to large dog cadavers, of various breeds, with 28.3 kg mean weight and of 5.3 years mean age, were used.

Femora were measured with a 3D scanner, obtaining 3D meshes. A CAD based software tool was purposely developed which allows the automatic calculation of morphometric parameters on a mesh model.

Anatomical and mechanical lateral proximal femoral angles (aLPFA, mLPFA), anatomical and mechanical lateral distal femoral angles (aLDFA, mLDFA), femoral neck angle (FNA), femoral torsion angle (FTA) and femoral varus angle, (FVA) were measured in 3D space. Also, angles were measured onto projected planes and radiographic images.

Mean values (±SD) of femoral angles measured in 3D space were: aLPFA 115.2°±3.9, mLPFA 105.5°±4.2, aLDFA 88.6°±4.5, mLDFA 93.4°±3.9, FNA 129.6°±4.3, FTA 45°±4.5, and FVA -1,4°±4.5. Onto projection planes aLPFA was 103.7°±5.9, mLPFA 98.4°±5.3, aLDFA 88.3°±5.5, mLDFA 93.6°±4.2, FNA 132.1°±3.5, FTA 19.1°±5.7, and FVA -1,7°±5.5. Adopting radiographic imaging methods, aLPFA was 109.6°±5.9, mLPFA 105.3°±5.2, aLDFA 92.6°±3.8, mLDFA 96.9°±2.9, FNA 120.2°±8.0, FTA 30.2°±5.7, and FVA 2.6°±3.8.

The proposed method gives reliable and consistent information about the actual 3D bone conformation. Results are obtained automatically and depend only on femur morphology, avoiding any operator-related bias. Angles in 3D space are different

from those measured with standard radiographic methods, mainly due to the different definition of femoral axes.

MATERIALS AND METHODS

Sixteen femora of 8 skeletally mature dogs, visually free of orthopaedic diseases of the hip and stifle joints, and euthanatized for reasons unrelated to the study, were used. Canine cadavers were medium to large size, of various breeds (Corso, German Shepherd, Border Collie, Dobermann, mixed breed Hounds, Collie, mixed breed, Border Collie, Pitt Bull) with mean weight of 28.3 Kg (range 20-40 Kg), and mean age 5.3 years old. The specimens were disarticulated and all soft tissues were removed, sparing the articular cartilage.

A three-dimensional geometrical model was obtained, measuring each femur with a 3D scanner (Vivid 910 Konica Minolta, 3D Scan Company, Atlanta, GA, USA equipped with a middle lens ensuring accuracy less than ±0.38 mm). The acquired geometrical model is a mesh that can be also derived by in vivo CT or MRI measurements

An automatic approach for the estimation of dog femur morphological and clinical parameters was developed taking into account both the veterinary definitions of the femoral axes and angles[1,2,7] and several methods proposed in human medicine,[14-17] enabling the computation of 3D parameters. Tools (www.food4rhino.com/project/rp), were developed in *Rhinoceros®* Version 5 environment using *IronPython* and *Meta.Numerics* (www.meta-numerics.net/), a library for advanced scientific computation. This CAD software was selected because it supports the management of mesh surfaces (for instance mesh visualization, mesh data structure management, geometric center calculation, sphere fitting), and the implementation of dedicated procedures for femur analysis. From a practical perspective, the mesh models were imported in Rhinoceros, where the only required user input is represented by the selection of a point close to the femoral head. This operation is required for aligning the femur with the z-axis. All the other steps are fully automated and do not require any other input.

In order to compute femoral angles, geometrical features (such as point, axes, plane, spheres) are identified with the methodology previously described (chapter 3: algorithm)

Preliminarily, a sensitivity study was performed in order to establish spherical neighbourhood sizes, as defined above, for femoral head, great trochanter tip and condyle evaluation; the same was done to identify the number of sections for the proximal femoral long axis and other parameters adopted for the femoral mesh analysis.

Femoral angles computed were aLPFA, mLPFA, aLDFA, mLDFA, FNA, FTA, FVA.

Except for FTA, all other angles were calculated in a projection plane positioned according to Dudley et al.[2] anatomical specimen preparation (distal femur inclined 25° to simulate the positioning of the femur during a hip-extended radiographic image) (Fig 5). FTA was computed in a projection plane perpendicular to the proximal femoral long axis (Fig 6).[2]

Moreover, the femoral length along the z-axis, the femoral head radius and the distance of the center of the femoral head from proximal femoral long axis were calculated.

Radiographs for each articulated hind limb were performed with digital radiographic equipment (Kodak Point of Care CR-360 System, Carestream Health, Inc., Rochester, USA), obtaining cranio-caudal and sagittal projections for each femur. The appropriate positioning of femora was carefully evaluated taking into account guidelines suggested by literature.[1-7]

All the angles were also measured through radiographic images, adopting the methods proposed by Dudley et al for FTA,[2] while the guidelines proposed by Tomlison et al. were adopted for the measurements of the other angles.[6]

RESULTS

Sixteen femora from 8 dogs of different breeds were analysed. The values for the femoral angles computed in 3D (mean ± standard deviation) are shown in table 1. Computed angles were calculated taking into account both mechanical and anatomical angles, and measured at the level of the proximal and distal femoral epiphyses. The range values for the computed angles were: aLPFA (108.3° - 122.9°), aLDFA (80.7° - 94.3°), mLPFA (98.9 - 111.2°), mLDFA (86.2° - 98.7°), FNA (123.0° - 136.2°), FTA (38.8° - 55.4°) and FVA (-9.3° - 4.3°). Table 2 summarizes the data obtained for the previously described angles, measured in a projected plane with the femur inclined at an angle of 25 ° with a caudal-cranial orientation. The range values for the angles measured were: aLPFA (93.3° - 113.8°), aLDFA (78.7° - 95.4°), mLPFA (90.7 ° - 105.4°), mLDFA (86.0 ° - 99.2°), FNA (126.1° - 142.0°), FTA (5.6° - 25.6 °) and FVA (-11.3° - 5.4°). Table 3 summarizes data relevant to bi-planar radiograph image analysis. The range values for the angles measured were: aLPFA (100.6° - 121.0°), aLDFA (84.4° - 97.5°), mLPFA (97.1° - 113.3°), mLDFA (89.9° - 101.3°), FNA (105.5° - 136.0°), FTA (15.9° - 39.0 °) and FVA (-5.6° - 7.5°). Finally, table 4 highlights the measurements computed for other parameters such as femur length, radius head and the distance from the femoral head center to the proximal femoral long axis.

3D	aLPFA°	mLPFA°	aLDFA°	mLDFA°	FNA°	FVA°	FTA°
MEAN	115.2	105.5	88.6	93.4	129.6	21.2	-1.4
SD	3.9	4.2	4.5	3.9	4.3	4.0	4.5

RX	aLPFA°	mLPFA°	aLDFA°	mLDFA°	FNA°	FVA°	FTA°
MEAN	109.6	105.3	92.6	96.9	120.2	30.2	2.6
SD	5.9	5.2	3.8	2.9	8.0	5.7	3.8

2D P.P.	aLPFA°	mLPFA°	aLDFA°	mLDFA°	FNA°	FVA°	FTA°
MEAN	103.7	98.4	88.3	93.6	132.1	19.1	-1.7
SD	5.9	5.3	5.5	4.2	3.5	5.7	5.5

Tab. 3: Mean values and standard deviations (SD) of angles computed on 3D femur models (top tab.), radiograph images (tab. in the middle) and on projected planes (bottom tab.) (degrees°): anatomic lateral proximal femoral angle (aLPFA), mechanical lateral proximal femoral angle (mLPFA), anatomic lateral distal femoral angle (aLDFA), mechanical lateral distal femoral angle (mLDFA), femoral neck angle (FNA), femoral torsion angle (FTA), femoral varus angle (FVA).

Femur	aLPFA°	mLPFA°	aLDFA°	mLDFA°	FNA	FVA	FTA	Fl	H.Rad.	H dist.
1	114.4	106.7	81.7	93.6	133.4	-1.8	13.4	216.6	12.0	17.0
2	114.1	105.6	80.1	94.1	133.3	-3.4	19.0	215.1	12.0	18.0
3	113.8	104.1	89.5	86.2	131.4	3.0	17.4	209.9	10.8	18.1
4	118.1	108.9	89.4	87.2	126.7	3.6	19.0	209.5	11.4	17.6
5	113.0	101.5	88.6	86.8	124.9	-0.8	22.4	175.5	9.9	16.3
6	110.9	99.5	89.7	85.4	126.4	-0.8	22.9	174.5	9.2	15.8
7	122.9	110.4	81,1	92.9	123.0	-5.0	23.5	214.3	11.4	20.2
8	122.4	111.5	82.9	90.5	127.6	-3.7	18.8	216.3	11.0	21.8
9	112.0	101.6	88,9	85.2	127.0	0.1	24.4	187.0	10.3	17.5
10	113.3	101.4	92,4	85.9	125.8	0.3	25.2	186.0	10.2	18.8
11	115.3	109.1	90,5	83.9	135.8	3.2	8.4	198.7	10.5	14.4
12	117.8	111.2	94.3	85.8	134.3	1.8	5.6	199.7	10.5	14.6
13	108.3	99.2	91	82.5	136.2	2.3	25.6	184.3	9.8	15.0
14	112.8	104.1	92.4	84.9	134.0	0.5	19.3	185.1	10.1	14.7
15	116.7	107.6	93,7	82.5	126.5	2.9	20.9	162.6	9.2	15.2
16	117.5	108.7	94.1	81.6	127.7	2.0	20.5	162.9	9.3	15.4
Mean	115.21	105.69	88.7	86.82	129.63	0.26	19.13	193.62	10.47	16.90
SD	3.91	4.15	4.50	3.95	4.31	2.67	5.72	18.93	0.90	2.15

Tab. 4: Angles measured with the 3D Approach with average and standard deviation values. Table also shows the measurements of three more parameters (FL, H. Rad. and H. Dist.).

DISCUSSION

This study proposes an automatic method to calculate femoral axes and angles in 3D geometrical models. Our approach several advantages related to diagnosis, preoperative planning and surgical treatment. First of all, the 3D evaluation of axis and angles gives reliable information about the actual bone conformation, which is intrinsically 3D and not planar. The proposed 3D computer aided methodologies compute axes and angles, regardless of the orientation of bone and points selected by the operator. Therefore, the variability of measurements related to the positioning of the patient as well as any operator-related bias, is reduced to a minimum. Due to the low number of manual operations, the use of the tools developed in a CAD environment requires minimal user input, and consequently, can be used with little if any CAD experience. Furthermore, automatic measurements are independent from the only manual operation needed (selection of a point close to the femoral head) and, therefore, the proposed procedure is very robust. Femoral angles computed through a 3D geometrical model substantially differ from those measured on bi-planar image. Consequently, new reference ranges for femoral parameters should be established.

Regarding the methodology, several methods have been developed to identify the proximal femoral long axis.[6,7,31] In agreement with Tomlison et al.,[6] using our method the above axis can be identified taking into account the geometric centers of femoral diaphysis cross sections ranging between one-third to one-half of the bone length. This approach allows the assessment of the proximal femoral long axis with a standardized protocol, as its evaluation is independent of femoral conformation, dimension and breed.

Literature suggests several definitions and proposes various methods to compute femoral head and neck axis.[4-8] Consequently, different values of angles related to this axis have been reported. When using 3D models, human medicine recommends the identification of the center of the femoral head through a spherical fitting.[14,15] Currently used protocols for the selection of the vertices of the femoral head for the fitting procedure are often unclear. In our protocol, the selection of the vertices is fully automated and is based on curvature analysis. Consequently, the computed sphere is operator independent. In human medicine, the center of the femoral neck is the geometric center of the minimal cross-sectional area in the neck. A generic cross-sectional area can be defined as a function of three independent variables which describes the position and orientation of the intersecting plane. Therefore, the minimal cross-sectional area in the neck is determined by an optimization procedure which iteratively varies these 3 variables.[14,15] The use of spherical sections, rather than planar sections for assessing the center of the femoral neck, decreases the number of variables to one (radius of the spherical section). As a result, the presented approach simplifies the computational process and simultaneously enhances the FNA and FTA evaluation, because of the increase of the distance between the femoral head and the center of the neck. Other approaches based on spherical sections were previously investigated and discussed.[21]

The estimation of the tip of the great trochanter includes a local fitting surface; thus, bias linked to local spikes, noise or similar mesh inaccuracies were avoided.

In order to correctly calculate the transcondylar axis, femoral condyles were analysed considering the kinematic of the stifle. Condyles, as proposed in human medicine, are computed fitting the distal articular surface of the femur with two spheres.[16,17] In 2D studies transcondylar axis traditionally assumes different orientations depending on the radiograph projection (cranio-caudal versus distal-proximal axial femoral radiograph).[2] Another advantage of the proposed method is the unique definition of this axis (always in the same position), based on the angle between a line perpendicular to the tibial plateau and the proximal femoral long axis. In our study, this angle is assumed to be 90° to simulate the orientation of transcondylar axis in a distal-proximal axial femoral radiograph.

In 3D space, infinite axes pass perpendicular to the midpoint of the transcondylar axis and, consequently, FVA loses its meaning. To bridge this gap, we suggested an alternative definition for FVA: the angle obtained between a plane perpendicular to the transcondylar axis and the proximal femoral long axis. Figure 29 shows how the mentioned plane becomes a line in a projection plane, explaining the proposed alternative for the FVA computation.

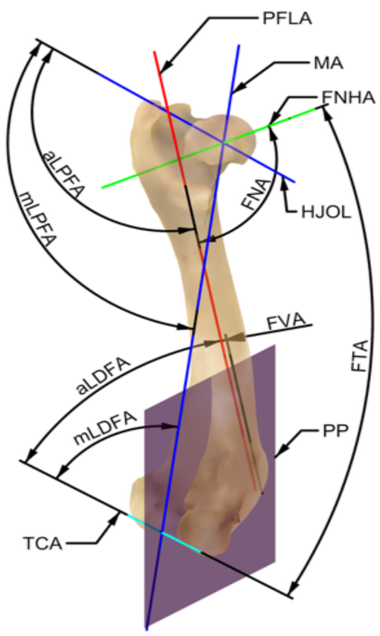

Fig. 29: femoral angles measured in 3D. Notice the sagittal violet plane in the distal femoral epiphysis (PP); this plane is perpendicular to TCA and was adopted for the FVA measurement of the DFLA.

Our results on femoral angles differ from available information in the literature as all past works are based on 2-D assessments.[1-7] Reasons of differences in femoral angles computed in projected planes are principally due to the definition of 3D axes. For instance, the proximal femur long axis in 3D features a geometric center as a set of sections that differs from the center of femoral diaphysis computed in 2D. Again, the orientation of the femur (z-axis coincident with the proximal femoral long axis) changes from the one achieved with radiographs and, therefore, the position of the trochanter tip. As a result the hip joint orientation line differs from those achieved with a bi-planar assessment. This peculiarity explains the differences between the values attained for aLPFA and mLPFA. Further explanations for these discrepancies could be related to the femur malposition and to an operator-effect. In our study, only FNA and FVA show for both projected planes values comparable with the literature. This does not necessarily mean that axes positioning is the same, but only that each pair of axes defining these angles has a common rotation.

Although 3D models are a well-established diagnostic tool for human medicine,[8-17] in veterinary medicine they represent a novelty. Recent efforts to develop consistent imaging techniques led to a 3D approach to investigate several areas of interest within the veterinary orthopedic field.[18-28] For instance, 3D models allow for volume measurement,[19] evaluation of joint congruency,[18,20] and rotation of deformed bones at a desired orientation creating cross-sectional views from any position.[24] However, little if any attention has been devoted to 3D measurements of femoral axes and angles, except for a recent study[26] which focuses on the evaluation of bone deformities through CT scan-reconstructed 3D images. Nevertheless, Yasukawa et al provide femoral measurements calculated in CT frontal or lateral view, thus in bi-planar projections.[26] In contrast, we present values for femoral angles calculated through 3D geometrical model.

Theoretically speaking, any model of femur (and femoral head) can be analysed by the proposed methodology, including pathological femora. Further work is necessary to better define 3D assessments of various pathological conditions of the canine femur especially regarding pathological femora characterized by a severe joint degeneration. For instance, the identification of the center of the femoral head may rely on different anatomical landmarks or criteria for the selection of the points for the spherical fitting.

REFERENCES

1. Swiderski JK, Radecki SV, Park RD, et al: Comparison of radiographic and anatomic femoral varus angle measurements in normal dogs. *Vet Surg* 2008;37:43-48
2. Dudley RM, Kowaleski MP, Drost WT, et al: Radiographic and computed tomographic determination of femoral varus and torsion in the dog. *Vet Radiol Ultrasound* 2006;47:546-552
3. Mostafa AA, Griffon DJ, Thomas MW, et al: Proximodistal alignment of the canine patella: radiographic evaluation and association with medial and lateral patellar luxation. *Vet Surg* 2008;31:201-211
4. Bardet JF, Rudy RL, Hohn RB: Measurement of femoral torsion in dogs using a biplanar method. *Vet Surg* 1983;12:1-6
5. Montavon PM, Hohn RB, Olmestead ML, et al: inclination and anteroversion angles of the femoral head and neck in the dog evaluation of a standard method of measurement. *Vet Surg* 1985;14:272-282
6. Tomlison J, Fox D, Cook JL, et al: Measurement of femoral angles in four dogs breeds. *Vet Surg* 2007;36:593-598
7. Petazzoni M: Radiographic measurements of the femur in Petazzoni M and Jaerger GH (eds): *Atlas of clinical goniometry and radiographic measurements of the canine pelvic limb*. Duluth, GA, Merial, 2008, pp 34-54
8. Jackson GM, Wendelburg KL: Evaluation of the effect of distal femoral elevation on radiographic measurement of the anatomic lateral distal femoral angle. *Vet Surg* 2012;41:994–1001
9. Gamage P, Xie SQ, Delmas P, et al: diagnostic radiograph based 3D bone reconstruction framework: application to the femur. *Comput Med Imag Grap* 2011; 35:427-437
10. Koh K, Kim YH, Kim K, et al: Reconstruction of patient-specific femurs using X-ray and sparse CT images. *Comput Biol Med* 2011;41:421-426
11. Otomaru I, Nakamoto M, Kagiyama Y, et al: Automated preoperative planning of femoral stem in total hip arthoplasty from 3D CT data: atlas-based approach and comparative study. *Med Image Anal* 2012;16:415-426

12. Metzler P, Geiger EJ, Alcon A, et al: Three-dimensional virtual surgery accuracy for free fibula mandibular reconstruction: planned versus actual results. *J Oral Maxillofac Surg* 2014;72:2601-2612
13. Zhu Z, Li G: Construction of 3D human distal femoral surface models using a 3D statistical deformable models. *J Biomech* 2011;44:2362–2368
14. Cerveri P, Marchente M, Bartels W, et al: Automated method for computing the morphological and clinical parameters of the proximal femur using heuristic modeling techniques. *Ann Biomed Eng* 2010;38:1752-1766
15. Kang Y, Engelke K, Fuchs C, et al: An anatomic coordinate system of the femoral neck for highly reproducible BMD measurements using 3D QCT. *Comput Med Imag Grap* 2005;29:533-541
16. Victor J: Rotational alignment of the distal femur: a literature review. *Orthop Traumatol Surg Res* 2009;95:365-372
17. Victor J, Van Doninck D, Labey L, et al: A common reference frame for describing rotation of the distal femur. A CT-BASED kinematic study using cadavers. *Bone Joint J* 2009;91-B:683-690
18. Lopez MJ, Lewis BP, Swaab ME, et al: Measurements obtained by use of computed tomography and radiography and scores of cartilage microdamage in hip joints with moderate to severe joint laxity of adult dogs. *Am J Vet Res* 2008;69:362-370
19. D'Amico LL, Xie L, Abell LK, et al: Relationship of hip joint volume ratios with degrees of joint laxity and degenerative disease from youth to maturity in a canine population predisposed to hip joint osteoarthritis. *Am J Vet Res* 2011;72:376-383
20. Andronescu A, Kelly L, Kearney MT, et al: Associations between early radiographic and computed tomographic measures and canine hip joint osteoarthritis at maturity. *Am J Vet Res* 2015;76:19-27
21. Savio G, Baroni T, Concheri G, et al: Mesh processing for morphological and clinical parameters computation in dog femur. *Research in Interactive Design* (Vol. 4) Springer 2016; 302-307
22. Wang C, Wang J, Zhang Y, et al: A canine model of femoral head osteonecrosis induced by an ethanol injection n navigated by a novel template. *Int J Med Sci* 2013;10:1451-1458
23. Fitzwater KL, Marcellin-Little DJ, Harrysson OL, et al: Evaluation of the effect of computed tomography scan protocols and freeform fabrications methods on bone biomodel accuracy. *Am J Vet Res* 2011;72:1178-1185

24. Verim O, Tasgetiren S, Er MS, et al: Anatomical evaluation and stress distribution of intact canine femur. *Int J Med Robotics Comput Assist Surg* 2013;9:103–108.

25. Zamprogno H, Nelson N, Schaeffer DJ, et al: Three Dimensional Morphologic Analysis of the Lateral Surface of the Canine Femur. *Vet surg* 2014;9999:1-7

26. Yasukawa S, Edamura K, Tanegashima K, et al: Evaluation of bone deformities of the femur, tibia, and patella in Toy Poodles with medial patellar luxation using computed tomography. *Vet Comp Orthop Traumatol* 2016; 29: 29–38

27. Kim SE, Jones SC, Lewis DD, et al: In-vivo three-dimensional knee kinematics during daily activities in dogs. *J Orthop Res* 2015;33:1603–1610

28. Jones SC, Kim SE, Banks SA, et al: Accuracy of noninvasive, single-plane fluoroscopic analysis for measurement of three-dimensional femorotibial joint poses in dogs. *Am J Vet Res* 2014;75:477–485

29. Savio G, Meneghello R, Concheri G: Optical Properties of Spectacle Lenses Computed by Surfaces Differential Quantities. *Advi Sci Lett* 2013;19:595-600

30. Di Angelo L, Di Stefano P: Bilateral symmetry estimation of human face. International Journal on Interactive Design and Manufacturing 2013; 7(4):217-225

31. Miles J, Mortensen M, Svalastoga E, et al: A comparison of anatomical lateral distal femoral angles obtained with four femoral axis methods in canine femora. *Vet Comp Orthop Traumatol* 2015;3:193-198

CHAPTER 5

REPEATABILITY AND REPRODUCIBILITY OF RADIOGRAPHY, COMPUTED TOMOGRAPHY AND THREE-DIMENSIONAL COMPUTATION FOR THE MEASUREMENT OF THREE FEMORAL ANGLES IN DOGS

This chapter was adapted from: Longo F, Nicetto T, Banzato T, Drigo M, Savio G, Conchieri G, Meneghello R and Isola M. Repeatability and reproducibility of radiography, computed tomography and three-dimensional computation for the measurement of three femoral angles in dogs: abstract for *ACVS meeting* 2017: submitted; *Veterinary Surgery* 2017: incoming submission.

SUMMARY

Objective: To introduce a novel method for three-dimensional computation of femoral angles in dogs, starting from 3D reconstructions of CT images. Repeatability and reproducibility of three diagnostic methodologies (RX, TC and 3D computation) were evaluated for the measurement of three femoral angles (aLDFA, FNA, FTA), which are usually assessed when a femoral deformity is questioned.

Study design: An ex-vivo diagnostic study.

Sample population: Twenty-two femurs obtained from 16 cadavers, of 7.8 year mean age with 29,3 kg mean weight, were used for the analysis.

Methods: Femoral angles were measured by three blinded observers in nine separate occasions; three assessments per diagnostic technique. An overall amount of 594 femurs was examined and the related measurements were analyzed by mixed effect linear models (for repeated measures) with femur as crossed random effect and diagnostic technique, observer and measurement repetition as fixed factors. Repeatability, reproducibility and ICC were, also, calculated.

Results:

Repeatability and reproducibility were acceptable (< 5%) for the measurement of aLDFA and FNA, for all the methodologies tested. FTA computation was neither a reproducible nor repeatable procedure (> 15%). However, 3D protocol was the only technique to show an acceptable repeatability (< 5%), for the computation of such angle. Calculated means among observers were: RX aLDFA (91,06° ± 4,6°) RX FNA (125,06° ± 5,3°) and RX FTA (23,91° ± 8,3°); TC aLDFA (91,38° ± 4,4°), TC FNA (125,8° ± 5,8°) and TC FTA (24,14° ± 7,5°); 3D aLDFA (89,75± 5°), 3D FNA (128,79 ° ± 4,3 °) and 3D FTA (20,44° ± 7,1°).

The intra-class coefficients (ICC) were excellent, being > 0,75 for almost to all the parameters considered.

Conclusions: Three-dimensional computation is a semi-automated and standardized protocol that resulted as the most repeatable technique among the methodologies tested. 3D computation allows for precise measurements, significantly decreasing user-inputs, thus minimizing operator-related bias that could affect RX and TC. FTA computation was not satisfactory, therefore further studies are encouraged to study anatomical landmarks that may cause errors in the torsional assessment.

MATERIAL AND METHODS

Sixteen skeletally mature dogs, euthanized for reasons unrelated with the current research, were primarily selected for the study. Cadavers were medium to large sizes of different breeds and age. The sex, weight and breed were, also, recorded.

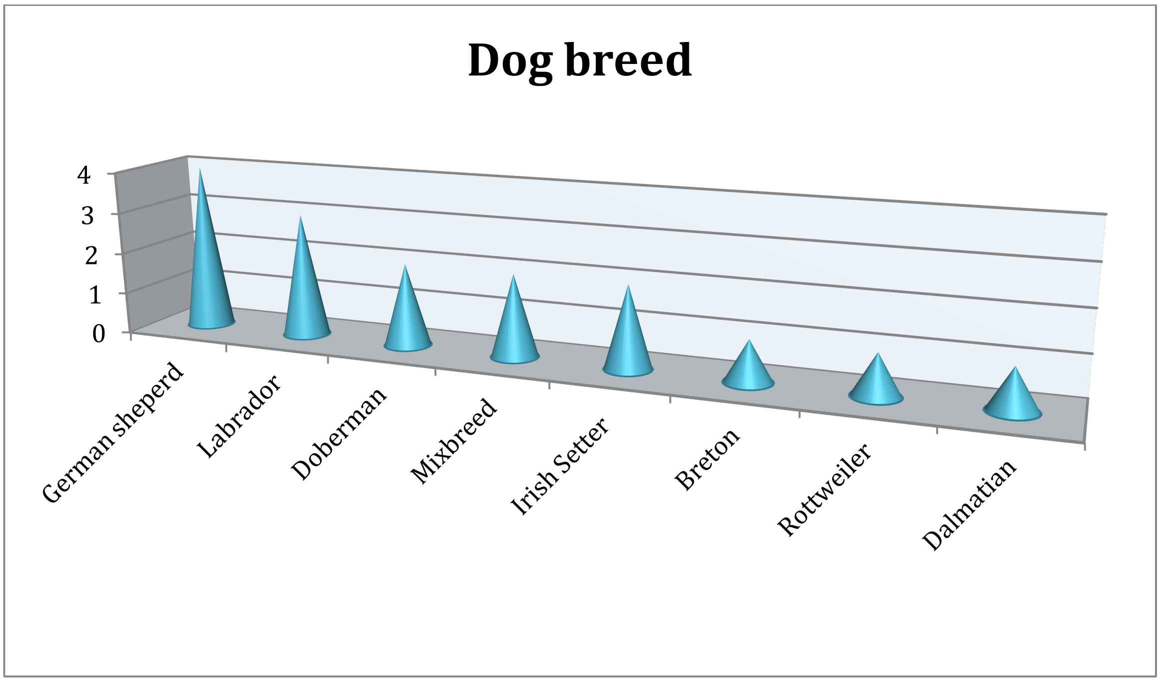

Fig. 30: graphic of the breeds used for this study. German shepherd was the prevalent breed (4), followed by Labrador retriever (3).

For this study, three blinded observers evaluated the images of femurs from November 2015 till March 2017. Observers were two experienced small animal orthopaedic surgeons (MI, TN) and one experienced radiologist (TB). The readers performed measurements in radiographic, CT images as well as three-dimensional bone models, independently, on several separate occasions with several weeks between the assessments. In addition, two collaborators actively participated in the study. The first operator executed the CT scans, radiographic exams, and prepared all the images for each femur. The second collaborator performed the randomization of all the samples using an open source program (*Research randomizer, Version 4.0. Retrieved on January 20, 2017, from http://www.randomizer.org/)* with the aim of changing the order of presentation of the anonymized samples for each series, differing it for every reader. A randomized set of three series of 30 samples each, was created for every examiner. The operation was, then, repeated for all the type of image (radiographic, computed tomographic and CT scans for 3D model). As a result, an overall number of 27 series of 810 randomized femur samples was produced.

28/10/2015 Research Randomizer

DOWNLOAD PRINT CLOSE

RESULTS

3 Sets of **30 Unique** Numbers Per Set
Range: From **1** to **30**

Set #1

1, 26, 10, 24, 15, 9, 18, 19, 14, 3, 2, 21, 17, 27, 5, 28, 8, 4, 30, 23, 25, 12, 20, 6, 22, 13, 16, 7, 29, 11

Set #2

27, 28, 4, 29, 18, 12, 6, 23, 24, 11, 7, 8, 16, 5, 10, 15, 13, 19, 17, 21, 14, 9, 1, 3, 22, 20, 26, 2, 30, 25

Set #3

24, 18, 11, 28, 16, 10, 21, 23, 19, 25, 7, 9, 17, 8, 14, 22, 4, 29, 27, 15, 1, 2, 12, 26, 30, 5, 6, 20, 13, 3

Fig. 31: example of a randomized set adopted in this study and obtained with *Research Randomizer.*

Images of every femur were anonymized before the assessment using a legend of letters for each series to prevent any conditioning for the observers. Only the second collaborator knew the interpretation key of the legend for being able to assemble all the data collected at the end of measurement assessment.

Sample	Series 1	Series 2	Series 3
1	T	IN	BUL
2	C	UM	CLE
3	F	ZL	MIL
4	K	SX	DET
5	D	LZ	IND
6	U	TC	TOR
7	M	NY	BRO
8	X	HU	NEW
9	S	OR	BOS
10	O	BO	PHI
11	Z	SA	MIA
12	L	DA	ATL
13	Q	MO	ORL
14	A’	NA	CHA
15	N	ME	WAS
16	O’	NE	LAL
17	H	TA	CLI
18	P	AT	PHX
19	I	XY	GSW
20	W	SE	SAC
21	A	PO	UTA
22	G	LA	DEN
23	Y	OA	POR
24	J	CH	MIN
25	R	DE	OKC
26	E	CL	DAL
27	B	TO	HOU
28	E’	OK	SAS
29	V	UT	MEM
30	U’	WA	NOH

Tab. 5: table of the legend. Every femur sample was associated with a single letter for the first series and a combination of two or three letters for the second and third series.

Sample	Femur	Dog
1	Right	1
2	Left	1
3	Left	2
4	Right	3
5	Left	3
6	Right	4
7	Left	4
8	Right	5
9	Left	5
10	Right	6
11	Left	6
12	Right	7
13	Left	7
14	Right	8
15	Left	8
16	Right	9
17	Left	9
18	Right	10
19	Left	10
20	Right	11
21	Right	12
22	Left	12
23	Right	13
24	Left	13
25	Right	14
26	Left	14
27	Right	15
28	Left	15
29	Right	16
30	Left	16

Tab. 6: correlation between sample and femur (right or left) for every cadaver.

Imaging procedures

All the femoral images used for the measurements were prepared through commercially available DICOM processing software for Macintosh (*Osirix*, pixmeo SARL, Switzerland).

For CT and 3D images, a volume rendered and surface shaded pre-set was adopted to isolate each femur from any other bony structures. 3D reconstructed femurs were, then, analysed with a commercial CAD software (*Rhinoceros* version 5, Robert McNell & associates, Usa), in which a specific plug-in was developed for the femur 3D computation.[1]

Radiographic examination

Digital radiographic equipment (*Kodak Point of Care CR-360 System*, Carestream Health Inc, Usa) was used to perform the radiographic examination of the cadavers. At the beginning of the study 30 femurs were tested. Defined exclusion criteria were radiographic diseases of the stifle and hip joints, as they may have altered the analysis during the measurement and computational process. Bearing in mind these guidelines, 8 femurs were excluded from the initial group, as they didn't match the inclusion criteria.

Fig. 32: examples of samples excluded from the study. On the left image, a severe osteoarthritic degeneration in proximal epiphysis is present. In the right view a neoplastic-like soft issue lesion is observable in the distal femur metaphysis.

The collaborator performed cranio-caudal and distal-proximal axial femoral projections for each femur of every cadaver, adopting the currently accepted patient positioning guidelines.[2-4] Briefly, in the cranio-caudal projection, the patient was positioned in dorsal decumbency with a sitting position, using a soft support to accommodate the alignment of the column of the cadaver. The femur was arranged parallel to the radiographic cassette with the x-beam perpendicular to it, the hip was extended and pelvic limbs internally rotated as well.

Fig. 33: radiographic positioning for a cranio-caudal projection. A dorsal wood support was used to obtain a sitting position. On the left, lateral view of the positioning with a parallelism between femur and radiographic cassette. On the right, a picture taken from a top view shows the hyperextension of the femur.

For the axial x-ray films, the limb was positioned in a way that the long axis of the femur resulted perpendicular to the table and parallel to the x-ray beam, paying close attention to avoid excessive adduction or abduction of the pelvic limb.[4] This positioning allowed for the optimal visualization of the anatomical landmarks such as the femoral head, neck and condyles with the femoral shaft forming a concentric ring.[4]

Fig. 34: radiographic axial positioning. On the left image a lateral view of the femur is exhibited. Notice the perpendicular position of the femur in relation to the radiographic table. On the right, the operator perspective is shown. The femur has to be relatively straight avoiding excessive adduction or abduction; otherwise the head and femoral neck could be not correctly detectable.

The collaborator reviewed the proper radiographic positioning of the femur to exclude the projections that didn't satisfy the positioning recommendations proposed by literature.[5-7]

Positioning was considered acceptable for the cranio-caudal projection, if the femur was disposed parallel to the long axis of the pelvis with fabellae bisected by the femoral cortex, patella in the middle of the trochlear groove and tip of less trochanter partially visible as well.[4-6]

As concerns the distal-proximal axial femoral projection, the intramedullary canal had to be visible and ideally superimposed with a best-fit circle. Moreover, the femoral head and condyles had to be anatomically observable with the caudal and cranial cortical margins of the femoral neck detectable.[4,7]

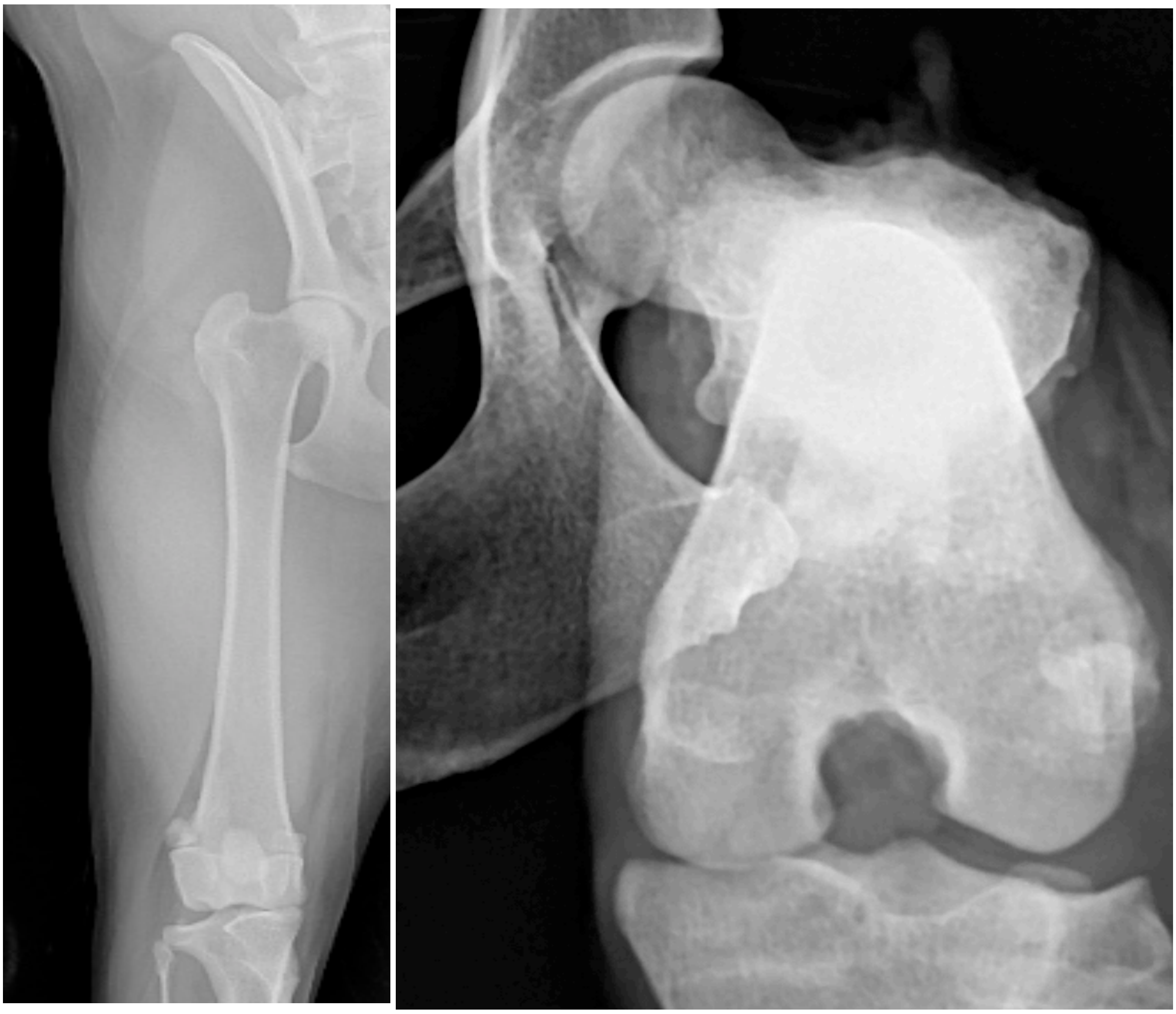

Fig. 35: example of a correctly positioned femur for the radiographic measurements. Cranio-caudal (left) and axial views (right).

CT examination

The CT examination started, once the collaborator performed, archived and tagged all the radiographs. For the computed tomographic study, the cadavers were positioned on a foam cradle in a supine position with the legs extended and adduced. Correct positioning was obtained using medication gauzes. Imaging was performed in a caudo-cranial direction using a 4-multi-detector-row CT scanner (*Toshiba Asteion S4*, Toshiba Medical Systems Europe, Zoetermeer, South Holland, The Netherlands) in helical acquisition mode. An exposure time of 0.725 seconds, voltage of 120 kV, amperage of 150 mA, and slice thickness of 1 mm (reconstruction interval: 0.8 mm) were always used. CT images were reconstructed with a high-resolution filter for the inner ear and bones (setting Fc81) and displayed in a bone window (window length, 1,000 HU; window width, 4,000 HU).

The images were reconstructed with *Osirix* using the 3D volume rendering option and then choosing a bone filter among the pre-set options.

Using the magnification function, the pelvis, tibia, tail and the contralateral hind limb were cropped to isolate the femur. During the cropping procedure, care was taken to avoid unintentional alteration of the profile of the femoral condyles.

Regarding the cranio-caudal position of the femur, a proper proximal-distal alignment was achieved following the procedure described by Oxley et al. (2013).[8]

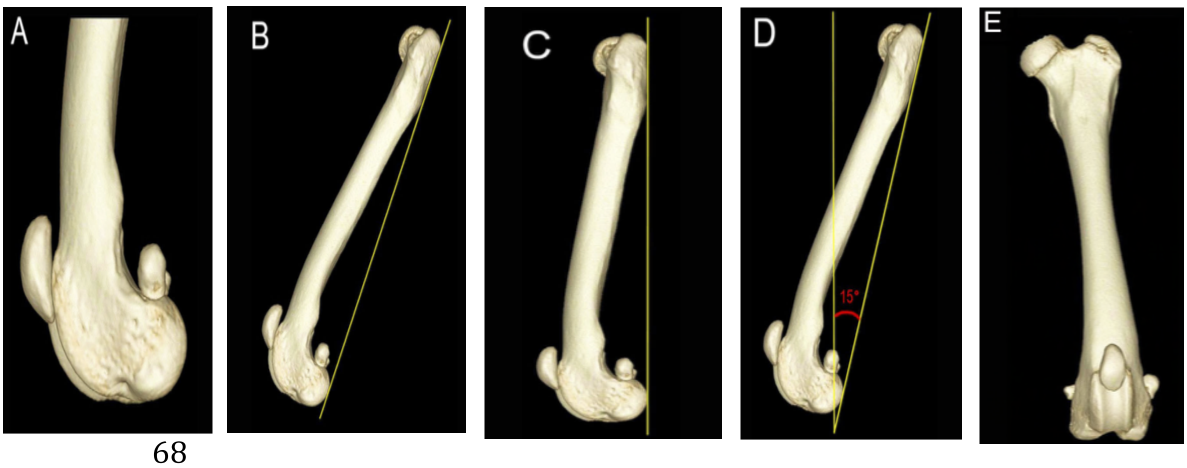

Fig. 36: methodology for the positioning of the reconstructed femur. The left image shows the medio-lateral femur orientation starting from the superimposition of the femoral condyles (A), drawing of a line that connects the most caudal point of the condyles and the proximal of the femur (B). Femur is then rotated in the sagittal plane until the axis has a caudal inclination of 15°(C, D) The image is finally rotated through a 90° in the transverse plane to obtain the definitive cranial view (E).(Images taken from Oxley et al., 2013).

For the CT axial projection, we used a different procedure for the positioning, that differs from the one previously described for the radiographic axial view and reported in the literature.[4,6,9,10]

In our protocol, femoral condyles were aligned parallel to the underlying measuring toolbar of *Osirix*, in a proximal-distal view to obtain an appropriate vision of the femoral head and neck.

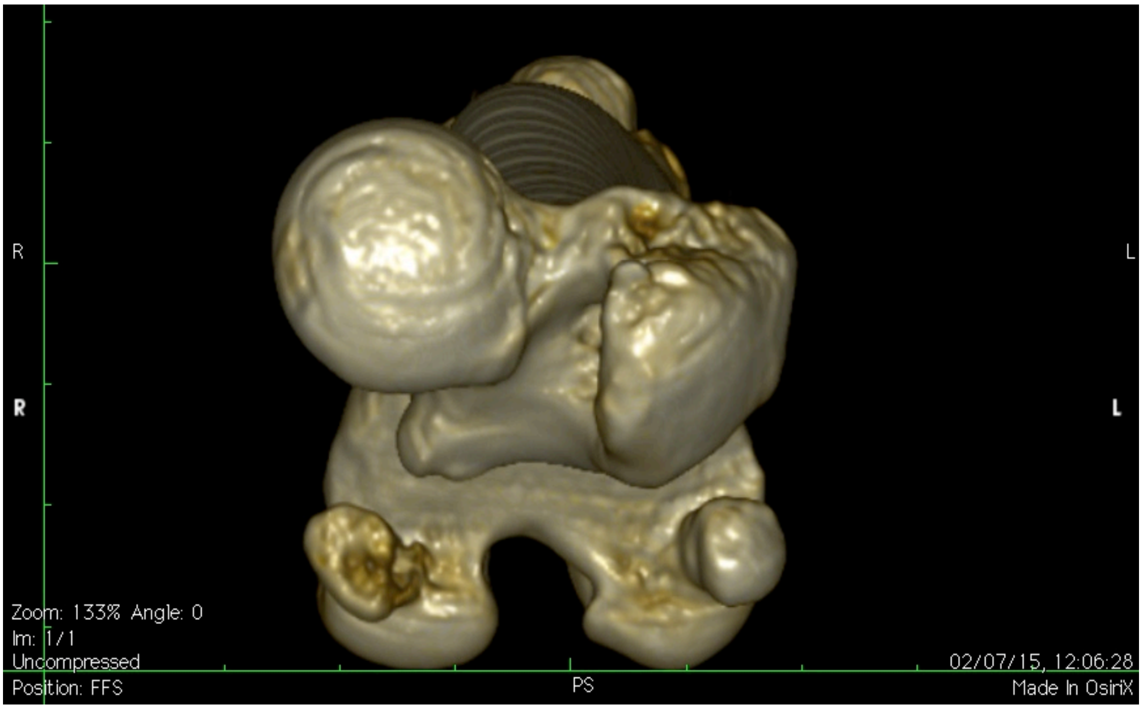

Fig. 37: proximal-distal positioning of the femur. Femoral condyles are aligned to a below toolbar. Then, the femur is moved on the transverse plane until the edges of the femoral neck and the conformation of the femoral head are visible.

Once the femur was correctly positioned in both projections, the file was firstly saved as a DICOM file. Then, the image, so obtained, was edited to eliminate any annotations, and was saved, as a JPEG file, and tagged as well, to be ready for measurements.

STL extraction using CT data

To perform the three-dimensional computation with *Rhinoceros* is necessary to import into it STL files. Therefore, examiners before the 3D analysis, imported in *Osirix* the DICOM datasets obtained through CT scans. Every CT scan included the pelvis with both femurs, hence each folder sent to readers, contained a JEPG image in which the reconstructed femur to be computed was labelled with a red dot located in the body of the ileum. The purpose of labelling was to guide the examiner for the selection of the right femur to analyse.

The segmentation phase started once the observer visualized the femur to isolate. Readers opened the CT scan and the 3D volume rendering function was used to completely isolate the labelled femur from any other bony structure with the goal of maintain intact the contour of the femur.

Fig. 38: example of a labelled 3D reconstructed pelvis. Note, in the zoomed image on the center, the presence of a red dot in the body of the ileum. On the right image, the femur is carefully isolated from the others bony structures.

Next, starting with an axial plane orientation, the ROI menu option in the upward toolbar of *Osirix* was selected, followed by the grow region (2D/3D segmentation) option.

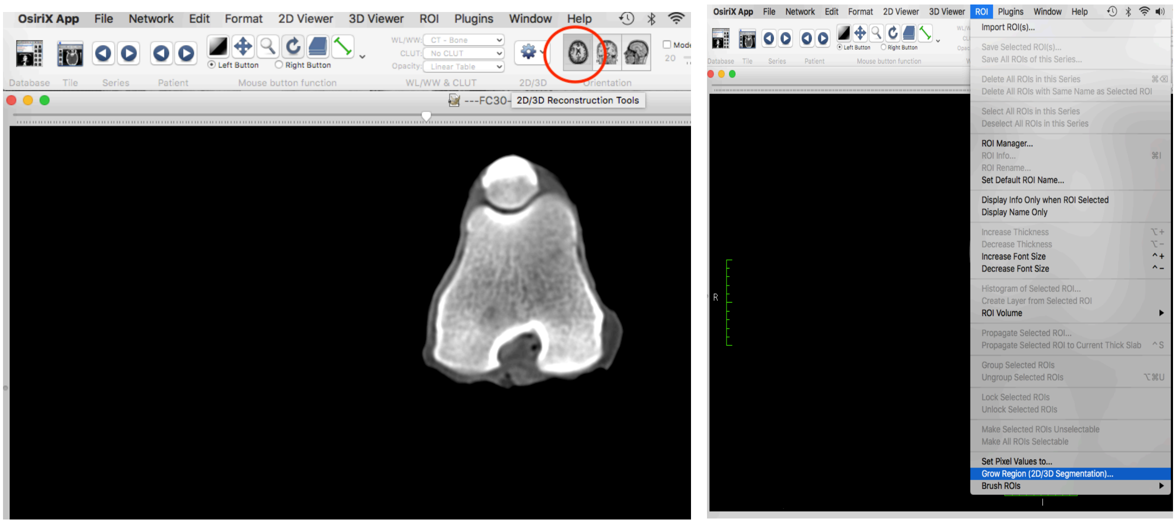

Fig. 39: on the left picture, a selection of the frontal orientation plan is chosen to begin the segmentation phase. On the right the grow region function is chosen.

The density of the bony target area was checked using an oval tool and expressed with Hounsfield attenuation numbers. A Hounsfield unit (HU) represents a normalized index of x-ray attenuation based on a reference scale. [11,12] Generally, in a typical CT scan, air measures -1000 HU, soft tissue between 30 HU and 70 HU and bone usually presents values that are greater than 300 HU.[11,12] The density measurement was necessary to set up the lower and upper thresholds. The target value was the mean density, which appears in a small script when the oval tool is positioned onto the tissue examined.

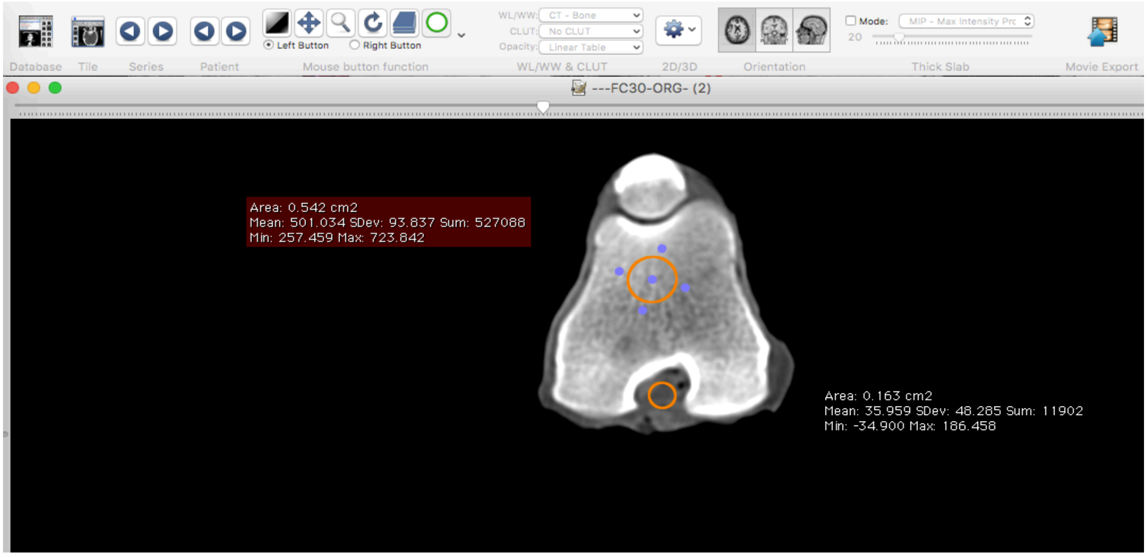

Fig. 40: density measurement using ROI tool. The circle in the upper part of the image is examining the density of the bone (mean value: 501 HU). The circle at the bottom is measuring the soft tissue density. The script at the top of the image shows an attenuation of the value (mean: 35 HU).

Subsequently, segmentations parameters are tagged in a specific window that pops up. Specifically, the 3D growing region function is picked; next the upper and lower thresholds (range values used: 200 to 4000) are inserted as well as the inside and outside pixels.

A starting point for the segmentation algorithm is selected, clicking inside the marked femur. Consequently, green crosshairs appeared, meaning that all the bone structures contiguous to the point selected are highlighted with the same colour.

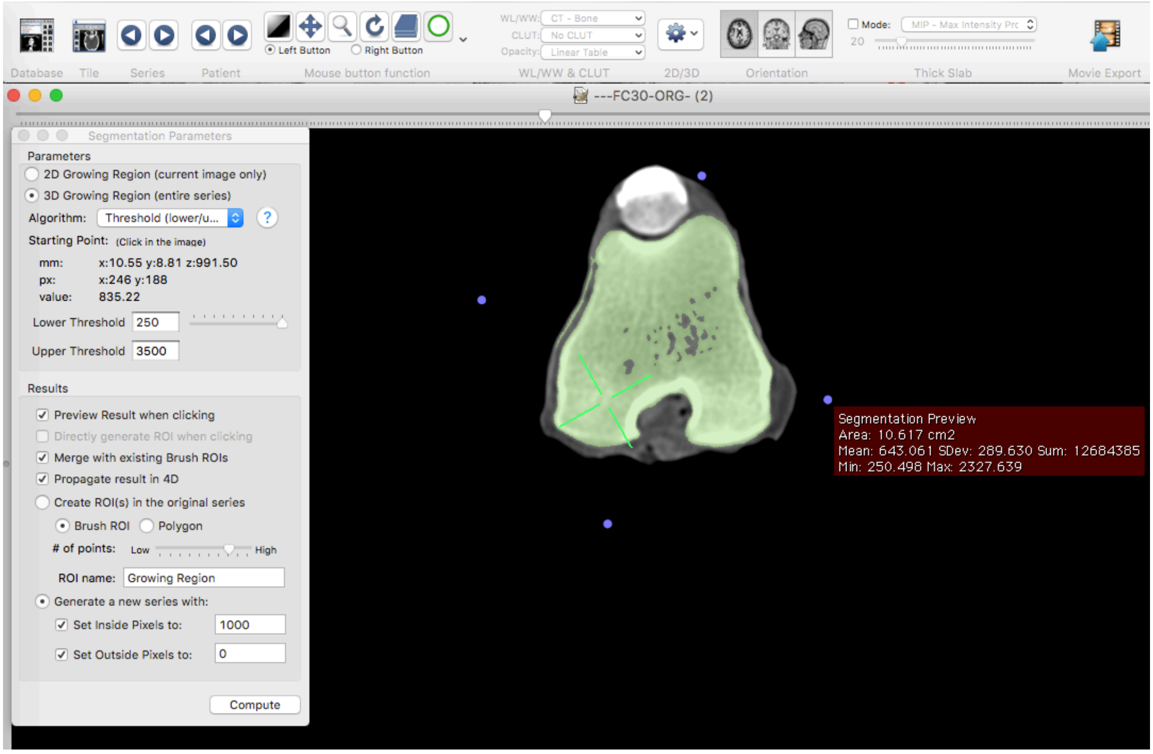

Fig. 41: the ROI is selected clicking on the bony structure the user want to isolate. In the grey window on the left, the operator inserts the parameters. In this study range values for the lower and upper threshold varied from 200 (minimum) to 4000 (maximum).

Finally, the compute button is clicked and, as a result, new series are generated. The latter ones appear as a darker image on one side of the CT scan. In fact, the software will generate new series with the bone being a single white colour with a value of 1000 (inside pixels) and everything else being a black colour with a value of zero (outside pixels).

The same procedure is, then, repeated for the other two planes (axial and sagittal), thus achieving a 360-degree segmentation.

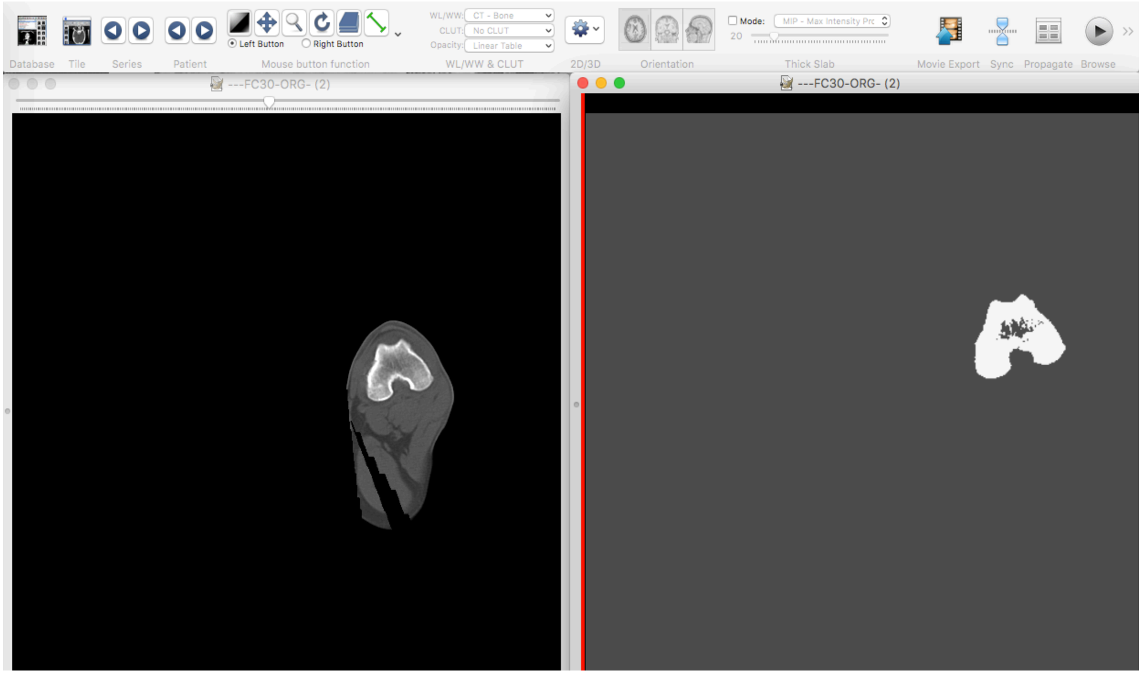

Fig. 42: the left windows shows a bone used for the segmentation. Different tissues with different densities (bone versus soft tissues) are observable. On the right image, a new bitmapped series is shown.

Once the bitmapped is generated and highlighted, the user clicks on the viewer menu and select 3D surface rendering option, leaving the settings tagged to their default values. Another window will pop up and parameters such as the resolution and pixel value must be inserted. For this study, the level of the resolution was set as high as possible and for the pixel value the CT-Bone option was chosen.

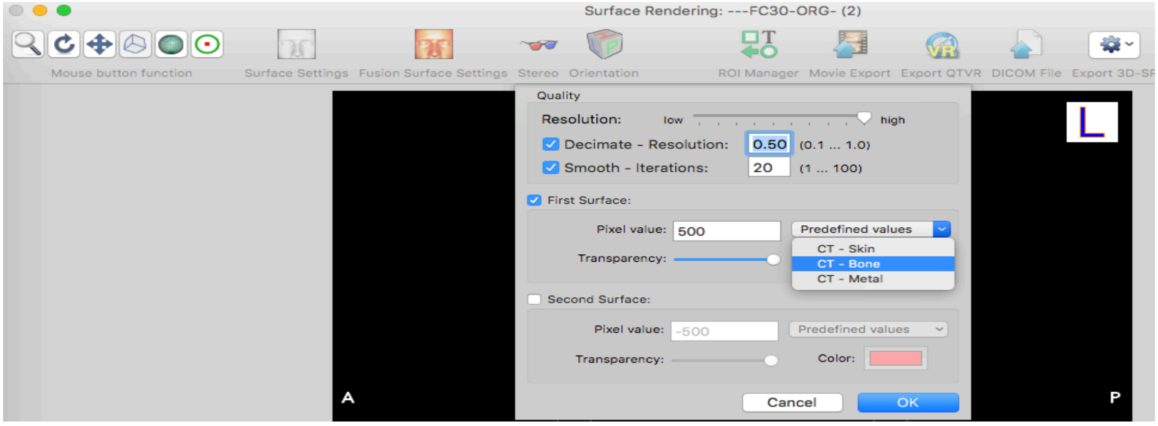

Fig. 43: setting of the 3D surface rendering parameters. The predefined value of CT-Bone filter is selected.

The user proceeds selecting the ok button and *Osirix* will, then, prepare the surface that will show a suitable approximation of the femur. Finally, the export 3D-SR MENU is selected in the upward toolbar and the file is exported as STL file.

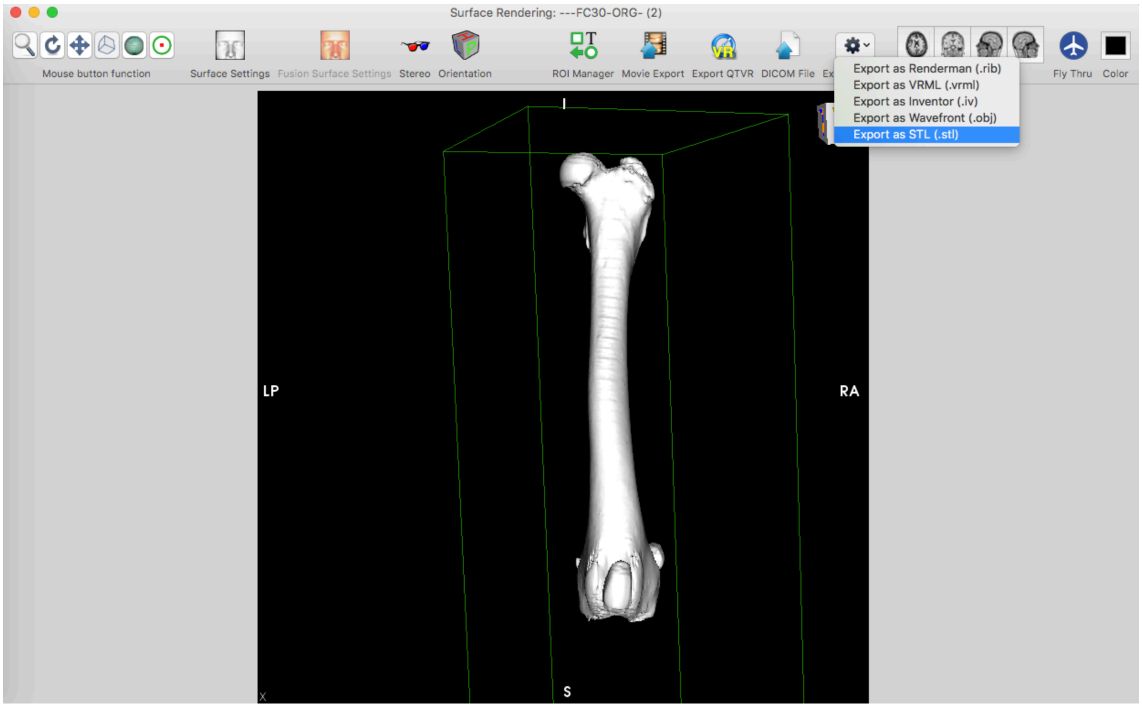

Fig. 44: appearance of the remodelled femur. When the setting of the bone model is over, the user saves the file as an a STL, selecting from the small window in the right upward toolbar.

Parameters measurement

In the study three angles were calculated (aLDFA, FNA and FTA) through three different diagnostic techniques. Examiners performed the measurements using always the same methodology for each diagnostic technique and for every angle assessed.

A folder including the anonymised femurs (RX and CT images) or pelvis (CT scans), and an excel file (excel), was given to the observers in 9 separate occasions in a frame of time of one year and half. Every examiner was asked to insert in the excel file the results of each measurement. All the excel files were sent back to the collaborator that collected all the data.

F29 *fx*

	A	B	C	D	E	F	G
1	3 d 1 serie						
2			AP	AP	AS		
3			aLDFA	FNA	FTA		
4	Samples						
5							
6	1	w	94	129,49	10,25		
7	2	e	87,89	124,57	24,72		
8	3	x	93,45	127,89	16,54		
9	4	j	90,3	134,99	6,12		
10	5	o	92,45	128,42	20		
11	6	k	89,99	123,48	23,32		
12	7	i	93,36	126,1	14,49		
13	8	s	92,94	124,07	16,49		
14	9	n	80,36	131,57	18,83		
15	10	v	97,51	128,89	19,8		
16	11	y	93,17	137,87	7,48		
17	12	d	96,3	122,9	30,92		
18	13	è	87,92	135,2	19,03		
19	14	r	89,92	128,34	24,07		
20	15	g	82,2	126,13	16,79		
21	16	f	95,09	126,2	28,44		
22	17	b	94,03	138,5	24,62		
23	18	a	82,38	125,18	23,71		
24	19	l	82,4	126,57	24,97		
25	20	ò	91,71	124,54	33,18		
26	21	à	82,48	134,97	15,36		
27	22	q	84,12	126,35	29,76		
28							

Fig. 45: example of an excel file in which the 3D measurements of a first series were recorded. Notice that the codified names are inserted in the column B.

Measurement technique

Radiographic and CT images:

To perform the measurements, the observers followed the general indications presented in literature.[2-7]

Anatomic lateral distal femoral angle (aLDFA):

The length of the femur was measured starting from the most proximal point of the femoral neck to the most distal aspect of the femoral trochlea. Then, two points were found at the center (equally spaced from the medial and lateral cortex) of the femoral diaphysis at one-third and one-half of the femur length. Finally, a line connecting these two center points was drawn and identified as the anatomic axis of the femur. Secondly, the distal joint line was depicted as a tangent connecting the most distal points of the medial and lateral condyles. The lateral distal angle obtained between these two lines represented the aLDFA.

Femoral neck angle (FNA)

First, the femoral head is superimposed using a best-fit circle; then the center of the sphere is found and it represents the first marked point. The midpoint in the narrowest region of the femoral neck is identified and it represents the second reference point. Thirdly, the axis if the femoral neck is drawn as it connected these two midpoints. The anatomic femoral axis is, then, depicted and the medial angle obtained is defined as the FNA.

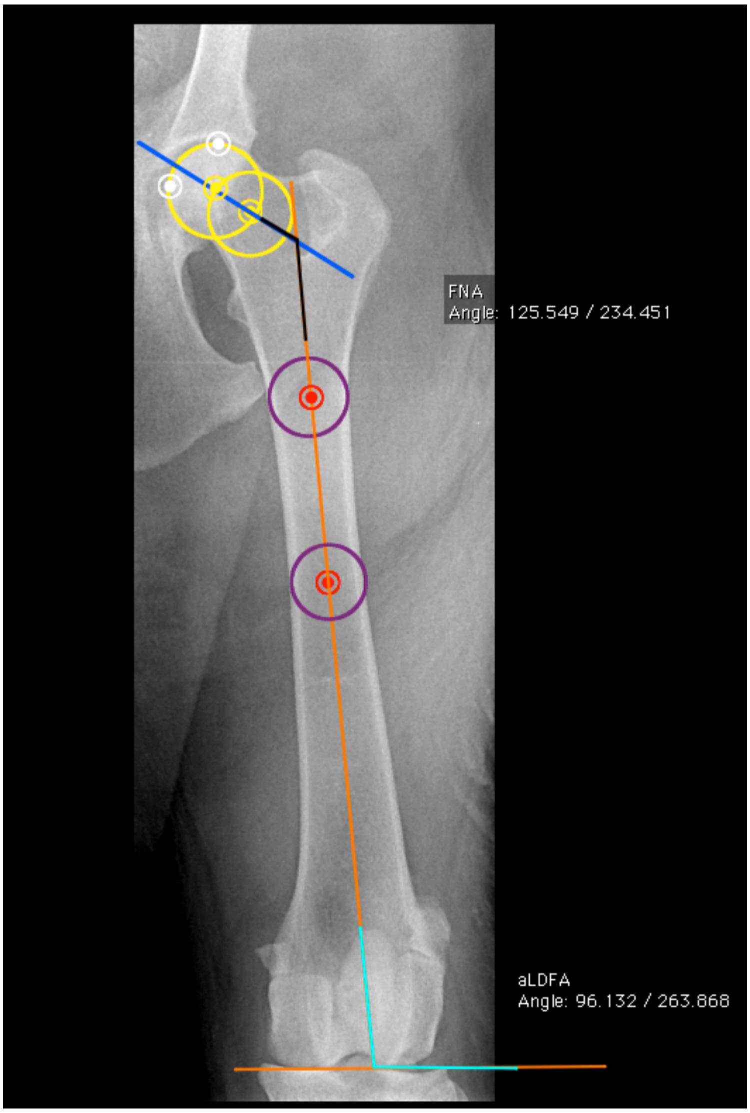

Fig. 46: radiographic measurement of aLDFA and FNA. Observe that circles were used to find the center in the femoral head and neck. Additionally, circles were put on the one-third and one-half of the femoral diaphysis to locate the referral points along which the PFLA passes. In this case, the FNA measures 125,54° and the aLDFA 96.13°.

Femoral torsion angle (FTA)

For the measurement of the radiographic FTA, the femoral head and neck axis was found using the same technique previously described for the FNA detection. Next, a line tangential to the caudal articular profile of the femoral condyles was found and defined as the transcondylar axis. The angle formed at the intersection of these lines was identified as the FTA or anteversion angle.

The FTA calculated in CT images was defined considering the identical referential points of the axial x-ray images but a different orientation of the femur was adopted. Again, the femoral head, neck and condyles were used as anatomical landmarks.

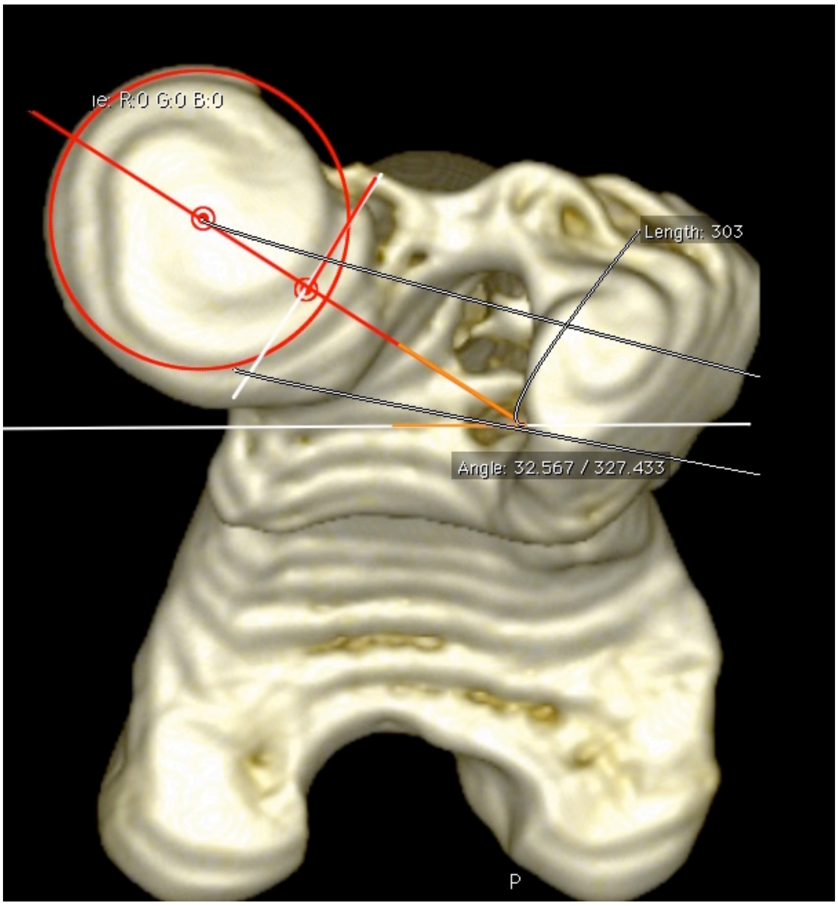

Fig. 47: tomographic measurement of the FTA. Notice the red circle that is superimposed to the femoral head with its own center as well as the white line crossing the femoral neck. To find the center of the femora neck, a line (white) connecting the edges of the neck was drawn and measured. The center of the neck corresponds to the half value of the length of the white line. In this case, the FTA was 32,56°.

3-D computation:

Prior to the start of 3D computational phase, examiners were trained to correctly use the program and practiced on some samples that were excluded from the study presented. Furthermore, a written manual was given as a reference to help them during the measurement assessment.

From a practical perspective, examiners imported in *Rhinoceros* the mesh models previously saved as STL files. After that, few user inputs are required to perform the computational process. First, the operator starts with the analysis of the mesh. Specifically, a coloured area appeared in inner part of the bone when the examiner clicks on the femur. This region is defined as the internal mesh. To impove the analysis of the bone, this internal region is eliminated as it may create some bias during the computational procedure. As a result, only the external mesh is adopted as a geometric model for the computation.

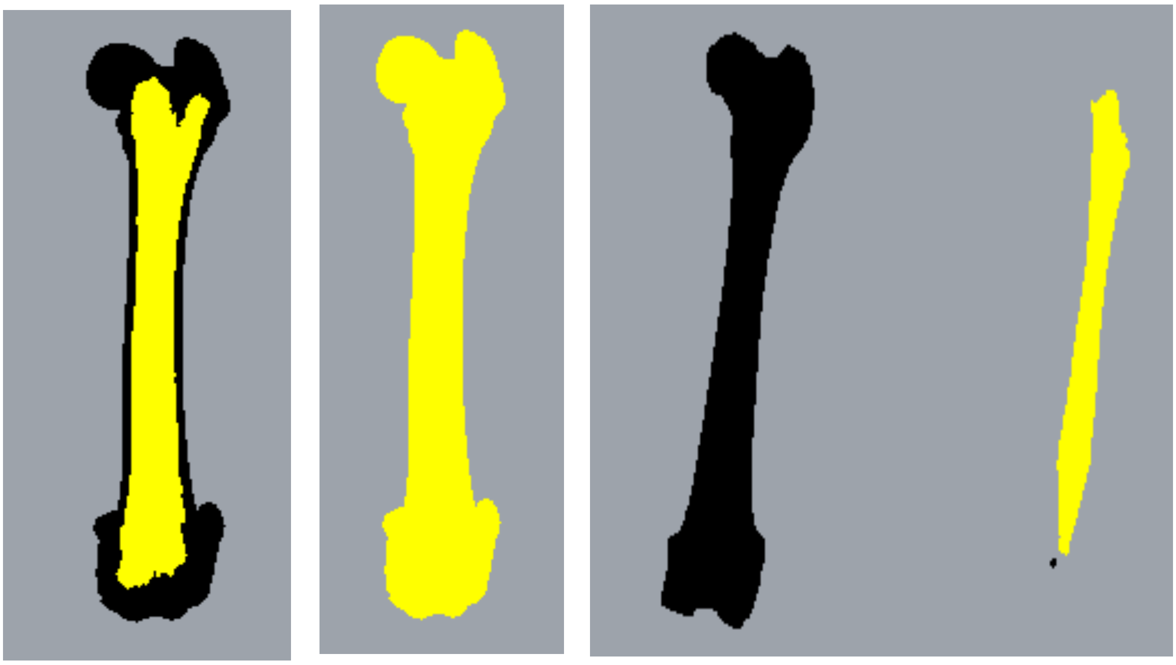

Fig. 48: pictures showing the selection of the internal (left image), external mesh (central picture) and the final aspect of the femur after the removal of the internal mesh.

After the cleaning phase, the second user input is represented by the selection of a point within the femoral head. This operation is necessary for the alignment of the femur along the z-axis. Prior to the start of the computation, the user had to modify some parameters in the anatomical distal axis section that were set for this study.

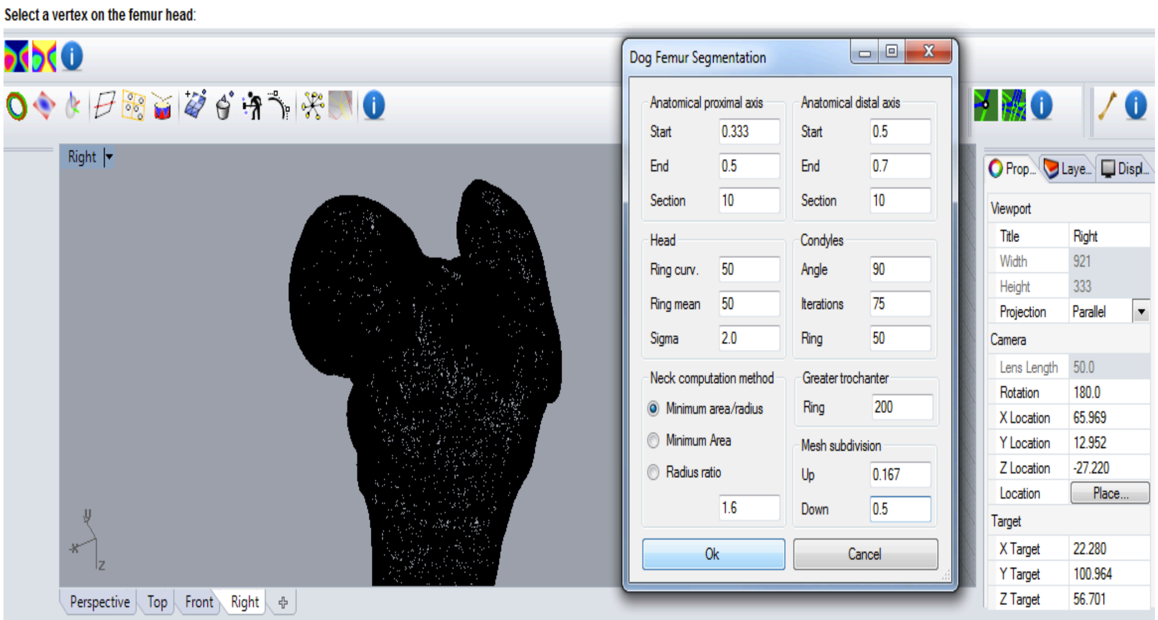

Fig. 49: after the selection of the femur icon, the command asks to select a vertex on the femur head. Next, the dog femur segmentation window appears (next to the femur) and the user modifies segmentation parameters.

To compute femoral angles, geometrical features such as point, axes, planes, spheres, must be primarily identified. As previously described (chapter 3), all the other phases are entirely computerized and do not require any other user inputs. Summarily, the algorithm proceeded with the following steps:

1. Femoral alignment
2. Analysis of the proximal femoral epiphysis
3. Analysis of the distal femoral epiphysis
4. Parameters computation

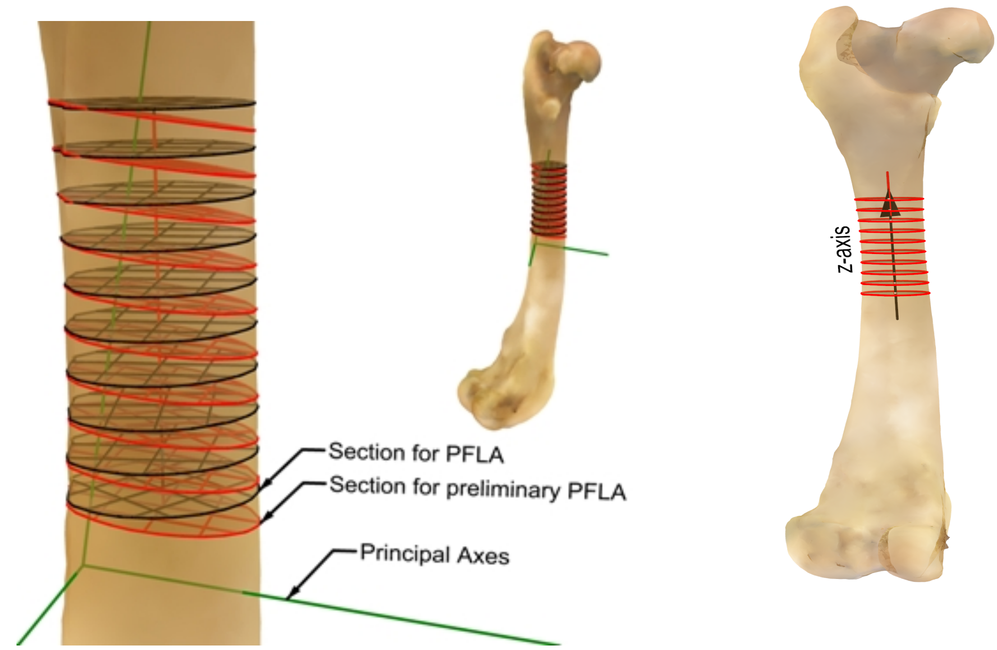

Fig. 50: phase 1: femoral alignment. The sections for the computing of PFLA are shown. They differ as sections for preliminary PFLA (red) and those for definitive PFLA (black). On the right, final orientation of the femur when alignment is compelted.

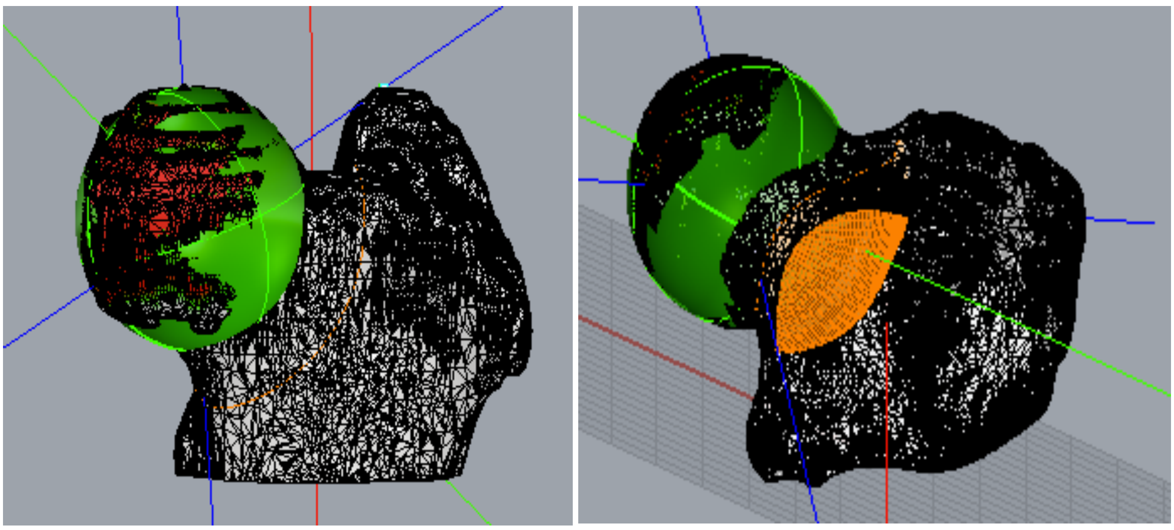

Fig. 51: phase 2: analysis of the proximal femoral epiphysis. The program, based on a curvature analysis, fitted the femoral head with a sphere. Since that the removal of the residual pieces of acetabulum and osteophytes is sometimes challenging during the segmentation and STL extraction phases; the algorithm was designed to avoid all the parts of the femoral head that do not fall within the curvature analysis set up. The red vertices in the left picture represent the portions of bone excluded

from the analysis. On the right, a distal to proximal transverse projection of the proximal epiphysis to show the spherical section of the neck (orange) that the algorithm has found.

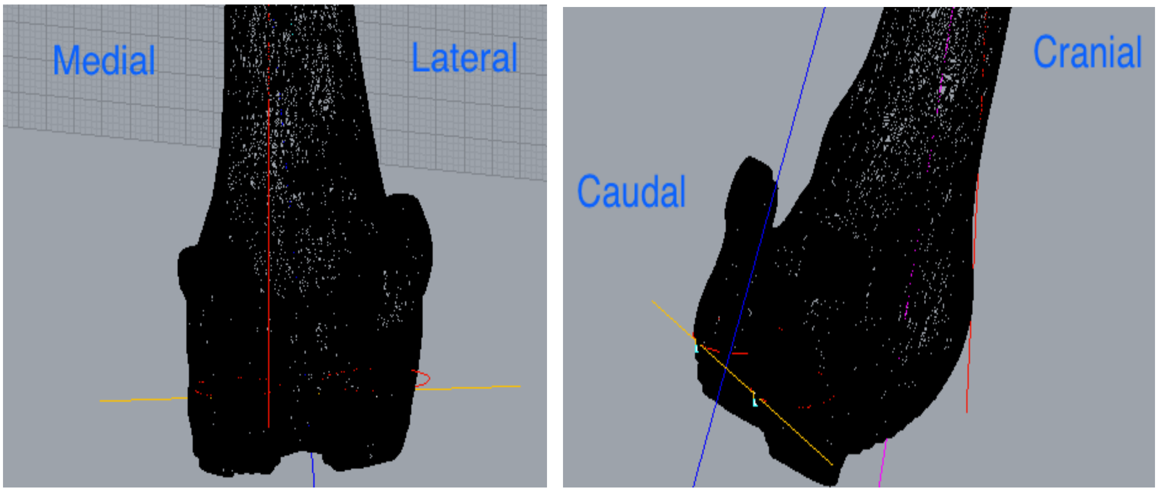

Fig. 52: phase 3: analysis of the distal femoral epiphysis. The PFLA (red line), TCA (gold line) and MA (blue line) are observable in both orthogonal images. Notice, also, the DFLA (purple line) in the right picture.

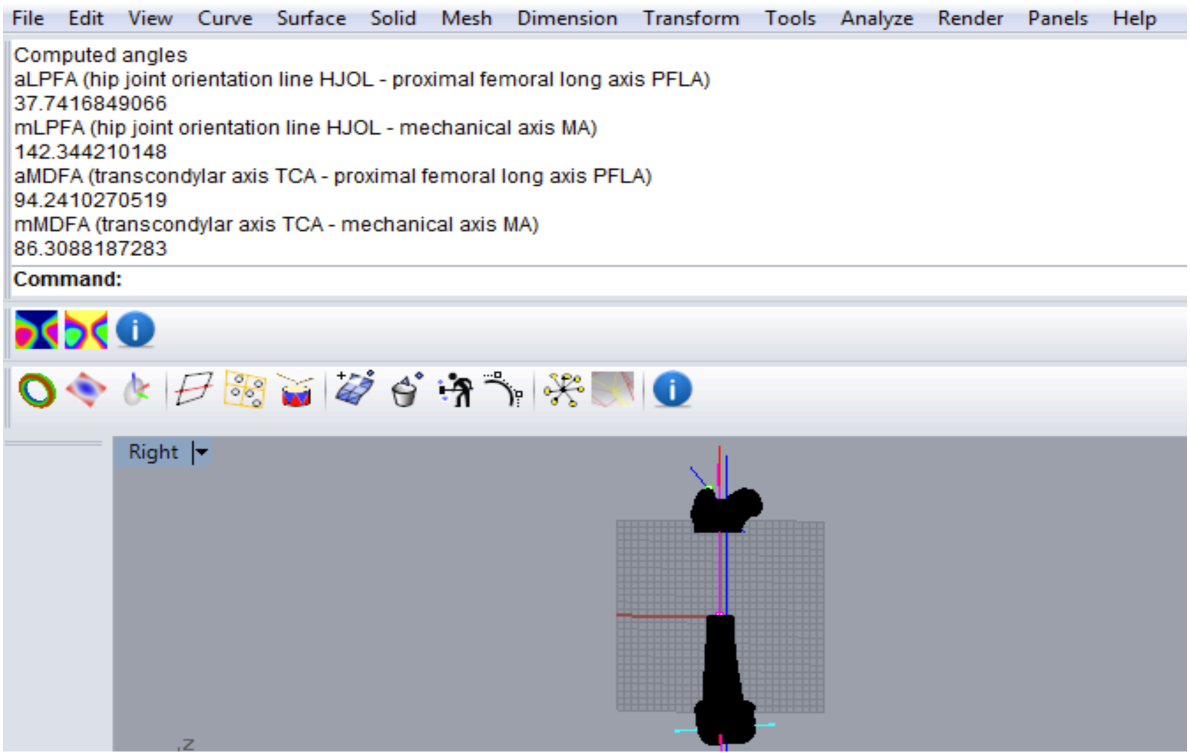

Fig. 53: phase 4: parameters computation. After the execution of the analysis, all the measurements will appear in an upper window.

When the algorithm of *Rhinoceros* finishes the computation phase, on the top view of the screen, all the femoral measurements appear (aLPFA, mLPFA, aLDFA, mLDFA, FNA, FTA, FVA, FL, H Rad, H Dist). For this study, observers only recorded the aLDFA, FNA and FTA.

STATISTICAL ANALYSIS

The measured values for each angle were analysed through the creation of three linear models for repeated measurements with fixed factors among which: observer, measurement repetition, diagnostic technique, as well as the interaction between them. Since that the repetition was not a significant factor, it was not included in any of the three models for the analysis of the angles.

Least square means method was adopted to compare the averages values and Bonferroni's correction was applied to evaluate differences present among the different levels of the analysed factors. Statistical significance was considered at P ($<0,05$). The repeatability (r) was measured as the coefficient of variance, calculated on the residual variance; reproducibility (R) was measured considering the variance of the diagnostic technique, repetition of measurements and interaction between these factors. Coefficients of variation < 5 % were considered acceptable.

Furthermore, means and standard deviations values were calculated for every measurement and summarized performing an average of the three sessions of measurement. Overall ranges for every angle measured with the three diagnostic techniques were, then, obtained.

RESULTS

Twenty-two femurs (10 right, 12 left) from sixteen dogs (10 males and 6 females) were included in the study. Eight femurs were excluded from the evaluation because they did not satisfy the inclusion criteria. Reasons for exclusion were: severe DJD of the proximal femoral epiphysis with femoral head deformation and neck thickening (5 cases); DJD of the distal femoral epiphysis with modification of the profile of femoral condyles (1 case), neoplastic-like alteration of the bone structure in the femoral head and in the distal epiphysis of the femur (2 cases).

The mean range age was 7.8 years (2.0-13.7), while the average of the weight was 29.3 Kg (15,5-43,2 kg). A total of 594 femurs samples were analysed from three blinded readers in 9 separate occasions. For each sample, three femoral angles (aLDFA, FNA and FTA) were calculated through three diagnostic techniques.

The range values (inter-observers means) for every angle were (table 7): for Rx aLDFA (90,75°-91,55°), FNA (123,93-126,56°) and FTA (22,03°-25,27°); for TC aLDFA (91,07-91,74°), FNA (125,16°- 127,25°) and FTA (23,05°- 25,84°); and for the 3D computation aLDFA (89,69°- 89,81°), FNA (128,11- 128,88°) and FTA (20,38°-21,28°). The overall ranges, regardless of the angle measured, for every diagnostic technique were: for Rx (0,8°-3,27°), for TC (0,67°-2,79°) and 3D (0,12°-0,9°).

The coefficients of variance, assessed considering observer and technique effect, for aLDFA within (repeatability) and between (reproducibility) examiners were (2,4 %-0,9 %); for FNA were (3,2% - 1,6%); whereas for FTA were (21,4%- 26,9%) (table 8).

For each reader, averages as well as standard deviation values of the angles measured in every session, are summarized (tables 9-17).

Diagn. Tech.	Observer 1			Observer 2			Observer 3		
	aLDFA°	*FNA°*	*FTA°*	*aLDFA°*	*FNA°*	*FTA°*	*aLDFA°*	*FNA°*	*FTA°*
RX	91,55°	123,93°	25,37°	90,75°	124,8°	22,03°	90,96°	126,56°	24,3°
TC	91,3°	125,16°	23,37°	91,74°	125,9°	23,05°	91,07°	127,25°	25,84°
3D	89,81	128,11	21,28°	89,75°	128,88°	20,38°	89,69°	128,69°	20,54°

Tab. 7: summary of the overall averages (mean of the three series) for angles measured through every diagnostic technique by every observer.

Angle	**Factor**	**level**	**LSE±SE§**	**F**	***P***	**Repeatability [CV]***	**Reproducibility [CV]****
FTA	Observer	1	23,10±1,34^{a}	6,67	<0,0031	21,4%	26,9%
		2	21,83±1,34^{b}				
		3	23,57±1,34^{a}				
	Diagn. Tech.	3D	20,44±1,34^{a}	35,34	<0,0001		
		RX	23,91±1,34^{b}				
		TC	24,14±1,34^{b}				
FNA	Observer	1	125,96±0,81^{a}	8,29	0,0009	3,2%	1,6%
		2	126,20±0,81^{a}				
		3	127,50±0,81^{b}				
	Diagn. Tech.	3D	128,79±0,81^{a}	46,74	<0,0001		
		RX	125,06±0,81^{b}				
		TC	125,81±0,81^{b}				
aLDFA	Observer	1	90,91±0,91	1,35	0,26	2,4%	0,9%
		2	90,76±0,91				
		3	90,54±0,91				
	Diagn. Tech.	3D	89,76±0,91^{a}	30,5	<0,0001		
		RX	91,06±0,91^{b}				
		TC	91,38±0,91^{b}				

Tab. 8: Analysis of the observer and diagnostic technique effect. Least square means of the measurements is reported with the standard error, supplied with value of the statistic test (F) and statistical significance (P). On the right, repeatability and reproducibility values calculated for each angle are expressed as coefficient of variance (CV).

*Repeatability (r) is expressed as the CV of the standard deviation of r, considering only the residual variance.

** Reproducibility (R) is expressed as the CV of the standard deviation R, considering the variance of the diagnostic technique, measurement repetition and factor interaction.

§ Different letters mean significant differences

FEMUR	aLDFA 1°	alDFA 2°	aLDFA 3°	FNA 1°	FNA 2°	FNA 3°	FTA 1°	FTA 2°	FTA 3°
1	92,69	94,38	93,8	124,32	132,2	130,95	25,44	33,98	29,97
2	97,37	98,94	93,86	120,98	117,68	124,85	31,06	46,43	25,72
3	98,85	98,74	99,46	123,37	120,62	122,65	26,59	39,77	40,34
4	95,76	95,18	95,19	126,22	126,19	124,52	27,85	32,77	38,73
5	93,94	93,74	94,21	123,16	124,06	119,6	19,17	27,79	18,31
6	93,46	95,26	93,48	128,21	124,32	123,3	23,87	31,16	16,61
7	90,36	87,82	87,83	123,92	117,19	117,53	23,07	26,58	22,47
8	88,18	91,55	90,64	120,08	122,43	118,31	30,19	27,32	26,35
9	84,7	86,23	82,95	133,08	130,46	127,37	19,17	14,71	9,13
10	87,76	80,81	79,86	129,88	127,83	129,3	15,4	17,68	14,56
11	93,66	89,47	92,47	128,67	125,27	123,6	37,18	25,72	32,32
12	91,27	91,83	93,89	121,76	123,16	115,48	23,88	21,02	20,12
13	95,39	98,81	98,55	123,31	122,44	129,73	14,1	38,37	28,3
14	88,98	84,56	86,27	121,43	118,89	120,47	18,89	30,09	21,47
15	86,17	87,14	85,36	120,22	121,9	119,23	16,62	15,5	19,5
16	92,08	83,37	87,64	134,27	121,28	118,93	22,98	22,38	15,05
17	92,53	94,4	95,01	121,9	129,22	127,08	16,03	12,79	14,43
18	92,07	89,78	89,44	124,08	122,05	120,9	16,3	16,57	19,36
19	88,6	90,47	88,81	119,94	119,47	119,83	27,55	22,53	46,02
20	91,79	94,01	91,68	124,53	130,56	130,83	27,25	31,47	23,44
21	92	91,48	92,21	130,28	124,98	127,36	38,98	35,72	18,85
22	97,26	94,77	94,29	121,87	120,32	120,16	41,07	32,54	28,36
MEAN	**92,03**	**91,42**	**91,22**	**124,79**	**123,75**	**123,27**	**24,66**	**27,40**	**24,06**
SD+-									

Tab. 9**:** RX measurements of the first observer.

FEMUR	aLDFA1°	alDFA2°	aLDFA3°	FNA1°	FNA2°	FNA3°	FTA1°	FTA2°	FTA3°
1	91,38	91,56	92,01	116,56	124,62	123,98	29,57	20,54	28,96
2	98,11	97,37	96,97	120,74	125,99	118,2	33,36	30,78	32,15
3	103,98	103,11	104,36	124	123,68	127,5	34,02	33,54	34,78
4	94,3	91,14	93	122,84	120,81	123,46	18,46	21,78	23,44
5	91,45	91	91,83	119,18	125,17	121,57	19,88	18,33	25,03
6	90,45	91,46	91,31	122,25	124,07	119,49	17,88	11,61	21,1
7	84,98	91	89,24	127,62	115,38	123,27	25,79	32,79	37,17
8	89,1	89,76	88,21	133,33	131,54	121,7	31,3	26,34	29,15
9	86,23	85,72	87,25	128,82	127,84	124,86	16,12	19,5	14,88
10	80,17	80,37	79,06	123,15	125,95	127,36	24,82	20,18	31,57
11	92,55	91,37	92,34	126,07	126,96	125,24	37,85	32,68	40,78
12	92,49	92,5	90,73	124,12	123,11	120,79	18,69	19,17	19,22
13	96,36	97,35	97,95	126,13	130,29	117,9	14,03	9,71	11,03
14	84,8	83,36	90,35	118,55	122,95	120,48	28,32	25,88	21,82
15	83,46	86,9	83,46	122,08	125,9	126,25	34,67	28,97	26,98
16	92,47	99,66	94,24	134,59	133,56	133,41	10,75	11,06	22,68
17	94,68	93,71	94,38	128,81	130,45	129,84	12,9	10,44	13,09
18	90,19	90,67	88,73	123,53	127,95	122,54	17,21	19,67	19,42
19	90,84	90,72	89,2	123,09	122,86	116,14	22,98	24,06	24,67
20	91,72	91,84	92,36	132,99	131	133,08	23,17	24,93	24,65
21	88,29	89,8	87,41	126,43	130,66	127,36	23,15	22,17	23,17
22	95,17	92,38	97,51	126,55	128,3	126,01	22,19	21,22	24,57
MEAN	**91,05**	**91,4**	**91,45**	**125,06**	**126,32**	**124,11**	**23,50**	**22,06**	**25,01**
SD+-	**5,25**	**5,0**	**5,24**	**4,70**	**4,15**	**4,58**	**7,62**	**7,19**	**7,44**

Tab. 10: TC measurements of the first observer.

FEMUR	aLDFA 1°	alDFA 2°	aLDFA 3°	FNA 1°	FNA 2°	FNA 3°	FTA 1°	FTA 2°	FTA 3°
1	95,09	93,23	94,3	126,2	126,9	126,56	28,44	28,85	27,8
2	89,99	90,09	88,91	123,48	124,85	119,01	23,32	24,42	25,15
3	96,3	97,13	96,1	122,9	125,5	123,18	30,92	30,52	28,23
4	93,45	94,7	94,42	127,89	129,11	128,73	16,54	14,74	17,41
5	92,94	93,5	92,97	124,07	126,88	126,14	16,49	17,81	15,45
6	92,45	93,15	92,31	128,42	126,8	128,51	20	19,75	19,86
7	82,4	83,38	83,89	126,57	127,58	124,58	24,97	24,73	26,46
8	84,12	84,72	85,23	126,35	125,2	126,27	29,76	31,77	25,52
9	82,48	82,85	82,79	134,97	134,08	134,09	13,36	11,93	12,02
10	80,36	80,93	81,16	131,57	130,45	132,97	18,83	18,27	17,87
11	91,71	93,6	91,38	124,54	126,8	126,81	33,18	30,5	30,49
12	93,36	92,27	93,3	126,1	127,1	127,9	14,49	13,03	14,79
13	94	93,45	93,67	129,49	129,14	129,5	10,25	15,1	11,3
14	82,38	82,79	82,15	125,18	125,72	124,91	23,71	23,65	23,35
15	82,2	82,85	81,54	126,13	126,6	126,28	16,79	17,04	16,75
16	93,17	92,7	91,7	137,87	137,89	138,08	7,48	7,02	8,02
17	90,3	90,8	90,1	134,99	134,9	134,91	6,12	6,1	5,12
18	89,92	90,3	89,91	128,34	125,5	128,34	24,07	23,05	24,21
19	87,89	88,47	87,8	124,57	124,6	124,57	24,72	24,65	24,71
20	94,03	94,12	93,3	138,5	136,49	136,88	24,62	24,82	26,3
21	87,92	87,98	88,7	135,2	135,24	135,1	19,03	17,4	18,79
22	97,51	98,18	97,45	127,92	128,89	128,9	19,8	22,26	21,32
MEAN	**89,72**	**90,05**	**89,68**	**128,69**	**128,91**	**128,73**	**20,31**	**20,33**	**20,04**
SD +-	**5,22**	**5,08**	**4,90**	**4,73**	**4,09**	**4,79**	**7,31**	**7,23**	**6,91**

Tab. 11: 3D measurements of the first observer.

FEMUR	aLDFA 1°	alDFA 2°	aLDFA 3°	FNA 1°	FNA 2°	FNA 3°	FTA 1°	FTA 2°	FTA 3°
1	93,4	92,51	92,78	129,41	122,61	127,22	26,3	30,81	27,8
2	99,31	98,12	90,95	124,18	123,31	122,12	31,62	30,31	7,4
3	100,22	100	99,54	124,73	125,33	129,72	27,27	32,41	28,6
4	94,4	97	92,05	128,27	120,42	118,13	13,27	23,51	11,6
5	95,09	93,44	93,8	120,23	122,32	121,34	17,73	16,39	17,23
6	96,23	99,03	93,44	123,03	122,53	126,52	10,04	24,05	12,22
7	87,63	88,93	87,11	125	118,71	117,2	27,33	28,43	21,3
8	88,45	90,81	87,29	130,11	121,52	115,6	31,23	25,12	29,21
9	82,23	82,81	82,96	127,72	131,81	129,81	20,3	18,04	17,34
10	82,61	81,22	82,22	125,83	132,56	128,83	7,82	22,51	21,22
11	90,08	89,42	89,17	128,05	128,33	133,34	41,51	40,09	44,02
12	91,51	89,92	91,09	124,55	125,71	120,6	19,04	17,5	18,4
13	94,13	95,52	94,73	131,63	139,31	140,97	13,7	20,63	16,2
14	84,79	86,55	83,27	129,61	126,22	116,95	17,51	10,77	21,2
15	89,43	86,33	86,51	120	120,21	115,.65	12,03	15,24	8,34
16	91,72	85,29	82,98	125,22	115,3	118,3	9,61	13,98	15,7
17	93	90,03	90,5	127,72	136,44	123,6	14,74	12,07	12,4
18	88,67	88,77	89,03	124,79	119,45	116,08	20,6	23,55	24,7
19	88,72	89,21	89,51	116,41	113,81	127,03	21,21	19,05	18,3
20	94	91,71	91,14	128,21	135,31	136,07	23,51	29,21	18,4
21	91,2	90,4	91,62	124,88	130,66	113,2	42,02	28,09	29,7
22	94,72	94,93	95,02	122,21	125,32	122,45	43,4	23,51	36
MEAN	**91,42**	**90,99**	**89,85**	**125,53**	**125,32**	**124,05**	**22,35**	**22,96**	**20,78**
SD +-	**4,71**	**5,02**	**4,45**	**3,68**	**6,74**	**7,32**	**10,55**	**7,32**	**8,99**

Tab. 12: RX measurements of the second observer.

FEMUR	aLDFA 1°	aLDFA 2°	aLDFA 3°	FNA 1°	FNA 2°	FNA 3°	FTA 1°	FTA 2°	FTA 3°
1	91,04	93,5	94,3	121,4	128	121,4	35,5	25,42	35,6
2	96,62	98,3	97,5	118,21	108,3	117,6	26,12	23,31	30,33
3	102,41	102,8	105	119,78	118,21	112,89	38,03	45,12	39,07
4	93,44	90,6	93,5	125,03	117,21	117,28	16,61	9,34	20,3
5	91,34	94	92,5	123,23	119,33	117,42	10,31	16,34	18,3
6	90,22	87	88	126,49	119,72	121,55	16,87	16,4	29,63
7	88,09	87,6	88	125,79	116,81	134	21,51	30,7	30,22
8	93,4	89,4	90	128,42	137,23	119,53	39,04	32,23	41,22
9	89,71	85,7	86	136,53	131,53	126,45	20,71	16,8	18,51
10	81,93	82,7	82,4	122,82	136,7	131	25,24	11	20,12
11	89,71	92	91,6	123,72	119,77	120,3	33,22	30,5	43,6
12	91,33	93,7	93	131,42	109,56	109,65	18,61	13,4	19,45
13	96,81	96	97	112,31	129,52	112,6	10,23	13,78	23,41
14	94,24	82,6	83,2	125,71	130,22	119,21	19,07	21,34	32,09
15	87,62	87,5	89,3	128,31	128,57	129,22	32,53	19,23	27,09
16	97,36	93,6	95,2	140,03	142,8	133	16,54	8,79	25,23
17	93,32	94,7	92,5	137,13	133,7	132,6	18,39	12,35	11,42
18	92,22	91	91,89	118,22	129,87	121,11	37,63	12,13	21,21
19	90,21	89	87,5	116,63	107	118	18,72	21,32	21,82
20	92,3	93	92,6	141,71	134	133,5	18,43	22,9	33,82
21	91,24	91,6	90,2	132,15	135,5	131,8	9,09	12,42	22,53
22	94,12	94,3	95	122,54	129,7	130	16,32	17,62	25,72
MEAN	**92,21**	**91,39**	**91,64**	**126,25**	**125,60**	**123,18**	**22,66**	**19,65**	**26,84**
SD+-	**4,08**	**4,81**	**4,98**	**7,70**	**10,05**	**7,59**	**9,37**	**8,93**	**8,26**

Tab. 13: TC measurements of the second observer.

FEMUR	aLDFA 1°	alDFA 2°	aLDFA 3°	FNA 1°	FNA 2°	FNA 3°	FTA 1°	FTA 2°	FTA 3°
1	94,03	93,36	93,49	126,17	126,04	128,59	28,42	28,81	28,63
2	89,99	88,87	89,81	123,43	123,97	124,8	23,21	25,34	27,56
3	96,3	97,1	97,96	122,81	124,8	123,19	30,98	30,56	28,35
4	93,44	94,71	94,42	127,71	128,12	128,72	16,58	14,75	16,11
5	93,03	93,54	92,96	127,04	128,14	126,14	17,87	16,11	15,43
6	90,58	91,95	92,06	128,38	128,73	128,66	20,02	20,54	20,87
7	82,43	81,89	82,5	126,59	125,3	125,89	24,99	26,78	24,76
8	84,16	86,31	85,94	126,34	126,89	125,81	29,84	27,74	32,78
9	83,54	83,71	82,27	134,93	133,98	134,07	14,41	11,98	11,95
10	80,36	81,73	81,44	131,53	132,51	132,51	18,44	17,83	17,83
11	90,73	91,37	91,24	124,52	126,75	126,75	32,19	30,84	30,53
12	92,67	92,86	93,26	126,12	125,43	127,86	14,45	15,22	14,76
13	93,94	93,71	93,96	129,43	129,33	129,45	10,26	11,23	12,04
14	82,38	82,78	82,14	125,15	124,99	125,01	23,74	23,67	23,4
15	82,16	82,82	81,51	126,08	126,24	126,17	16,83	17,01	16,77
16	93,1	91,67	92,54	137,85	138,05	138,13	7,5	8,04	7,93
17	90,33	90,76	90,4	134,96	134,89	134,95	6,13	6,12	6,27
18	89,89	90,28	89,88	128,17	125,43	128,29	24,18	23,12	24,22
19	88,81	88,41	87,75	124,5	124,29	124,54	24,76	24,76	24,71
20	94,02	93,96	93,3	136,95	136,47	136,87	24,64	24,96	26,33
21	87,91	89,63	88,68	135,18	135,24	135,1	19,06	18,91	18,81
22	96,54	97,92	96,91	128,87	128,87	128,13	20	22,27	20,66
MEAN	**89,56**	**89,97**	**89,74**	**128,75**	**128,83**	**129,07**	**20,38**	**20,29**	**20,48**
SD+-	**4,95**	**4,88**	**5,10**	**4,49**	**4,34**	**4,29**	**7,17**	**7,14**	**7,32**

Tab. 14: 3D measurements of the second observer.

FEMUR	aLDFA 1°	alDFA 2°	aLDFA 3°	FNA 1°	FNA 2°	FNA 3°	FTA 1°	FTA 2°	FTA 3°
1	92,95	92,4	94,15	120,86	129,1	133,22	30,5	34,2	33,41
2	98,88	94,4	91,44	115,66	122,8	124,81	34,28	33,9	7,96
3	97,96	100	100,31	124,93	118,9	117,17	28,8	34,2	34,25
4	95,14	96,1	93,7	128,46	124,6	125,72	22,79	15,3	28,29
5	93,82	93,8	94,9	123,35	125,9	130,14	21,02	22,6	20,21
6	97,13	94,7	93,13	129,48	124,1	124,46	19,8	15,1	25,52
7	90	88,5	87,66	124,07	123,8	115,78	28,57	25,2	23,29
8	90,18	90,9	87,44	124,49	126	121,47	33,29	31,2	33,31
9	85,23	88	86,41	133,21	135	135,09	21,06	15,4	12,31
10	83,63	81,4	82,75	122,3	131,2	135,43	21,6	21,7	18,92
11	90,49	91,6	89,77	127,08	123,3	125,08	39,5	33,1	37,92
12	90,13	91,4	92,43	124,83	124,2	123,33	14	18,2	14,41
13	96,62	97,4	95,41	119,21	124,1	131,91	17,02	25,3	23,35
14	84,6°	83,4	83,05	124,6	127,6	136,71	22,7	30,9	30,32
15	86,7	86,4	86,04	119,76	127,6	123,21	20,49	18,8	21,51
16	82,33	82,5	83,33	135,71	127,9	125,82	22,65	12,8	16,42
17	92,34	91,2	89,73	127,74	131,8	132,32	14,28	8,5	18,88
18	91,79	89,2	89,44	127,69	126,7	128,32	25,13	25,5	26,12
19	88,52	89,7	90,72	118,04	120,7	122,81	23,23	27,2	21,02
20	90,14	92,8	90,91	127,95	135,6	136,62	20,26	27,3	26,22
21	90,91	91,7	91,42	130,06	136,6	130,94	19,59	26,2	25,43
22	94,46	95,3	96,12	120,8	125,2	129,81	34,07	35,4	32,71
MEAN	**91,39**	**91,03**	**90,46**	**125,01**	**126,94**	**127,73**	**24,30**	**24,45**	**24,17**
SD+-	**4,53**	**4,72**	**4,52**	**4,92**	**4,67**	**5,99**	**6,74**	**7,89**	**7,70**

Tab. 15: RX measurements of the third observer.

FEMUR	aLDFA 1°	alDFA 2°	aLDFA 3°	FNA 1°	FNA 2°	FNA 3°	FTA 1°	FTA 2°	FTA 3°
1	91,27	91,2	90,02	128,42	135,4	126,87	34,49	33,5	32,64
2	96,54	94,3	90,2	122,44	117,6	122,1	31,91	33,9	30,2
3	95,15	91,6	92,98	128,29	134,3	132,13	37,46	29,4	32,23
4	92,09	93,7	94,31	120,54	125,5	124,48	21,07	25,9	23,22
5	93,45	92,1	90,18	122,59	126	123,8	19,24	17,2	16,51
6	90,91	92,5	89,74	124,95	132,5	126,5	24,3	31,6	23,73
7	88,41	90,1	92,76	130,23	130,3	135,4	24,03	34,6	29,05
8	90,63	90,3	90,17	127,2	131,1	128,39	33,89	36,9	34,72
9	89,05	87,2	88,3	138,7	134,1	137,12	32,15	21,2	23,31
10	83,82	81	81,4	133,45	128,7	127,4	21,9	21,8	21,56
11	91,62	91,9	94,3	124,43	121,5	122,36	36,18	31,5	29,42
12	92,52	92,1	92,65	124,6	123,4	125,13	17,73	21,7	19,42
13	98,07	98,2	96,17	125,4	120,9	122,81	20,7	27,5	23,25
14	83,1	84,6	82,95	125,17	126,3	125,32	25,37	30,1	28,77
15	86,3	86,4	87,2	126,43	126,1	125,82	28,49	24,4	26,82
16	93,65	94,3	91,1	130,14	132,2	129,44	17,34	24,7	18,71
17	92,81	92,7	91,12	129,44	130	128,34	13,73	16,6	12,23
18	91,57	90	91,91	131,79	123,5	124,33	29,82	29,4	30,9
19	89,53	89,8	89,93	118,63	122,9	121,1	24,63	24,6	25,67
20	93,71	91,7	94,26	131,33	125,8	126,33	23,56	27,7	23,21
21	88,8	90,8	91,25	136,81	123,8	126,51	24,41	20,1	20,34
22	97,69	95,9	94,93	131,94	125,4	126,63	25,95	22,4	24,83
MEAN	**91,39**	**91,01**	**90,81**	**127,86**	**127,15**	**126,74**	**25,83**	**26,66**	**25,03**
SD+-	**3,90**	**3,74**	**3,57**	**5,02**	**4,81**	**4,01**	**6,50**	**5,72**	**5,66**

Tab. 16: TC measurements of the third observer.

FEMUR	aLDFA 1°	alDFA 2°	aLDFA 3°	FNA1°	FNA2°	FNA3°	FTA1°	FTA2°	FTA3°
1	94,05	94,39	93,22	126,18	126,19	127,03	28,42	28,44	28,48
2	87,83	89,98	89,38	127,75	123,46	123,18	26,05	26,89	25,73
3	96,31	96,3	97,2	122,8	122,86	124,81	30,97	30,92	30,57
4	93,44	93,24	94,71	127,72	127,72	129,12	16,58	16,58	14,74
5	93,08	93,03	93,54	125,02	124,07	126,89	14,49	16,44	17,78
6	92,71	92,41	93,15	129,39	128,39	129,3	21,02	20,02	20,3
7	81,72	82,43	83,5	125,98	126,58	125,89	24,19	24,99	24,76
8	83,53	84,16	84,34	125,14	126,34	125,21	29,04	29,84	31,77
9	82,94	81,87	82,28	133,95	132,18	134,09	12,01	13,78	11,94
10	80,58	80,36	80,68	132,38	131,54	132,47	17,4	18,44	17,21
11	91,54	91,71	91,42	124,92	124,53	126,76	32,29	32,19	30,17
12	93,88	93,37	91,26	126,91	126,11	127,1	15,23	14,45	13,95
13	94,12	93,94	93,94	131,39	129,92	129,44	15,65	13,12	10,22
14	83,24	82,38	82,78	125,76	125,15	124,99	23,07	23,74	23,67
15	82,17	82,16	82,82	126,98	126,08	126,24	17,23	16,84	17,01
16	93,83	93,1	91,74	137,25	137,85	137,5	8,2	7,48	7,63
17	90,2	89,68	90,8	133,62	134,96	134,67	6,93	6,13	6,64
18	89,39	89,89	90,28	127,62	128,18	126,43	24,98	24,18	23,12
19	88,45	87,81	88,41	124,01	124,51	124,29	25,26	24,76	24,67
20	94,02	94,02	93,36	136,05	136,95	136,56	24,03	24,63	26,73
21	88,42	87,89	88,69	133,79	135,19	134,47	20,63	19,05	19,74
22	97,94	96,54	98,11	127,79	128,15	128,56	20,72	20	22,39
MEAN	**89,69**	**89,57**	**89,80**	**128,74**	**128,49**	**128,86**	**20,65**	**20,58**	**20,41**
SD+-	**5,24**	**5,15**	**5,04**	**4,11**	**4,45**	**4,22**	**6,97**	**7,17**	**7,40**

Tab. 17: 3D measurements of the third observer.

DISCUSSION

This study investigated the repeatability (intra- observer variability) and reproducibility (inter-observer variability) of three diagnostic techniques for the measurement of three femoral angles that are usually assessed when a femoral deformity is questioned.[2-7,13-16]

Whereas protocols adopting radiographs and CT-scans have been reported to explore the repeatability and reproducibility of femoral measurements,[2-8] little if any mention to 3D femoral computation was made. To bridge this gap a recent publication described a novel 3D approach for the computation of canine femoral angles.[17] The outcomes of that research highlighted the benefits of automatically measuring femoral angles with minimal of user-input application. The conclusions of that paper stated that the proposed method offers reliable information about the 3D bone conformation with the possibility of performing the computation of morphometric parameters. One of the most relevant advantages highlighted is the decreasing of operator-related bias. However, the source of data developed for the 3D femoral analysis was obtained through a 3D scanner[17]; thus, not a commonly available diagnostic tool.

Considering the larger availability of CT equipment in veterinary practices, one of the aims of the present study was to explore the feasibility of a 3D femoral computation, through the elaborations of mesh models derived from CT imaging. Moreover, repeatability and reproducibility were investigated as the precision of a methodology is defined by the variation of results achieved, by testing the same samples in several occasions.[2-4,8] To achieve this purpose, two universally adopted diagnostic techniques (RX and CT) and a novel methodology (3D), were compared.

Our outcomes emphasize that the femoral measurements exhibited a different trend in relation to diagnostic technique adopted, having the 3D computation the most consistent and precise protocol (table 7). In fact, looking at the overall ranges differences, 3D approach has only 0,12° of range excursion (inter-observer mean difference) for aLDFA, 0,77° FNA and 0,9° for FTA. On the contrary, examiners performed differently with RX and CT, showing a less robust trend. Measurements obtained through radiographic projections had a 0,8° excursion for aLDFA, 2,63° FNA and 3,27° for FTA. For CT, the ranges for aLDFA, FNA and FTA were respectively: 0,67°; 2,09° and 2,79°. These results support the conclusions of Savio et al. (2016)[16], confirming the thesis that an automatic 3D computation remarkably decrease the operator-related bias as well as the errors linked to the positioning. As reported in table 8, also RX and TC performed well in two of three angles but their assessment was not consistent as 3D. The most frequent causes for a not perfect agreement of the measurements could be ascribable to errors due to positioning, measuring, and recording of data that could occur at the time of image acquisition, at the stage of orientation of the reconstruction plane.[18-20]

Our methods were consistent with the commonly accepted guidelines for the positioning of the femur,[2-6] except for a TC projection.

As concerns radiography, literature reports several criterions to correctly position and different approaches to compute femoral axes and angles are described. [xx] In our study, the axes and angles were assessed taking the same reference anatomical landmarks described by Tomlison et al.[5] for the cranio-caudal view and Dudley et al.[4] relative to axial projection.

With regard to the CT technique, two different protocols were adopted for each projection. For the cranio-caudal view, we positioned the femur using the procedure described by Oxley et al.[8] In that paper a standardized approach for the determination of the FVA was presented to evaluate its precision. The conclusions of the study encouraged the use of the methodology reported, in view of the low intra- and inter-observer variability. Therefore, a valid purpose to select this approach is ascribable to the critical importance of adopting a standardization of the sagittal and rotational plane orientation, especially when a bone characterized by a physiological procurvatum is assessed. [8]

The estimation of the FTA, in the CT axial view, was performed using a different positioning of the femur. In fact, traditionally, the torsion angle could be assessed simulating a radiographic projection (distal-proximal view)[9,10] as well as performing multi-planar reformatting scans of the proximal and distal femoral epiphyses.[4] On the contrary, we positioned the femur in a proximal to distal orientation, with the femoral condyles tangent to a horizontal reference line, femoral head and neck supra-elevated and diaphysis partially visible. The proposed positioning allowed for a suitable alignment of the femoral condyles on the same plane (transverse), simplifying, therefore, the assessment of the TCA. Moreover, the width and the edges of the femoral neck were detectable, hence likely reducing the frequent struggles for the finding of the neck midpoint. However, the technique adopted for the measurement of the FTA was the same used in the x-ray images, indeed it was performed considering the identical referential points as well as drawing the same axes.

The results concerning the radiographic and tomographic assessments show that the aLDFA computation was the most easier and consistent angle to measure, while the FTA measurement was the most challenging. This trend may find an explanation in both femur positioning and anatomical landmarks considered for the computation. aLDFA and FNA are measured in the frontal plane, so even though several papers report that these angles are susceptible to malpositioning,[3,8,18,20] the identification of the correct anatomical landmarks is not as challenging as the one needed for the FTA computation. For instance, the identification, in the transverse plane, of the edges of femoral neck is sometimes frustrating because of the superimposition of the distal femoral epiphysis that may be augmented when a femoral varus is present. Furthermore, the precise fitting of the femoral head could be difficult, especially in the case of a femoral retroversion. Finally, the positioning of the femoral diaphysis with the intramedullary canal entirely visible could be harder to obtain as well either during the radiographic positioning or the TC femoral orientation. For this reason, we opted for a different transverse TC projection, that allowed us to put into the foreground the proximal femoral epiphysis and have the femoral condyles on the same plane.

Three-dimensional measurement of morphometric parameters such as angles represented a novel topic for veterinary literature. As a result, the methodology used to perform the computation was not entirely known and required an in-depth practical training for the readers. In fact, to avoid operator-related bias caused by the inexperience of using the recently described 3D software, observers were trained to use the program and were given a written manual as a reference to assist them during the primary phases of the computation. Additionally, examiners practiced on some samples excluded from the research prior to the start of the evaluation. Once the examiners learnt to correctly use the CAD software, they could easily perform the computation and the time spent for the 3D assessment progressively decreased among the three sessions.

The three-dimensional averages of the three sessions of measurements performed by each reader, evidenced a similar trend to RX and TC in identifying the more easiest and most difficult angle to calculate (aLDFA and FTA, respectively). However, 3D approach resulted the more precise protocol, showing a major consistency, testified by the maximum values for range excursion (0,12°, 0,77° and 0,9 °) in the aLDFA, FNA and FTA computation. All these values are lower than those obtained with the other two diagnostic techniques.

Looking at the overall repeatability and reproducibility, weighed on operator and instrument effect, we considered the coefficients of variance for the aLDFA (2,4%; 0,9%) and FNA (3,2%;1,6%) acceptable, whereas those related to FTA (21,4%; 26,9%) resulted unacceptable (table 8). The present synthesis of data confirmed the previously explained considerations. First, the aLDFA measurement was the most repeatable and reproducible. Additionally, table 8 shows that, for this angle, no statistically significant difference was detected between observers; whereas a significant difference was found in the comparison between 3D approach with RX and TC. Again, 3D was the most consistent technique, presenting a 0,55° difference in excursion range from the TC measurement, and a 0,68° of excursion from Rx assessment, hence more than 0,5° of difference.

Second, FTA is the most challenging angle to measure with both observers and diagnostic technique have an impact on its measurement. Also in this case, a significant difference in the comparison of the diagnostic techniques was found. Additionally, the discordancy detected among observers have actively contributed to increase the coefficients of variance (table 8).

Finally, analysing the timing employed to prepare the images on which performing the measurements, we can state that radiography is the faster technique, since the isolation of bone structures, is not required. However, the radiographic study is more difficult to perform rather than the acquisition of CT data. Furthermore, it is a biplanar approach and, thus, affected by all the shortcomings previously cited.[2-6] TC and 3D share the same timeframe needed for bone isolation with the remarkable difference that TC measurements, like radiographs, are performed in 2D images.

Considering only the computation process, 3D analysis is the faster technique, since that, once it started, the program usually needs nearly less than a minute and a half to compute all the parameters. All the potential bias user-dependent are only restricted to the accuracy with which the femur is isolated from the other bony structures. In this sense, an occasional difficulty encountered by the examiners, during the STL extraction phase, was the isolation of the femoral head from the acetabulum. This operation could be sometimes complicated, above all when severe osteoarthritis alters bone profiles. The latter consideration was critical as the more precise is the bone isolation, the more accurate will be the computational process performed by the software. To bypass this potential problem, as well as to expand the possibility of analysing more easily, also, pathological femurs, some modifications to the algorithm were developed and supplied. As shown in figure 51, the algorithm was set up to exclude from the femoral computation all that bone parts that do not fall within the curvature analysis. As a result, the algorithm did not select anymore the upper vertex in the femoral head but only a point within it.

REFERENCES

1. Savio G, Baroni T, Concheri G, et al: Mesh processing for morphological and clinical parameters computation in dog femur. *Research in Interactive Design* (Vol. 4) Springer 2016; 302-307
2. Palmer RH, Ikuta CL, Cadmus JM: Comparison of femoral angulation measurement between radiographs and anatomic specimens across a broad range of varus conformations. *Vet Surg* 2011;40:1023-1028
3. Swiderski JK, Radecki SV, Park RD, et al: Comparison of radiographic and anatomic femoral varus angle measurements in normal dogs. *Vet Surg* 2008;37:43-48
4. Dudley RM, Kowaleski MP, Drost WT, et al: Radiographic and computed tomographic determination of femoral varus and torsion in the dog. *Vet Radiol Ultrasound* 2006;47:546-552
5. Tomlison J, Fox D, Cook JL, et al.: Measurement of femoral angles in four dogs breeds. *Vet Surg* 2007;36:593-598
6. Petazzoni M: Radiographic measurements of the femur in Petazzoni M and Jaerger GH (eds): *Atlas of clinical goniometry and radiographic measurements of the canine pelvic limb*. Duluth, GA, Merial, 2008, pp 34-54
7. Hauptman J, Cardinet GH, Morgan JP, et al: Angle of inclination and anteroversion in hip dysplasia in the dog. *Am J Vet Res* 1985; 46:2033-2036
8. Oxley B, Gemmill TJ, Pink J, et al: Precision of a novel computed tomographic method for quantification of femoral varus in dogs and an assessment of the effect of femoral malpositioning. *Vet Surg* 2013;42:751-758
9. Towle HA, Griffon DJ, Thomas MW, et al: Pre-and postoperative radiographic and computed tomographic evaluation of dogs with medial patellar luxation. *Vet Surg* 2005;34:265-272
10. Mostafa, A. A., Griffon, D. J., Thomas etal.: Radiographic Evaluation of Femoral Torsion and Correlation With Computed Tomographic Techniques in Labrador Retrievers With and Without Cranial Cruciate Ligament Disease. *Vet Surg* 2014; 43: 534–541
11. Schreiber JJ, Anderson PA, Rosas HG, Buchholz AL and Anthony G: Hounsfield units for assessing bone mineral density and strength: a tool for osteoporosis management. *J bone joint surg*, 2011;93:1057-1063.

12. Shapurian T, Damoulis PD, Reiser GM, Griffin TJ and Rand WM: Quantitative Evaluation of Bone Density Using the Hounsfield Index. *Int J Oral Maxillofac Implants*, 2006;21 (2):290-297.
13. Gibbons SE, Macias C, Tonzing MA, et al: Patellar luxation in 70 large breed dogs. *J Small Anim Pract* 2006;47:3-9
14. Yasukawa S, Edamura K, Tanegashima K, et al: Evaluation of bone deformities of the femur, tibia, and patella in Toy Poodles with medial patellar luxation using computed tomography. *Vet Comp Orthop Traumatol* 2016; 29: 29–38
15. Johnson AL, Broaddus KD, Hauptman JG, et al: Vertical patellar position in large-breed dogs with clinically normal stifles and large-breed dogs with medial patellar luxation. *Vet Surg* 2006;35:78-818
16. Soporat C, Wangdee C, Chuthatep S, et al.: Radiographic measurement of femoral varus in Pomeranian dogs with and without medial patellar luxation. *Vet Comp Orthop Traumatol* 2012;25: 195-201
17. Savio G, Baroni T, Concheri G et al.: Computation of femoral canine morphometric parameters in three-dimensional geometrical models. *Vet Surg* 2016; 45(8):987-995
18. Barnes DM, Anderson AA, Frost C, et al: Repeatability and reproducibility of measurements of femoral and tibial alignment using a computed tomography multiplanar reconstructions. *Vet Surg* 2015;44:85-93
19. Franklin SP, Franklin AL, Wilson H, et al.: The relationship of the canine femoral head to the femoral neck: an anatomic study with relevance for hip arthroplasty implant design and implantation. *Vet Surg* 2012;41: 86-93
20. Jackson GM, Wendelburg KL: Evaluation of the effect of distal femoral elevation on radiographic measurement of the anatomic lateral distal femoral angle. *Vet Surg* 2012;41:994–1001

CHAPTER 6

COMPUTER-ASSISTED SURGICAL CORRECTION OF A FEMORAL DEFORMITY IN A DOG: THE TRASLATIONAL APPLICATION OF A 3D GEOMETRICAL MODEL FOR CORRECTIVE OSTEOTOMIES

This chapter was adapted from: Longo F, Savio G, Conchieri G and Isola M.: Computer-assisted surgical correction of bone deformities: a case series. Incoming submission.

SUMMARY

A third-degree medial patella luxation was diagnosed in a 13 months old female Labrador Retriever. A complete radiographic study was primarily performed to confirm the diagnosis, followed by a CT scan. A 3D reconstruction, based on a tomographic evaluation of the affected limb was, then, executed. Next, a 3D computation was performed and compared to CT measurements previously taken in biplanar images. Custom-made guides were designed using the 3D reconstruction of the pathological femur as a reference model onto which the guides were created. As a result, a unique matching between the surgical guides and the femur was obtained. The custom-made guides were successfully used intra-operatively and allowed for an easy detection of the anatomical CORA as well as they actively guided the orientation of the osteotomy cutting plane. The latter aspects represent the main benefits in using such surgical tools, as they act both as precise intraoperative localizers of osteotomy corrective landmarks and surgical saw guides.

MATERIAL AND METHODS

CASE HISTORY:

The clinical case reported was a 13 months old female, Labrador retriever of 26,5 kg presented at the Veterinary Teaching Hospital of the University of Padova for a sub-acute onset of a left pelvic limb lameness.

On presentation, the dog exhibited lameness (grade 2/4) at walking that got worsen at trot (grade 3/4) with an internal rotation of the stifle.

Physical inspection showed a significant swelling in the left stifle with a III degree medial patellar luxation (grade 3/4) and pain demonstrated during the extension phase of the stifle joint. On the right pelvic limb, a mild medial patellar luxation (grade 1/4) was found with no pain detectable during the passive motion of the stifle.

The subject was sedated using 0,010 mg/kg I/M medetomidine (Sedator, A.T.I. s.r.l., Bologna, Italy) and 0,2 mg/kg I/M butorphanol tartrate (Dolorex, Animal Health, Milano, Italy) and a complete radiographic study of the pelvis and left hind limb was performed.

The ventro-dorsal standard view and the left cranio-caudal projection of the femur confirmed the presence of the medial patellar luxation with an apparent varus deformity. Femoral varus was also manifest with the medio-lateral view in which a lower position of the lateral femoral condyle was present. The radiographic study of the tibia did not show any signs of frontal or transverse deformity. Next, after discussing with owner diagnosis and possible surgical therapies, a tomographic study of both pelvic limbs was proposed with the aim of verifying the presence of torsion on the femur affected and to obtain a 3D reconstruction of the bone model.

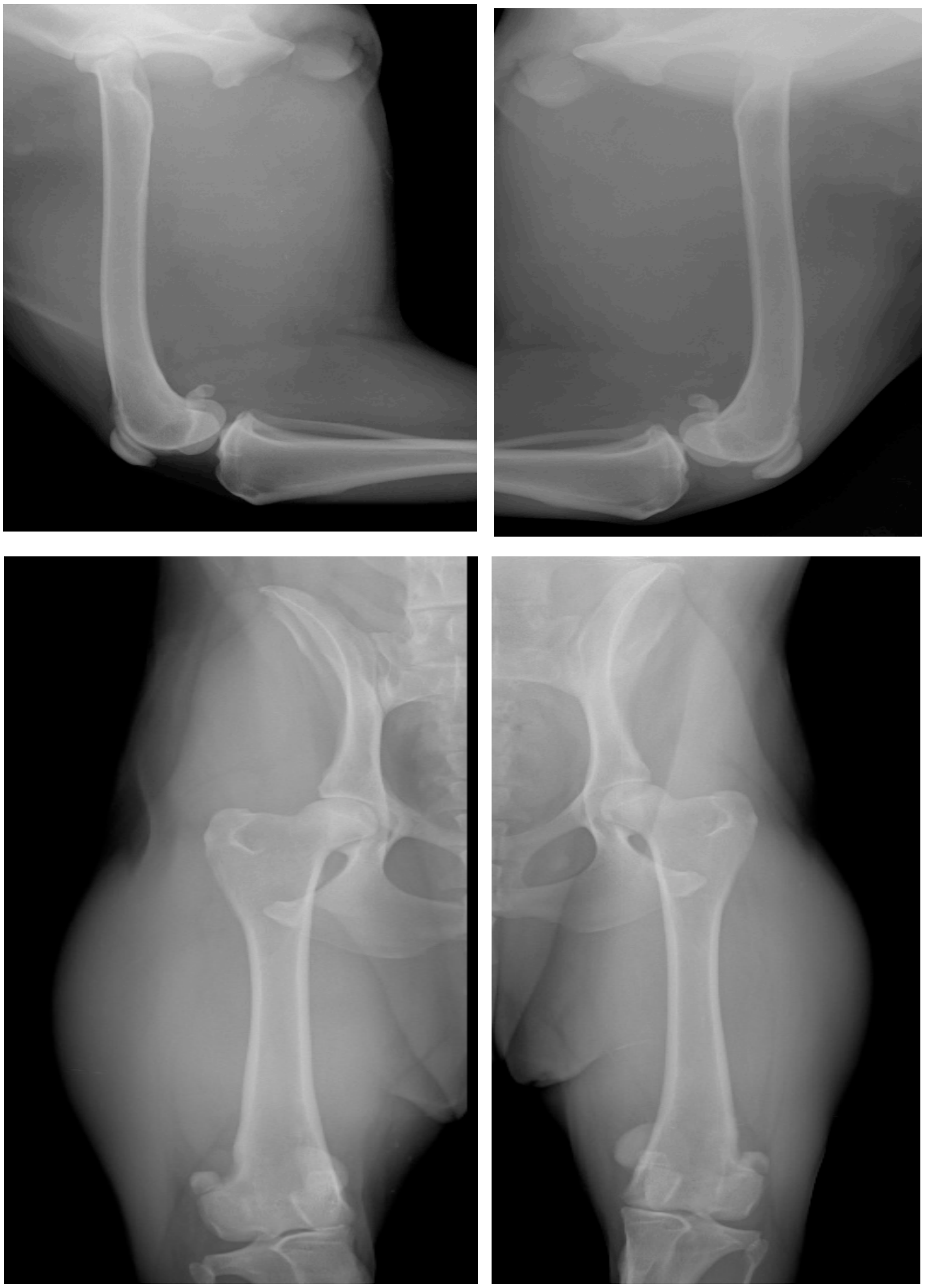

Fig. 54: radiographic study that includes two medio-lateral projections as well as two cranio-caudal view of each femur obtained through a sitting position. Notice the bilateral medial patellar luxation, with the left stifle (right image at the bottom) having a worse grade.

Under sedation, the dog was positioned on a foam cradle in dorsal recumbency with the hind limbs legs extended and slightly intra-rotated. Imaging was performed in a caudo-cranial direction using a 4-multi-detector-row CT scanner (Toshiba Asteion S4, Toshiba Medical Systems Europe, Zoetermeer, South Holland, The Netherlands) in helical acquisition mode with a slice thickness of 1 mm. CT images were reconstructed with a bone filter in a commercial software (Osirix) and the femur was positioned and aligned following the procedure described in the previous chapter. After that, the computation of femoral angles was primarily performed in biplanar images saved (Fig. 55). A left pathological femoral varus was confirmed (aLDFA: 102,13°), the CORA was identified and quantified (8,16°). The FTA was 27,63 ° and thus was not considered pathological since it matched the values of the contra-lateral limb and, most of all, was within the range values proposed by literature.[1-3]

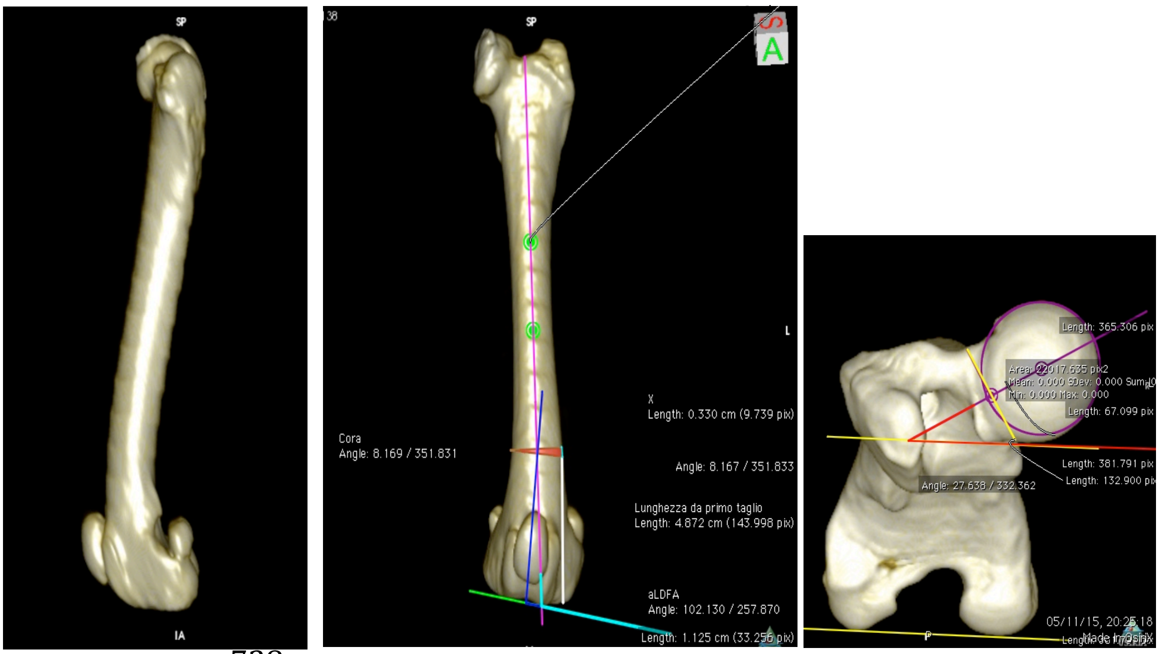

Fig. 55: tomographic images of the femur. Medio-latera, cranio-caudal and axial views are shown. Measurements of CORA (8,16°), aLDFA (102,13°) and FTA (27,63°) were performed.

Next, the 3D reconstructed model (DICOM) was converted and saved as a STL file to be imported and manipulated in Rhinoceros. The CAD software analysed the femur using the algorithm previously described. The 3D computation was performed with two purposes. The first was to compare the 3D values with those measured in CT images. Secondly, we used the 3D approach in order to obtain a geometrical model on which we could create and customize two surgical guides that would have intra-operatively assist the corrective osteotomy.

Once the femur was imported in Rhino, we started the analysis and computational process. The angles measured were slightly divergent from those calculated in CT images as the 3D aLDFA was 104,3° and FTA 23,5°.

The surgical guides were customized starting from the geometrical model developed in Rhino, and then using a protocol that has been developed during this study but won't be here described in detail, as it is not the object of the present research.

Fig. 56: Preoperative image of the femoral model onto which the two surgical guides were customized and applied.

Briefly, the distal femoral joint surface was located using the software and a plane perpendicular to the line was found. Then, the plane was advanced in distal to proximal direction until meeting of the CORA previously detected. Another plane, perpendicular to the PFLA was created and located in a point where it met the distal plane in the medial femoral cortex. The wedge, so defined, was removed and the femoral fragments manipulated until the gap was closed with apposition of the bone cortices with a different frontal alignment achieved. The surgical guides customized were exactly contoured to the bone and, then, produced with a 3D printer. They were made of polymetylmethacrylate (PMMA) and, later, hardened and set aside for surgical sterilization.

Finally, the computer-assisted femoral corrective osteotomy was proposed to the owner once the customized surgical guides were set and laboratory evaluation had excluded any type of diseases that could have prevent the surgery.

RESULTS

TREATMENT:

The surgical plan included localization of the CORA in cranial surface of the femoral distal metaphysis, positioning of the customized surgical guides, closing wedge osteotomy, osteosynthesis using an angle stable implant (Fixin Intrauma,Rivoli (TO)) and trocheoplasty.

The corrective femoral osteotomy was performed with the patient under general anaesthesia (induction with I/V propofol 2mg/kg, and maintenance with isofluorane in oxygen) and performing a sciatic block.

A lateral longitudinal skin incision, starting from the mid femoral diaphysis region till the tibial tuberosity, close to the fibular head, was performed. The subcutaneous tissue was then dissected and the biceps fascia incised. Gelpi retractors were positioned between the *biceps femoris* and the *vastus lateralis* muscles and caudal femoral vessels were ligated. The joint capsule was incised and incision extended in proximal to distal direction, taking care to preserve the *exstensor digitorum longus* muscle. The capsule was retracted from the lateral femoral condyle in order to better visualize the fat pad and, thus, cruciate ligaments and menisci were inspected for their integrity. The deepening and the torsion of the trochlear groove were evaluated before the osteosynthesis. After that, the joint capsule was further retracted in a caudo-distal direction with the aim of visualize the most proximal point of the lateral femoral *labrum.* From this anatomical landmark, a distance of 3.3 cm was taken with a surgical ruler to locate in the femoral shaft the anatomical CORA. The Cora position was marked in the formal cortices with a cautery. After that, the distal customized saw guides were slide along the femur until their matching with the bone surface. Moreover, they were held in place with a 1.0 mm K-wire. Next, a Fixin plate (6 holes, 3.5 mm of diameter and mm long) was pre-positioned along the lateral surface of the femoral shaft to check the position, direction of the screws, as well as distal screw bone purchase.

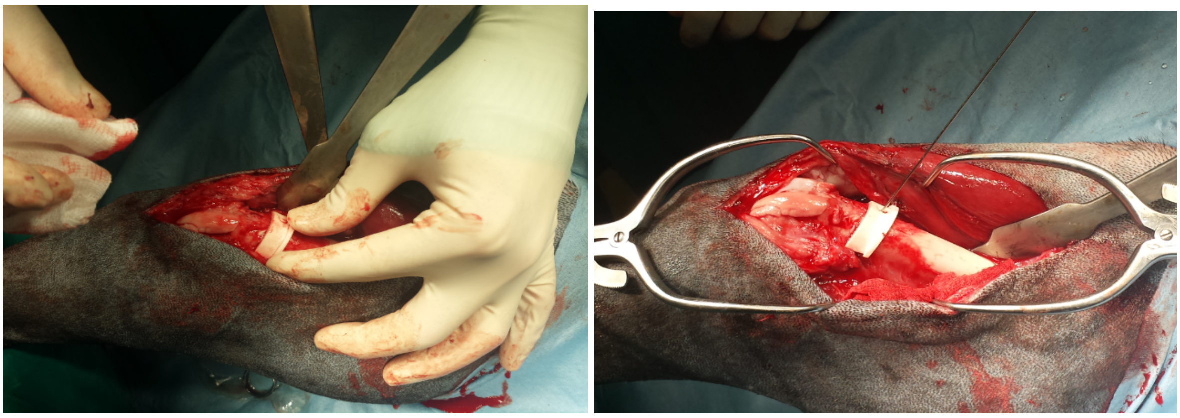

Fig. 57: insertion and fixation of the distal surgical saw guide. One of the benefits in using this tool is the unique matching with the bone surface.

The distal pin of the jig was inserted at the middle of cranial femoral metaphysis, slightly proximal to the trochlear sulcus and perpendicular to the bone surface. The proximal pin was then, positioned parallel to the first one and in a such position that must be between the first and second hole of lateral plated area. Next, the proximal customized saw guide was inserted in the femoral diaphysis in its matching point and fixed with another 1.0 mm K-wire as well.

The wedge resulting from the apposition of the saw guides was measured to confirm the matching with the preoperative measurement. The jig was positioned as well as hohmanns and periosteal elevator were used to retracted soft tissues from the osteotomy site. The caudal area of the femur was also packed with gauzes to prevent iatrogenic lesions to the muscles.

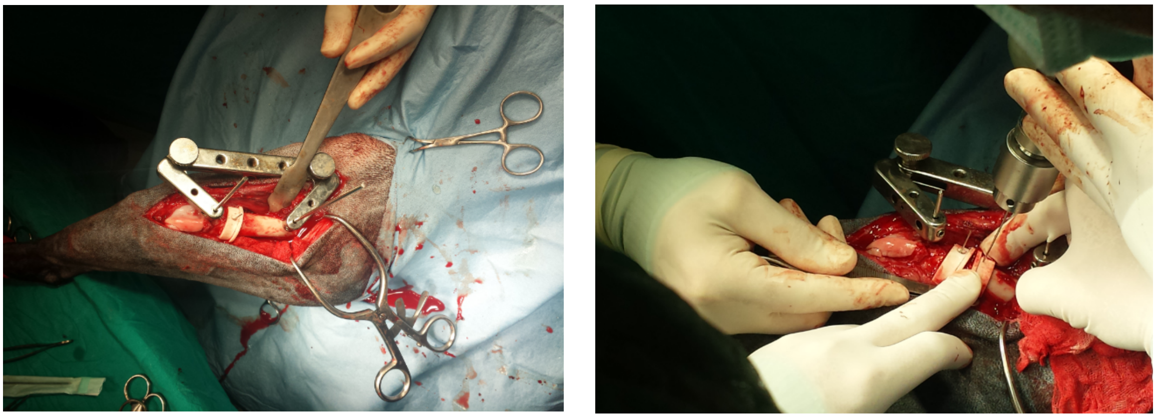

Fig. 58: jig application on the dorsal aspect of the femur, followed by the fixation of the proximal surgical guide.

Finally, the osteotomy was performed using surface of the saw guide as a support for the saw blade. When the ostectomy was executed, width and length of the wedge were checked and the saw guides were then removed from the femur. The osteotomy gap was reduced and held in place with a large pointed reduction forceps placed between the two pins of the jig.

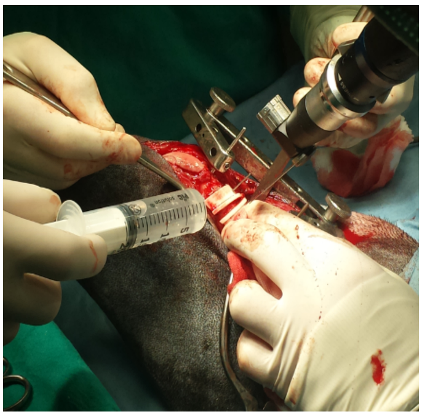

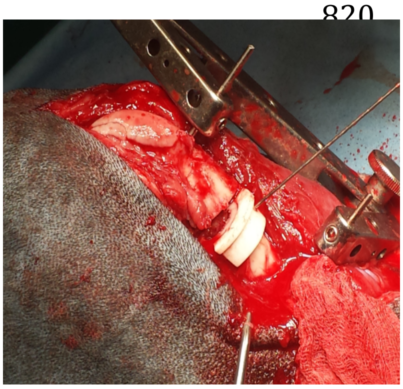

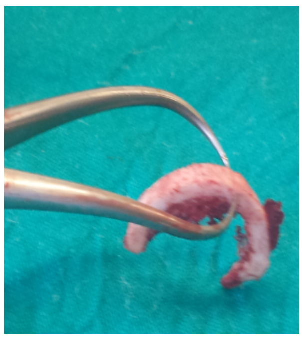

Fig. 59: ostectomy in the anatomical CORA. Notice the cutting and the width of the wedge removed in the central and lateral pictures.

Finally, the plate was positioned and fixed starting with the second distal hole. To complete the surgery an *en bloc* trochleoplasty was performed to improve the accommodation of the patella, onto the trochlear groove as well a lateral imbrication of the capsule. Joint capsule, biceps fascia, subcutaneous tissue and skin were sutured according to standard closure.

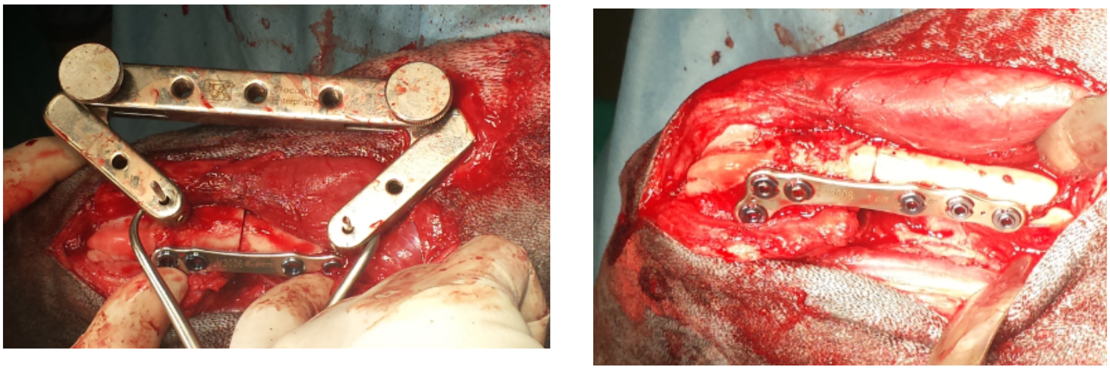

Fig. 60: ostectomy reduction (lefty image) and osteosynthesis using a Fixin 3.5 mm plate (right image)

Standard ventro-dorsal, cranio-caudal and medio-lateral radiographs obtained immediately after the surgical procedure revealed that the implant was correctly positioned with a good sagittal alignment and revealed an appropriate varus correction with a aLDFA of 93 °. Moreover, the patella was centred in the trochlear groove. A modified Robert Jones bandage was applied post-operatively for 24 hours to protect the hind limb until the lumbar-sacral plexus block was finished and to prevent post-surgical swelling.

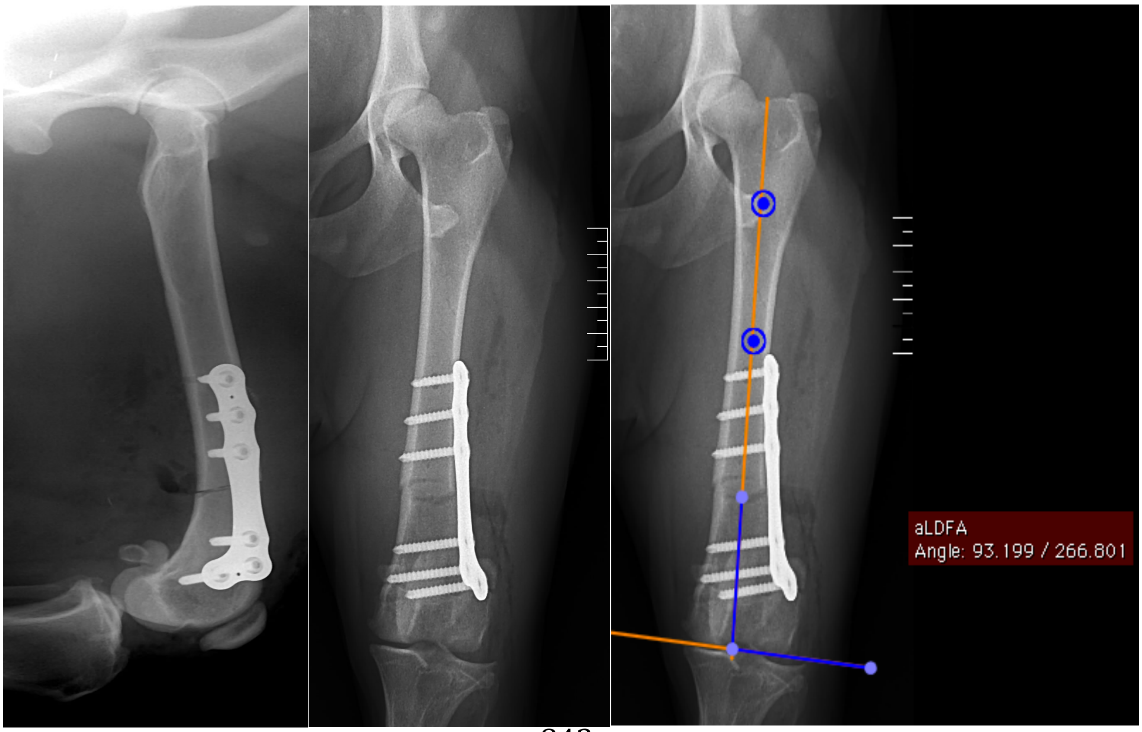

Fig. 61: orthogonal postoperative radiographic films. The medio-lateral view shows a correct longitudinal plate fixation with anatomical reduction of the corrective osteotomy. Central and right images evidenced the femoral varus correction with postoperative aLDFA of 93°. Note the patellar location in the middle of the trochlear groove.

Postoperative therapy included 4mg/kg carprofen (Rimadyl, Pfizer Italia s.r.l., Latina, Italy) *per os* every 24 hours for 7 days, then 2 mg/kg for other 7 days; 25 mg/kg cefazoline sodium *per os* every 12 hours for 8 days and tramadol hydrochloride (Hexal AG, Holzkichircen, Germany).

The convalescence recommendations included a cage limitation period for 8 weeks by and room restriction for other 4 weeks. Discharge instructions also recommended that the patient had to be walked three to four times per day on a leash for an increasing amount of time until full recovery at 3 months of the follow-up.

Physical examination 8 days after surgery, during stiches removal, showed a mild swelling in the medial compartment of the left stifle with little discomfort throughout the manipulation of the joint. The central position of patella was checked and confirmed.

Physical inspection and follow-up radiographic monitoring were not performed, as the patient was not taken to the hospital for re-checks. However, at 4 months telephone follow-up the owner reported that the dog was doing fine without perceived lameness.

DISCUSSION

Angular deformities of long bones are typically challenging for the orthopaedic surgeons.

Such skeletal malformations often cause apparent and functional modifications that may cause significant defects in the weight bearing of the subject as well as osteoarthritic degenerations in the medium and long term.[4,5]

The purpose of the corrective surgery in the affected limb aims to re-establish the natural alignment of the bone, thus decreasing the strain in the affected joints. To achieve this goal, the accurate study of all the bone alterations is crucial.[4]

Surgical simulation has been adopted in preparation for complicated reconstructive surgeries as well as for surgical training.[6-8] The simulation allows for the evaluation of a fracture configuration, methods to reduce it and selection of the more appropriate implants to use.[6-8]

Furthermore, pre-operative planning is necessary for measurements that the surgeon must carry-on intra-operatively.

However, even when an accurate preoperative planning is performed to treat a bone deformity, a certain degree of under- or over- correction could happen. Reasons behinds this leaning included: incorrect methods of planning, image-related bias for instance caused by poor positioning of the patient when a planning is performed through radiographs. Additionally, the complexity of deformity (multiplanar versus monoplanar) and the tendency of resorting to free-hand surgical correction may cause a mismatch between planning and final surgical outcome.[4-9]

In view of these considerations, the use of 3D reconstructed models can avoid or at least decrease the frequency of image-related errors, thus simplifying the surgical procedure as well as reduce the of range of potential errors.[6]

Three-dimensional reconstruction allows for detecting simultaneously all the bone deformities and precisely quantifying the degree of an angular deviation in all three axes of the space. The last feature is remarkably significant as the assessment of the bone morphology is accomplished in 3D and thus not in a biplanar image. This advantage is even more so relevant when a bone is affected by multiplanar deformities.

The minimization of intra-operatively bias is crucial for the surgeon because, depending on the size of the treated bone, a 1 mm error could translate in larger mistakes, achieving an outcome with an over- or under-corrected angular deformity.[6-9]

About computer-assisted surgery, the case here reported represents the objectification of the final goal of our research that was the development of surgical devices to perform assisted-correction of bone deformities.[9-11] In the authors' opinion, the translation of the application of a 3D computation on mesh model to the surgical field would have completed and enhanced the whole research.

Starting from the preoperative planning, we had compared the measurements of CT aLDFA and FTA with those computed in 3D. A mild difference was detected in both cases as for the aLDFA there was an increase of 2.2° while the 3D FTA resulted lower than the CT FTA. In the first case, since a femoral varus was clearly apparent with all the three diagnostic techniques used, we decided to take the 3D aLDFA as our surgical reference value. As a results, the length of the wedge removed was bigger compared to the one calculated in the CT preoperative planning. The postoperative films showed that the new aLDFA value was similar to the one measured in the not pathological hind limb and thus the femoral varus was considered corrected.

As concerns the femoral torsion, we opted not to correct it, even if the 3D indicated a minimum of retroversion of the femoral head but it was still within the range values that are usually taken as reference parameters from literature.

The use of the CAD software was critical for both the surgical planning and the customization of the surgical guides. In fact, the manipulation of the bone fragments, once the wedge was defined, allowed us to perform a simulation of the closing wedge ostectomy. As a result, we obtained a preoperative reconstruction of the femur with a corrected frontal alignment. The planning information were crucial to obtain the surgical outcome as the simulation of the closure of the wedge gap allowed for the awareness of the postoperative alignment of the femur.

Although this was not the case, the cad software simulation offers also a trustable idea of amount of the limb shortening or lengthening in relation to the use of closing or opening wedge.[10] Moreover, it is possible to use the model as a direct comparison during the surgery, confirming for instance the length of the wedge to remove with those of the wedge model.

In order to improve the surgical outcome of the corrective osteotomy, customized saw guides were made on the geometrical model, thus they have been generated taking into account the femoral surface contour. This feature represented a remarkable advantage and simplified the surgical procedure. In fact, these surgical tools fit correctly only in the planned site of the osteotomy and, therefore, the anatomical CORA was easily detectable. However, a re-check measurement was taken with a ruler starting from the most proximal point of the lateral femoral *labrum* to confirm the point of the osteotomy site.

To better fixate the guides, avoiding any possibility of minimal displacement, they were held in position through the insertion of K-wire pins. This step was not mandatory but considering our poor experience in using such devices; we felt more comfortable with an intra-operatively secondary fixation to the femur.

Another advantage of the proposed surgical devices is that they literally assist the osteotomy. In detail, we used each edge of the saw guides to direct the position and plane of the saw blade. The profit of the latter aspect is obvious since the surgeon has on his hands the planned inclination of the cutting plane. With the purpose of accommodating the contact between the saw blade and guides on 3D model prototyping, we increased the height of the saw guides; otherwise a portion of the saw blade would have not been in contact with the guides, hence increasing the risk of losing the direction of the cutting plane.

REFERENCES

1. Dudley RM, Kowaleski MP, Drost WT, et al: Radiographic and computed tomographic determination of femoral varus and torsion in the dog. *Vet Radiol Ultrasound* 2006;47:546-552
2. Tomlison J, Fox D, Cook JL, et al: Measurement of femoral angles in four dogs breeds. *Vet Surg* 2007;36:593-598
3. Petazzoni M: Radiographic measurements of the femur in Petazzoni M and Jaerger GH (eds): *Atlas of clinical goniometry and radiographic measurements of the canine pelvic limb*. Duluth, GA, Merial, 2008, pp 34-54
4. Paley D: Principles of Deformity correction. Berlin. Germany, Springer-Verlag, 2003
5. Dobbe J, du Prè KJ, Kloen P, et al: Computer-assisted and patient-specific 3-D planning and evaluation of a single-cut rotational osteotomy for complex long-bone deformity. *Med Biol Eng Comput* 2011;49:1363-1370
6. Lattanzi R, Baruffaldi S, Zannoni C, et al: Specialised CT scan protocols for 3-D pre-operative planning of total hip replacement. *Med Eng Phys* 2004;26:237–245
7. Pozzi A: surgical simulation and custom made guide in *Esvot proceedings,* 2016, pp 253
8. Fitzpatrick N: Emergence of personalised implants in *Esvot proceedings,* 2016, pp 112
9. Dismukes DI, Fox DB, Tomlinson JL, et al: Use of radiographic measures and three-dimensional computed tomographic imaging in surgical correction of an antebrachial deformity in a dog. *J Am Vet Med Assoc* 2008; 232:68–73
10. Crosse KR, Worth AJ: Computer-assisted surgical correction of an antebrachial deformity in a dog. *Vet Comp Orthop Traumatol* 2010;23:354–361
11. Domenech L, Soler C, Soriano J: Development of a customized device for correction of angular deformities of long bones in small animals. A case report. *17th Conference of the European Society of Veterinary Orthopaedics and Traumatology*. October 2-4, 20

CHAPTER 7

CONCLUSIONS OF THE RESEARCH

The whole research was conceived with the purpose of introducing to the literature a newly developed protocol for the measurement of morphological femoral parameters with a 3D approach. To obtain this goal, a validation of the three-dimensional technique represented the first mandatory step to take. In this regard, the rationale of our first study was to define a 3D assessment of bone morphometric parameters on a mesh model. We satisfied this goal, demonstrating the feasibility of the 3D technique. However, because 3D morphometric parameter evaluation is a relatively new topic in veterinary medicine, and due to the substantial difference in the nature of past measurements (mostly done in 2D), our results cannot be compared with literature, hence new reference ranges for femoral parameters should be developed from CT and MRI images.

The software we developed allows to elaborate mesh models derived not only from a 3D scanner but also from CT and MRI, therefore enabling the development of databases which can be helpful in veterinary practice both for diagnostic and treatment purposes.

Since the introduction of new a technique needs the investigation of its repeatability and reproducibility to be considered a reliable diagnostic method, and due to better availability of CT and MRI in veterinary daily practice, we put the basis for our second study. The outcomes were encouraging and satisfied our hypotheses as the 3D approach resulted the most precise and consistent technique in light of the average values as well as coefficients of variance obtained. The conclusion of the second study reinforced and supported the hypothesis proposed with our first report, thus underlining the importance of adopting an automatic and independent protocol. Moreover, the standardization of the femoral computation minimizes the user-related computation bias and may avoid all the minor variations in the bone positioning that could be expected either with conventional radiography or computed tomography.

The increased emphasis on 3D computation is not only pertinent to diagnostic imaging, but also to surgery. For instance, 3D computation could be considered as a more reliable methodology for corrective osteotomies since it might improve the evaluation of skeletal deformities and occurring joints malalignment. As a result, surgeons may rely on a more detailed planning, potentially carrying out a better quality corrective osteotomy and, conceivably, decreasing complication rates.

Furthermore, three-dimensional assessment of a bone deformity improves the localization of the CORA as well as offers a more accurate idea of the orientation of the osteotomy-cutting plane, thus simplifying the surgical procedure and perhaps decreasing the complication rate. In support of this thesis, 3D models are regarded as indispensable for the design of customized templates and surgical devices used to perform assisted-correction of bone deformities.

Our initial surgical experience using saw bone guides was positive and encouraging as we found out that these devices are user-friendly and can be easily adaptable to the bone surface.

In the context of future perspectives, a prospect study will investigate the accuracy of 3D approach for the measurement of femoral angles in normal and pathologic femurs.

Second, a report of the methodology used to create the surgical guides will be presented, describing all the passages required for the elaboration of such intra-operatively tools. Finally, future researches will focus on the composition and configuration of the saw bone guides with the aim of to improving the fixation of these surgical tools to the bone, avoiding the use of temporarily reduction instruments.